



EX LIBRIS
UNIVERSITATIS
ALBERTENSIS

The Bruce Peel.
Special Collections
Library



Digitized by the Internet Archive
in 2025 with funding from
University of Alberta Library

<https://archive.org/details/0162012506166>

University of Alberta

Library Release Form

Name of Author: *Arthur Thomas Gerald Fuller*

Title of Thesis: *Design and Implementation of Bode-Type Variable-Amplitude Digital Equalizers*

Degree: *Doctor of Philosophy*

Year this Degree Granted: *2000*

Permission is hereby granted to the University of Alberta Library to reproduce single copies of this thesis and to lend or sell such copies for private, scholarly, or scientific research purposes only.

The author reserves all other publication and other rights in association with the copyright in the thesis, and except as hereinbefore provided, neither the thesis nor any substantial portion thereof may be printed or otherwise reproduced in any material form whatever without the author's prior written permission.

THE UNIVERSITY OF ALBERTA

DESIGN AND IMPLEMENTATION OF BODE-TYPE
VARIABLE-AMPLITUDE DIGITAL EQUALIZERS

by

Arthur Thomas Gerald Fuller



A THESIS

SUBMITTED TO THE FACULTY OF GRADUATE STUDIES
IN PARTIAL FULFILLMENT OF THE REQUIREMENTS FOR THE
DEGREE OF DOCTOR OF PHILOSOPHY

DEPARTMENT OF ELECTRICAL AND COMPUTER
ENGINEERING

EDMONTON, ALBERTA

Spring 2000

University of Alberta

Faculty of Graduate Studies and Research

The undersigned certify that they have read, and recommend to the Faculty of Graduate Studies and Research for acceptance, a thesis entitled *Design and Implementation of Bode-Type Variable-Amplitude Digital Equalizers* submitted by Arthur Thomas Gerald Fuller in partial fulfillment of the requirements for the degree of Doctor of Philosophy.

To my wife,
my best friend and partner in crime.

ABSTRACT

This thesis presents analytical and computational techniques for the design and implementation of Bode-type variable-amplitude digital equalizers. The important practical feature of the resulting variable-amplitude digital equalizers is that their frequency response may be varied continuously from that of a specified shaping transfer function to its inverse by varying the value of a single variable digital multiplier only. Three different design techniques are proposed, including (a) the indirect design based on the translation of a continuous-time s -domain analog prototype network into the digital domain by using wave-digital synthesis techniques, (b) the direct discrete-time z -domain design using a novel set of three realizability conditions, and (c) the computational design by enumeration. Moreover, an approximation technique is presented for the design of general-order shaping transfer functions with maximally flat or equiripple lowpass, highpass, or bandpass magnitude-frequency response characteristics. The theoretical basis of Kharitonov's stability theorem is used for the development of a novel BIBO stability condition for general-order Bode-type variable-amplitude digital equalizers. In addition, the effect of the "dynamic" variations of the variable digital multiplier on the stability and the transient signal behaviour of Bode-type variable-amplitude digital equalizers is investigated. The proposed techniques are illustrated through their application to the design and microprocessor hardware implementation of a real-time stereo 4-band digital graphic equalizer. The resulting digital graphic equalizer provides CD-quality equalization of a 2-channel audio input signal by using eight second-order Bode-type variable-amplitude digital equalizer sections.

ACKNOWLEDGEMENTS

The author wishes to thank his supervisor Dr. B. Nowrouzian for his guidance, advice, and encouragement throughout the course of this work, and for the constructive criticism he offered during the writing of this thesis. This thesis would not have been possible without his mentorship, input, and support.

The author gratefully acknowledges the financial support of NSERC through the *1967 Science and Engineering Scholarship*, of Micronet, and of the Departments of Electrical and Computer Engineering at the University of Alberta and the University of Calgary.

The author wishes to thank all the staff within the Department of Electrical and Computer Engineering for their support and assistance during the course of his studies.

The author wishes to extend his deepest thanks to his parents, Drs. Gerald and Norma Fuller, for their help, their example, and the wonderful home environment they have provided. One could not wish for better role models.

The author wishes to thank his wife, Darla, for putting up with him during his studies and the long nights. Her friendship and moral support through the good and the bad have made the difference.

Finally, the author wishes to acknowledge God for Life, and for the precious opportunities that the author has been given.

Contents

1	Introduction	1
1.1	Survey of Existing Design Techniques for Digital Audio Graphic Equalizers	3
1.1.1	Design based on Parallel Connection of IIR Bandpass Digital Filters	4
1.1.2	Design based on Parallel Connection of FIR Bandpass Digital Filters	6
1.1.3	Design based on Digital Parametric Equalizers using Allpass Digital Filters	8
1.1.4	Design based on Digital “Bump” Equalizers	9
1.2	Bode-Type Variable-Amplitude Digital Equalizers	11
1.3	Overview of the Thesis	13
2	Design of Bode-Type Variable-Amplitude Wave-Digital Equal- izers	18

2.1	Design of First-Order Fan Bode-Type Variable-Amplitude Wave-Digital Equalizers	23
2.2	Design of Second-Order Bump Bode-Type Variable-Amplitude Wave-Digital Equalizers	29
2.3	BIBO Stability of Bode-Type Variable-Amplitude Wave-Digital Equalizers	34
2.3.1	BIBO Stability of First-Order Fan WD Equalizers . . .	35
2.3.2	BIBO Stability of Second-Order Bump WD Equalizers	38
2.4	Application Examples	41
2.5	Conclusions	45

3 Realizability Conditions for Bode-Type Variable-Amplitude

	Digital Equalizers	47
3.1	Background	48
3.2	Realizability Conditions for Bode-Type Variable-Amplitude Digital Equalizers	51
3.3	Design of Bode-Type Variable-Amplitude Digital Equalizers .	55
3.4	BIBO Stability Condition for Second-Order Bode-Type Variable-Amplitude Digital Equalizers	57
3.5	Computational Design of Bode-Type Variable-Amplitude Digital Equalizers by Enumeration	60

3.5.1	A Class of Infinite-Precision Bode-Type Variable-Amplitude	
	Digital Equalizers	64
3.5.2	A Class of Finite-Precision Bode-Type Variable-Amplitude	
	Digital Equalizers	65
3.6	Selection of Bode-Type Bump Variable-Amplitude Digital	
	Equalizer with Minimal Internal Signal Wordlength	71
3.6.1	Application Example	76
3.7	Conclusions	78
4	Design of General-Order Bode-Type Variable-Amplitude Dig-	
	ital Equalizers	81
4.1	Introduction	81
4.2	Effective Shaping Transfer Function	83
4.3	Development of the New Design Technique	85
4.4	Design of General-Order Bode-type VA digital equalizer Shap-	
	ing Transfer Functions	88
4.4.1	Design of Normalized Prototype Lowpass Shaping Trans-	
	fer Functions	90
4.4.2	Derivation of Shaping Transfer Functions with Maxi-	
	mally Flat Passbands	92

4.4.3	Derivation of Shaping Transfer Functions with Equiripple Passbands	96
4.4.4	Derivation of Shaping Transfer Functions with Equiripple Stopbands	99
4.5	BIBO Stability of Bode-type VA digital equalizers	102
4.5.1	Theoretical Background	103
4.5.2	Development of BIBO Stability Condition	106
4.6	Application Example	110
4.7	Conclusions	116

5 Implementation Issues for Bode-type VA Digital Equalizers

	with Time-Varying Coefficients	119
5.1	Introduction	119
5.2	Stability Analysis of Bode-type VA Digital Equalizers Consisting of a Dynamically-Varying Variable Digital Multiplier .	122
5.2.1	Stability under Infinite-Precision Arithmetic	122
5.2.2	Stability under Finite-precision Arithmetic	126
5.3	Analysis of the Transient Behavior of Bode-type VA Digital Equalizers Consisting of a Dynamically-Varying Variable Digital Multiplier	127
5.4	Application Example	131

5.4.1	Investigation of Dynamic Stability	133
5.4.2	Investigation of Output Signal Transients	133
5.5	Conclusions	137
6	Implementation of a Real-Time Multi-Band Digital Graphic	
	Equalizer	140
6.1	Introduction	140
6.2	Overview of DSP56002EVM Microprocessor System	142
6.3	Design and Implementation of the DE Subsystem	144
6.4	Development of Parallel Interface	150
6.5	The GUI Subsystem	151
6.6	Conclusions	154
7	Conclusions	156
7.1	Review of Material Presented	156
7.2	Contribution of the Thesis	160
7.2.1	Chapter 2	160
7.2.2	Chapter 3	161
7.2.3	Chapter 4	161
7.2.4	Chapter 5	162
7.2.5	Chapter 6	162
7.3	Proposed Areas of Future Investigation	163

A	MATLAB Design Files	174
A.1	Design of Maximally Flat Lowpass Transfer Function	174
A.2	Design of Cheybshev Lowpass Transfer Function	175
A.3	Calculation of Cheybshev Polynomial	177
A.4	Design of Inverse-Cheybshev Lowpass Transfer Function . . .	177
A.5	Normalized Lowpass to Lowpass Transformation Function . .	179
A.6	Normalized Lowpass to Highpass Transformation Function . .	180
A.7	Normalized Lowpass to Bandpass Transformation Function . .	181
A.8	Polynomial Addition Function	183
A.9	Polynomial Power Function	183
A.10	Polynomial Pad Function	184
A.11	Polynomial Pad Left Function	184
B	DSP56002EVM Code for 4-Band Equalizer Implementation	185
C	IBM-PC Code for 4-Band Equalizer Implementation	200
C.1	C Code	200
C.2	TCL/TK Code	202

List of Tables

2.1	Definition of b_1 and b_0 for fan equalizers	24
2.2	Definition of impedance $\frac{R_x}{R_n} s^\lambda$ for fan equalizers	24
2.3	Multipliers α_1 and α_2 for first-order fan VA WD equalizers . .	28
2.4	Definition of X and Y for fan WD equalizers	37
2.5	Design specification for the first-order lowpass and highpass fan equalizers	41
2.6	Multiplier values for the first-order lowpass fan equalizer . . .	42
2.7	Multiplier values for the first-order highpass fan equalizer . .	42
2.8	Design specification for the second-order bump equalizer . . .	43
2.9	Multiplier values for the second-order bump equalizer	45
3.1	Positive-valued transmittances a_{ij} for infinite-precision Bode- type bump digital equalizers	65
3.2	Negative-valued transmittances a_{ij} for infinite-precision Bode- type bump digital equalizers	66

3.3	Multiplier transfer functions for equalizer 20	77
3.4	Positive-valued finite-precision bump Bode-type VA digital equalizers class interconnections	79
3.5	Negative-valued finite-precision bump Bode-type VA digital equalizers class interconnections	80
4.1	Coefficient values for $T_{se}(z)$	111
4.2	Multiplier coefficient values for $t_{22}(z)$	115
5.1	Coefficient values for variable multiplier v	132
6.1	Band 1 $T_{se}(z)$ coefficient values	147
6.2	Band 2 $T_{se}(z)$ coefficient values	148
6.3	Band 3 $T_{se}(z)$ coefficient values	148
6.4	Band 4 $T_{se}(z)$ coefficient values	149
6.5	Band 1 Bode-type VA digital equalizer coefficient values . . .	149
6.6	Band 2 Bode-type VA digital equalizer coefficient values . . .	149
6.7	Band 3 Bode-type VA digital equalizer coefficient values . . .	150
6.8	Band 4 Bode-type VA digital equalizer coefficient values . . .	150
6.9	Bode-type VA digital equalizer variable digital multiplier v values	155

List of Figures

1.1	Digital graphic equalizer consisting of a parallel connection of IIR bandpass digital filters	5
1.2	Non-constant- Q equalizer section magnitude-frequency response characteristics for various values of g_n	6
1.3	Digital graphic equalizer consisting of a parallel connection of FIR bandpass digital filters	7
1.4	FIR bandpass equalizer magnitude-frequency response char- acteristics for various values of g_n	8
1.5	Digital graphic equalizer consisting of cascade connection of digital parametric equalizers	9
1.6	Constant- Q equalizer section magnitude-frequency response characteristics	10
2.1	Analog prototype network for WD realization of $T_v(s)$	20
2.2	Analog prototype network for first-order fan VA WD equalizers	25

2.3	Identification of interconnections for the first-order fan VA	
	WD equalizer realization	25
2.4	First-order fan Bode-type VA WD equalizer realization	26
2.5	Two-pair parallel adaptor realization	27
2.6	Three-pair series adaptor realization	27
2.7	Analog prototype network for the second-order bump VA WD	
	equalizers	30
2.8	Identification of connections for the second-order bump VA	
	WD equalizer realization	31
2.9	Second-order bump VA WD equalizer realization	32
2.10	Magnitude-frequency response characteristics for the first-order	
	lowpass fan equalizer	43
2.11	Magnitude-frequency response characteristics for the first-order	
	highpass equalizer	44
2.12	Magnitude-frequency response characteristics for the second-	
	order bump equalizer	46
3.1	Schematic diagram representing a Bode-type VA digital equal-	
	izer	51
3.2	Network N_2 obtained by extracting multipliers α_2 and α_3 ,	
	and the two unit-delays from network N_1	63

3.3	One of the 14 new Bode-type VA bump digital equalizers . . .	67
3.4	Objective function values for the finite-precision class of 40 digital equalizers	77
4.1	Normalized magnitude-frequency response	92
4.2	Normalized prototype magnitude-frequency responses	111
4.3	Magnitude-frequency response of $T_{se}(z)$	112
4.4	Phase-frequency response of $T_{se}(z)$	113
4.5	Fourth-order bump digital equalizer	114
4.6	Magnitude-frequency response of digital equalizer	116
4.7	Plot of poles of $T_v(z)$ for $v \in (V_{Ie}, V_{Fe})$	117
5.1	Time-domain response of 4th-order Bode-type VA digital equal- izer	134
5.2	Transient output signal	135
5.3	Illustration of settling-time verification	136
5.4	Illustration of incremental transition steps	137
5.5	Illustration of transitions between incremental steps	138
6.1	Digital graphic equalizer system overview	142
6.2	Block diagram of DSP56002EVM	145
6.3	Schematic diagram for 2nd-order Bode-type VA digital equalizer	146
6.4	Desired DE subsystem response	147

6.5	Transmission protocol (IBM-PC side)	152
6.6	Transmission protocol (DSP56002EVM side)	152
6.7	Digital graphic equalizer GUI	153

Chapter 1

Introduction

The trend in today's commercial audio marketplace is towards digital audio products and formats. The Compact Disc (CD), Laser Disc (LD), and Digital Video Disc (DVD) formats have obtained widespread acceptance due to their ability to permit high-quality audio signal reproduction. Digital signal processing techniques are making in-roads in the field of high-quality audio signal reproduction, even in applications which were once solely based on analog signal processing techniques (such as hearing aid applications). In the emerging digital audio signal processing applications, it is desirable that the processing of the audio signals be contained entirely in the digital domain so as to maintain the high-quality feature of the underlying signal.

The present thesis is concerned with the digital processing of audio signals by employing digital graphic equalizers. In digital graphic equalizer

applications, the audio frequency spectrum is split into a number of frequency bands, with each band being equalized separately by using a digital equalizer section. The constituent digital equalizer sections realize transfer functions having gains¹ at band center-frequencies that can be changed in real-time by varying the value of a single variable digital multiplier. Ideally, it is required that the quality factor Q (the ratio of center-frequency and bandwidth) of these equalizer sections remain constant as the gains at the band center-frequency are changed [1]. This “constant- Q ” behavior is essential for the design of graphic equalizers if it is required to minimize the interband interference in an attempt to obtain an overall digital graphic equalizer magnitude-frequency response which correctly reflects the gain setting at the band center-frequencies. Ideally, it is also required that the gain at the band center-frequency be controlled by the value of a single variable digital multiplier. In an actual hardware implementation, this minimizes the memory requirements for pre-computed gain settings and avoids the high computational cost of recalculating digital multiplier values in real-time. Finally, in some applications, it may be desirable to have higher-order (> 2) digital equalizer sections in order to obtain sharp transition bands, which in turn, reduces the interband interference. Digital graphic equalizers with

¹Here and in the following, the term “gain” is used to refer to an actual gain or loss through a digital equalizer.

such features find practical applications in multimedia, in digital audio signal processing, in digital signal enhancement/correction, and in hearing aids [2].

1.1 Survey of Existing Design Techniques for Digital Audio Graphic Equalizers

The existing techniques available for the design of digital audio graphic equalizers can be classified into four distinct categories:

1. Design based on parallel connection of IIR bandpass digital filters [3].
2. Design based on parallel connection of FIR bandpass digital filters [4–6].
3. Design based on digital parametric equalizers using allpass digital filters [2, 7].
4. Design based on digital “bump” equalizers [8, 9].

The digital graphic equalizers in these categories are briefly reviewed in the following four subsections, accordingly.

1.1.1 Design based on Parallel Connection of IIR Band-pass Digital Filters

In this design technique, the audio input signal is passed through a set of N second-order IIR bandpass digital filters connected in parallel as shown in Figure 1.1, where $X(z)$ and $Y(z)$ represent the z-transformed input and output signals, respectively, where the equalizer sections $H_n(z)$'s (for $n = 1, 2, \dots, N$) represent bandpass IIR transfer functions with magnitude-frequency responses aligned at various band center-frequencies, and where g_n 's represent variable digital multipliers (serving as frequency independent gain factors). In this way, the digital graphic equalizer in Figure 1.1 realizes an overall magnitude-frequency response $|H(e^{j\omega})|$ given by

$$|H(e^{j\omega})| = |1 + \sum_{n=1}^N g_n H_n(e^{j\omega})|. \quad (1.1)$$

However, in order to facilitate the independent adjustment of the gains at the band center-frequencies by using the variable digital multipliers g_n , it is desirable to have

$$|H(e^{j\omega})| = 1 + \sum_{n=1}^N g_n |H_n(e^{j\omega})|. \quad (1.2)$$

This can be achieved approximately by ensuring that

$$|1 + H_n(e^{j\omega})| \approx 1 + |H_n(e^{j\omega})|. \quad (1.3)$$

If the conditions in Eqn. 1.3 are not adequately satisfied, then

$$|1 + H_n(e^{j\omega})| \approx 1 + |H'_n(e^{j\omega})|, \quad (1.4)$$

and the resulting effective weighted magnitude-frequency responses $|g_n H'_n(e^{j\omega})|$ will have the typical characteristics as shown in Figure 1.2². Unfortunately,

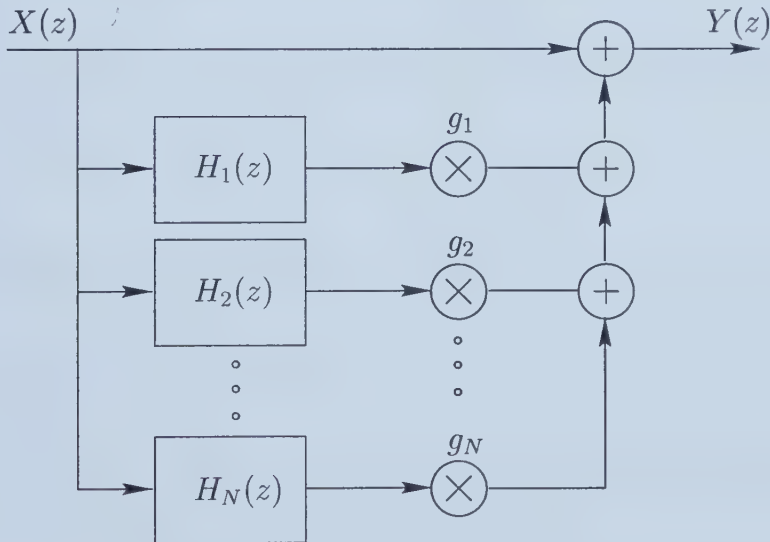


Figure 1.1: Digital graphic equalizer consisting of a parallel connection of IIR bandpass digital filters

as evident from Figure 1.2, the effective band digital equalizer sections do

²In the following graphs, “normalized frequency” refers to actual frequency (in rad/s) normalized to half the sampling frequency (i.e. the Nyquist frequency).

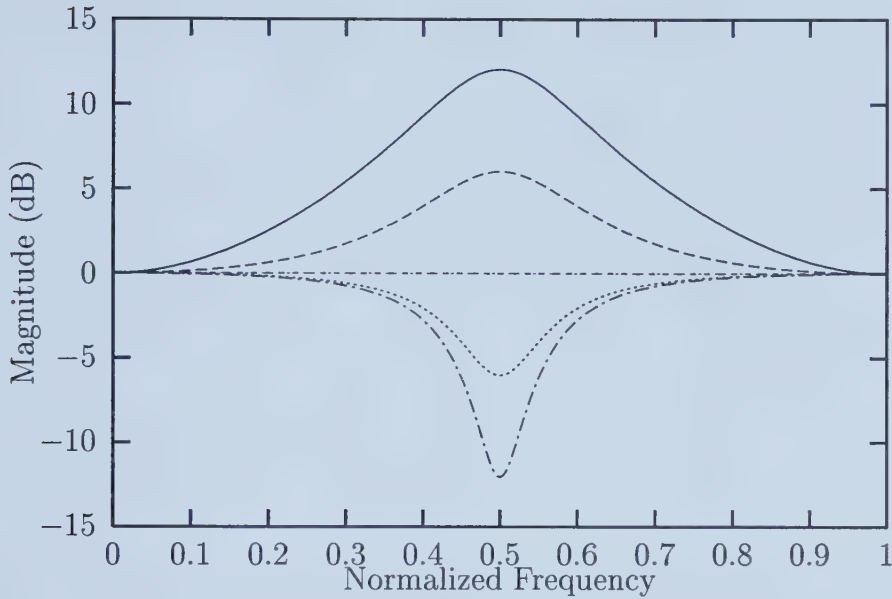


Figure 1.2: Non-constant- Q equalizer section magnitude-frequency response characteristics for various values of g_n

not exhibit the above mentioned desirable constant- Q magnitude-frequency response characteristics.

1.1.2 Design based on Parallel Connection of FIR Band-pass Digital Filters

This design technique is essentially the same as that in the preceding subsection, except that there is no direct feed-through path from the input to the output, and that the constituent transfer functions $H_n(z)$ are realized as FIR bandpass digital filters (c.f. Figure 1.3). As before, single variable digital multipliers g_n change the gains at the band center-frequencies by utilizing the magnitude-frequency response characteristics associated with the FIR

bandpass digital filters $H_n(z)$. The effective digital equalizer sections exhibit

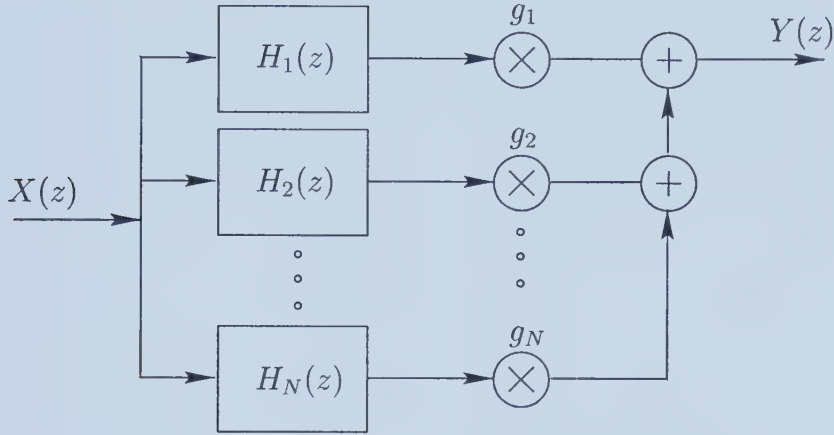


Figure 1.3: Digital graphic equalizer consisting of a parallel connection of FIR bandpass digital filters

typical magnitude-frequency response characteristics as shown in Figure 1.4.

The salient feature of the above technique is that it can be used to obtain a linear-phase digital equalizer section. However, this technique typically requires FIR bandpass digital filters having high orders and a substantial computational requirement. In addition, the use of high-order FIR bandpass filters leads to an overall digital graphic equalizer exhibiting a long latency which renders them unsuitable for use in live performance or in the processing of audio synchronized with video images (e.g. TV).

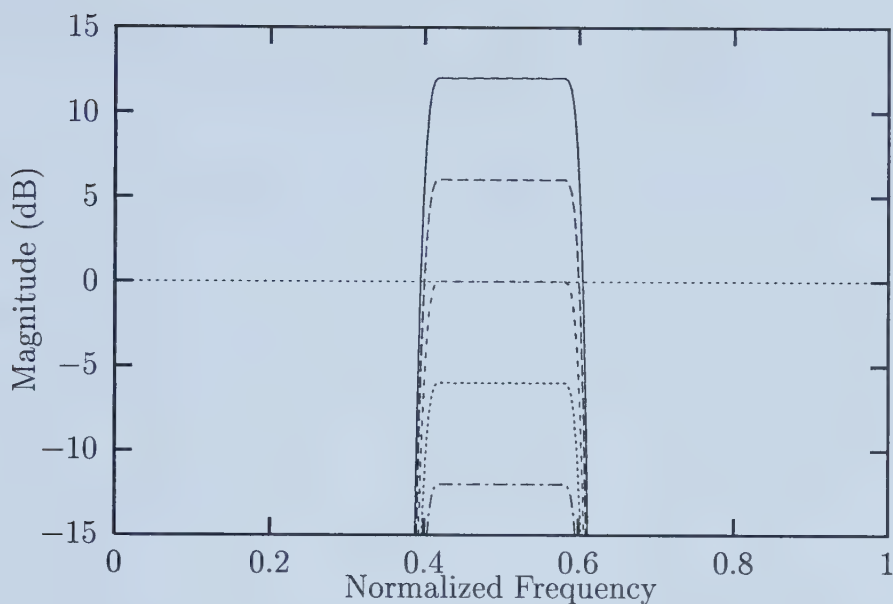


Figure 1.4: FIR bandpass equalizer magnitude-frequency response characteristics for various values of g_n

1.1.3 Design based on Digital Parametric Equalizers using Allpass Digital Filters

In this design technique, the audio input signal is passed through a set of N digital filters connected in cascade as shown in Figure 1.5, where the equalizer sections $H_n(z)$ are realized in accordance with

$$H_n(z) = \frac{1}{2} [1 + A_n(z)] + \frac{1}{2} g_n [1 - A_n(z)], \quad (1.5)$$

where $A_n(z)$'s represent second-order allpass transfer functions, and where g_n 's represent variable digital multipliers.

The salient feature of the above design technique is that the variable

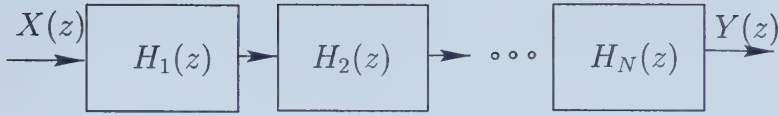


Figure 1.5: Digital graphic equalizer consisting of cascade connection of digital parametric equalizers

digital multipliers g_n can be used to control the gains at the band center-frequencies, while the multiplier coefficients contained in the allpass digital filter sections can be used to independently control other characteristics of the magnitude-frequency response (i.e. the center frequency, bandwidth, etc.) associated with the equalizer section. However, the resulting digital graphic equalizers still do not exhibit the desirable constant- Q characteristics, but instead exhibit non-constant- Q characteristics as shown in Fig 1.2. Moreover, this technique is only applicable to the case of first- and second-order parametric digital equalizer sections.

1.1.4 Design based on Digital “Bump” Equalizers

In this design technique, the values of the coefficients of a traditional digital biquad are determined in terms of the required bandwidth, center frequency, and the maximum gain associated with the “bump” magnitude-frequency response characteristic. In this way, a symmetric constant- Q magnitude-frequency response can be obtained as shown in Figure 1.6. In this approach, the desirable constant- Q magnitude-frequency response characteristics are

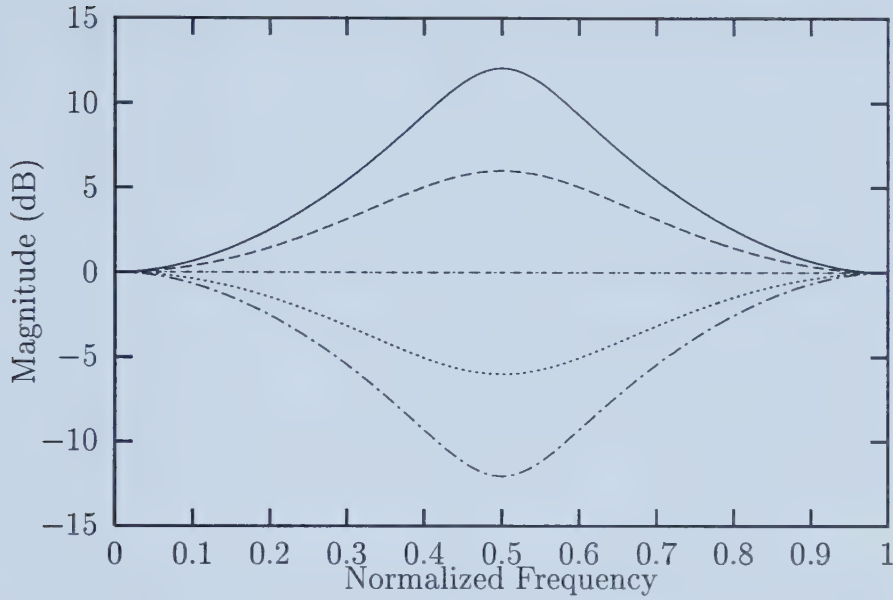


Figure 1.6: Constant- Q equalizer section magnitude-frequency response characteristics

obtained in a simple and straight-forward manner. However, this technique suffers from two drawbacks: (1) the multiplier coefficient values associated with the biquad must be re-computed in real-time each time the gain of the equalizer section is changed, and (2) this technique can only be applied to the case of second-order digital equalizer sections in which the corresponding multiplier coefficients can be easily determined analytically in terms of second-order bump magnitude-frequency response characteristics.

1.2 Bode-Type Variable-Amplitude Digital Equalizers

In the past, the design of Bode-type variable-amplitude (VA) equalizers has been investigated mainly from an analog point of view [10–15]. The present thesis is concerned with the design and hardware implementation of the corresponding Bode-type VA *digital* equalizers. The resulting VA digital equalizers are required to incorporate a single variable digital multiplier only to realize a symmetrical constant- Q magnitude-frequency response variation as shown in Fig. 1.6. In addition, they are required to realize second- or higher-order shaping transfer functions.

In his classical paper of 1938, Bode introduced the concept of variable amplitude equalizers [10]. Ideally, the logarithmic magnitude-frequency response characteristic of such an equalizer is required to satisfy a relationship of the form

$$\ln |T(j\omega)| = \ln |T_o(j\omega)| + f(R_v) \ln |T_s(j\omega)|, \quad (1.6)$$

where $T(s)$ is the transfer function of the equalizer, where $T_o(s)$ and $T_s(s)$ are fixed shaping transfer functions, and where $s = j\omega$ is the analog complex frequency-variable. In this equation, $f(R_v)$ represents a frequency indepen-

dent adjustment parameter whose value can be varied from -1 (via 0) to $+1$ by varying the value of R_v from 0 to ∞ . In the case of analog equalizers, R_v is usually a variable resistor.

In his paper, Bode [10] has shown that the relationship in Figure 1.6 cannot be exactly satisfied by a physically realizable equalizer, but that an acceptable approximation can be achieved by using a transfer function of the form

$$T(s) = T_o(s) \frac{1 + r_v T_s(s)}{r_v + T_s(s)}. \quad (1.7)$$

In Eqn. 1.7, $r_v = R_v/R_n$, where R_n is a suitable reference resistance. Then, r_v varies from 0 (via 1) to ∞ as R_v varies from 0 (via R_n) to ∞ . By using a power series expansion of $T(j\omega)$ in accordance with

$$\begin{aligned} \ln |T(j\omega)| &= \ln |T_o(j\omega)| + \frac{r_v - 1}{r_v + 1} \ln |T_s(j\omega)| + \\ &f_3(r_v) \Re\{\ln^3 T_s(j\omega)\} + \dots, \end{aligned} \quad (1.8)$$

one can obtain an acceptable approximation to the ideal frequency response characteristic in Eqn. 1.6.

In the design of variable amplitude equalizers, the transfer functions $T_o(s)$ and $T_s(s)$ are usually specified at the outset. Then, the design problem can

be further simplified to that of the realization of the transfer function $T(s)$ satisfying Eqn. 1.7. The problem under consideration can further be reduced by realizing the equalizer as a cascade connection of two separate sections, one of which realizes a fixed transfer function

$$T_f(s) = T_o(s), \quad (1.9)$$

and the other realizes a variable transfer function

$$T_v(s) = \frac{1 + r_v T_s(s)}{r_v + T_s(s)}, \quad (1.10)$$

so that

$$T(s) = T_f(s)T_v(s). \quad (1.11)$$

The ensuing discussions are concerned with the variable transfer function $T_v(s)$ only.

1.3 Overview of the Thesis

The thesis is organized into seven chapters and is supported by three appendices.

In Chapter 2, a synthesis technique is presented for the design of first- and second-order Bode-type VA wave-digital (WD) equalizers. The proposed first-order VA WD equalizers consist of one unit-delay and two digital multipliers and produce a fan-shaped (shelving) magnitude-frequency response, while the proposed second-order VA WD equalizers consist of two unit-delays and three digital multipliers and produce bump-shaped (peaking) magnitude-frequency response characteristics. In the resulting WD equalizers, a single digital variable multiplier is employed to control the fan amplitude in the first-order equalizer and the bump amplitude in the second-order equalizer without affecting their other important magnitude-frequency response characteristics (e.g. the cut-off frequency in the fan equalizer and the center frequency and quality factor in the bump equalizer). Moreover, these equalizers remain bounded-input bounded-output (BIBO) stable under infinite-precision arithmetic for all possible values of the variable digital multiplier. Application examples are given to illustrate the design of such Bode-type VA WD equalizers.

In Chapter 3, a novel approach is presented for the computational design of Bode-type VA digital equalizers by enumeration. In this approach, it is required that the frequency response of the resulting VA digital equalizers can be varied from that of an arbitrary shaping transfer function to its inverse by changing the value of a single variable digital multiplier only. A set of three

novel realizability conditions are developed to facilitate the design of these VA digital equalizers realizing arbitrary shaping transfer functions. Moreover, a mathematical technique is developed to place in evidence the interdependence between the range of variable digital multiplier values and the constituent shaping transfer functions. The results thus obtained are applied to the design and enumeration of two classes of second-order bump digital equalizers for both infinite-precision as well as finite-precision implementations. In the case of the finite-precision implementation, the digital equalizers are classified in terms of their required internal signal wordlength for guaranteed stable operation without overflow saturation and limit-cycles.

In Chapter 4, a novel approach is presented for the design of arbitrary-order Bode-type VA digital equalizers. In this approach, the interdependence between the range of variable digital multiplier values and the shaping transfer function is eliminated. This elimination leads to a substantial simplification in the realizability conditions associated with the VA digital equalizer, and, in turn, leads to a reduction in the cost of the corresponding hardware implementation of the digital equalizer. Moreover, it restricts the variable digital multiplier values to an effective range which is devoid of impractically large extreme values. In addition, a novel approximation technique is presented for the design of general-order shaping transfer functions with maximally flat or equiripple lowpass, highpass, or bandpass magnitude-frequency

response characteristics. This is achieved by first deriving a corresponding normalized prototype lowpass shaping transfer function, and then by applying a lowpass-to-lowpass, lowpass-to-highpass, or lowpass-to-bandpass frequency transformation to obtain the desired (denormalized) shaping transfer function. These shaping transfer functions can be employed in the design of VA digital equalizers having magnitude-frequency responses with sharp transition bands and reduced interband interference in the corresponding digital graphic equalizers. This is followed by exploitation of the theoretical basis of Kharitonov's stability theorem for the development of a novel BIBO stability condition for general-order Bode-type VA digital equalizers. The proposed design technique is illustrated through its application to the design of a fourth-order VA digital equalizer.

In Chapter 5, an investigation is undertaken into the effect of changes in the variable digital multiplier values on the "dynamic" stability and time-domain response characteristics of the Bode-type VA digital equalizer. A technique is developed for the estimation of the time required for the transients in the output of the VA digital equalizer as caused by changes in the value of the variable digital multiplier to reduce to a specified small level. The results thus obtained are illustrated in connection with a fourth order Bode-type VA digital equalizer.

Chapter 6 is concerned with the design and real-time microprocessor

hardware implementation of a stereo 4-band digital graphic equalizer using the above Bode-type VA digital equalizers. This digital graphic equalizer consists of two subsystems: (a) a graphical user interface (GUI) subsystem implemented on an IBM PC (or compatible) running the Microsoft Win32 operating system, and (b) a digital equalizer (DE) subsystem running on a Motorola DSP56002EVM microprocessor system. The GUI subsystem facilitates real-time changes to the variable multiplier values by the user via a set of 9 sliders (8 band controls and 1 volume control). The DE subsystem uses the resulting digital multiplier values to perform CD-quality equalization of a 2-channel (stereo) audio input signal using eight second-order VA digital equalizer sections (4 digital equalizer sections per channel).

Chapter 2

Design of Bode-Type

Variable-Amplitude

Wave-Digital Equalizers

This chapter¹ is concerned with the exploitation of the existing literature concerning Bode-type variable-amplitude (VA) analog equalizers [10–15] and its application to the development of a design technique [16] for the corresponding VA wave-digital (WD) equalizers. This technique is based on the design of a corresponding VA analog prototype network and its translation into the digital domain by using the conventional continuous-time to

¹A version of this chapter has been published. Fuller and Nowrouzian 1998. Canadian Journal of Electrical and Computer Engineering. 23: 155-162.

discrete-time bilinear frequency transformation

$$s = \frac{2}{T} \frac{z - 1}{z + 1}, \quad (2.1)$$

where z represents the discrete-time complex frequency variable, and where T represents the sampling period. A direct consequence of this approach is that the resulting VA WD equalizers inherit the well known practical features and robustness [17] normally associated with the corresponding WD filter realizations.

To facilitate the design of Bode-type VA WD equalizers, [10–15] the corresponding analog prototype network transfer function $T_v(s)$ is usually realized in terms of a normalized driving-point impedance function $\hat{Z}(s)$ and a normalized variable resistance \hat{R}_{1v} in accordance with

$$T_v(s) = \frac{\hat{Z}(s) - \hat{R}_{1v}}{\hat{Z}(s) + \hat{R}_{1v}}. \quad (2.2)$$

This is achieved by making the substitutions

$$T_s(s) = \frac{\hat{Z}(s) - 1}{\hat{Z}(s) + 1} \quad (2.3)$$

and

$$r_v = \frac{1 + \hat{R}_{1v}}{1 - \hat{R}_{1v}} \quad (2.4)$$

for r_v and $T_s(s)$ in Eqn. 1.10, where $\hat{Z}(s) = Z(s)/R_n$ and $\hat{R}_{1v} = R_{1v}/R_n$, where $Z(s)$ is a suitable impedance function, where R_n is a normalizing resistor, and where R_{1v} is a resistor varying from $-R_n$ (via 0) to R_n .²

The proposed Bode-type VA WD equalizer design technique makes use of the analog prototype network shown in Fig. 2.1, where $\hat{Z}(s)$ and \hat{R}_{1v} can

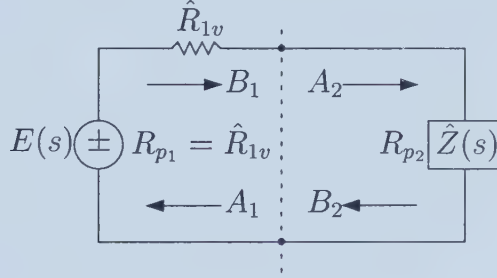


Figure 2.1: Analog prototype network for WD realization of $T_v(s)$

be obtained from Eqns. 2.3 and 2.4 in terms of the given shaping transfer function $T_s(s)$ and the variable resistance r_v as

$$\hat{Z}(s) = \frac{1 + T_s(s)}{1 - T_s(s)}, \quad (2.5)$$

²Equivalently, the normalized resistance \hat{R}_{1v} varies from -1 via 0 to 1 .

and

$$\hat{R}_{1v} = \frac{r_v - 1}{r_v + 1}. \quad (2.6)$$

The reflected wave B_1 in the prototype reference filter in Fig. 2.1 is independent of the incident wave A_1 in accordance with

$$B_1 = E(s), \quad (2.7)$$

but the reflected wave B_2 is related to the incident wave A_2 in accordance with

$$B_2 = \frac{\hat{Z}(s) - R_{p_2}}{\hat{Z}(s) + R_{p_2}} A_2, \quad (2.8)$$

where R_{p_1} and R_{p_2} are appropriate port resistances. Similarly, the incident wave A_2 is related to the reflected wave B_1 in accordance with

$$A_2 = B_1. \quad (2.9)$$

Then, from Eqns. 2.7, 2.8 and 2.9, one has

$$\frac{B_2}{E(s)} = \frac{\hat{Z}(s) - R_{p_2}}{\hat{Z}(s) + R_{p_2}}. \quad (2.10)$$

In this way, the variable transfer function $T_v(s)$ in Eqn. 2.2 can be realized as the reflectance of $\hat{Z}(s)$ with respect to \hat{R}_{1v} in the prototype network in Fig. 2.1 (via Eqn. 2.10).

If the desired Bode-type VA WD equalizer is realized directly from the analog prototype network of Fig. 2.1 by using the existing techniques, i.e. if R_{p2} is set to R_{p1} , then the values of *all* digital multipliers in the corresponding WD equalizer *realization* of $\hat{Z}(s)$ become dependent on the value of the variable resistance \hat{R}_{1v} . This renders the resulting VA WD equalizers impractical as they would require changes in more than one digital multiplier in order to implement a single change in the value of \hat{R}_{1v} .

In [18], the above problem was resolved by inserting a two-port parallel interconnection at the dotted intersection in the prototype network in Fig. 2.1 prior to the WD realization, making it possible to set the port resistance R_{p2} independently of the port resistance R_{p1} . This in turn isolates the digital multipliers constituent in the WD realization of $\hat{Z}(s)$ from \hat{R}_{1v} without any increase in the total number of multipliers required. This technique is exploited in and applied to the design of first-order fan and second-order bump Bode-type VA WD equalizers, permitting the desired magnitude-frequency response equalization through the use of a single variable digital multiplier *only*.

The design of first-order fan Bode-Type VA WD Equalizers is discussed in

Section 2.1. The resulting VA WD equalizers require two digital multipliers, one of which can be used independently for adjusting the fan height of the equalizer magnitude-frequency response. The design of the corresponding second-order bump Bode-type VA WD equalizers is discussed in Section 2.2. These equalizers require three digital multipliers, one of which can again be used for the independent adjustment of the bump height of the equalizer magnitude-frequency response. Finally, in Section 2.4, two examples are given to illustrate the design of fan and bump VA WD equalizers and their magnitude-frequency response characteristics.

2.1 Design of First-Order Fan Bode-Type Variable-Amplitude Wave-Digital Equal- izers

The continuous-time shaping transfer function $T_s(s)$ for the design of a first-order fan Bode-type VA WD equalizer is of the form [13]

$$T_s(s) = \frac{s + \omega_0}{b_1 s + b_0}, \quad (2.11)$$

where the coefficients b_1 and b_0 are as given in Table 2.1, and where $\omega_0 > 0$

Table 2.1: Definition of b_1 and b_0 for fan equalizers

Coefficient	Equalizer Type	
	Low-Pass	High-Pass
b_1	1	h
b_0	$h\omega_0$	ω_0

is the cut-off frequency and $h > 1$ is the maximum height of the fan-shaped equalizer magnitude-frequency response.

By substituting Eqn. 2.11 into Eqn. 2.5, the normalized impedance function $\hat{Z}(s)$ is obtained in the form

$$\hat{Z}(s) = \frac{R_x}{R_n} s^\lambda + \frac{R_{2f}}{R_n}, \quad (2.12)$$

where

$$\hat{R}_{2f} = \frac{R_{2f}}{R_n} = \frac{h+1}{h-1} \quad (2.13)$$

is a normalized resistance, and $\frac{R_x}{R_n} s^\lambda$ is a normalized inductive or capacitive impedance as given in Table 2.2 for low-pass and high-pass VA WD equalizers, respectively. By using Eqn. 2.12, the network in Fig. 2.1 can be

Table 2.2: Definition of impedance $\frac{R_x}{R_n} s^\lambda$ for fan equalizers

Parameter	Equalizer Type	
	Low-Pass	High-Pass
$\frac{R_x}{R_n}$	$\frac{2}{(h-1)\omega_0}$	$\frac{2\omega_0}{h-1}$
λ	1	-1

represented as shown in Fig. 2.2.

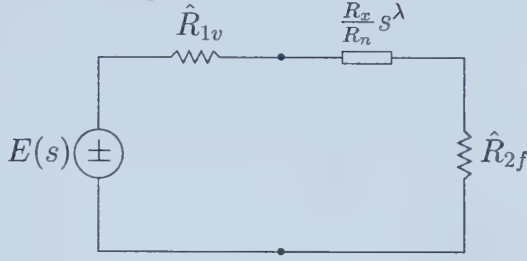


Figure 2.2: Analog prototype network for first-order fan VA WD equalizers

In order to arrive at the desired WD realization, the network in Fig. 2.2 is replaced by that shown in Fig. 2.3 through the incorporation of a two-port parallel and a three-port series wire interconnection (as indicated by dashed lines). The former wire interconnection has the important practical feature of

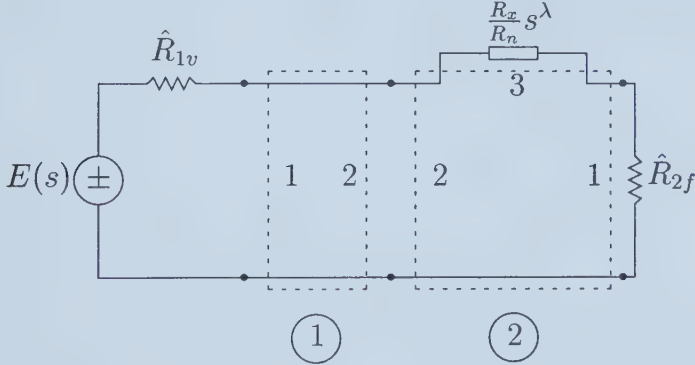


Figure 2.3: Identification of interconnections for the first-order fan VA WD equalizer realization

making the resulting WD equalizers adjustable with respect to \hat{R}_{1v} without increasing the total number of digital multipliers required for the realization.

Consider the i^{th} interconnection in the network in Fig. 2.3 (for $i = 1, 2$), and represent the resistance associated with its j^{th} port (for $j = 1, 2, 3$) by R_{ij} . Then, the port resistances R_{ij} can be assigned as follows.

Interconnection ②:

$$R_{21} = \hat{R}_{2f}; R_{23} = \left(\frac{2}{T}\right)^\lambda \frac{R_x}{R_n}; \text{ and } R_{22} = R_{21} + R_{23}. \quad (2.14)$$

Interconnection ①:

$$R_{11} = \hat{R}_{1v}; \text{ and } R_{12} = R_{22}. \quad (2.15)$$

Subsequently, the WD realization of the network in Fig. 2.3 can be obtained as shown in Fig. 2.4. The two-pair parallel adaptor in this realization is as

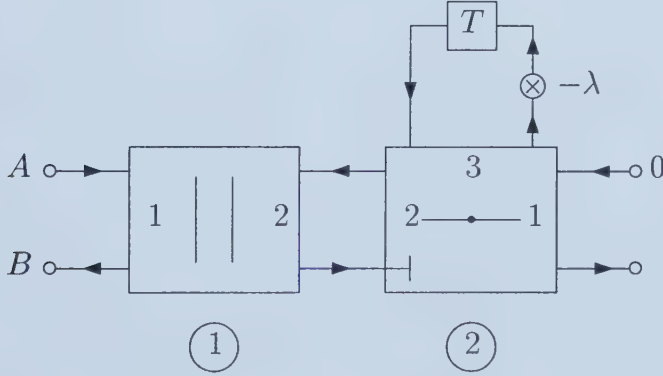


Figure 2.4: First-order fan Bode-type VA WD equalizer realization

shown in Fig. 2.5, where the value of the digital multiplier α_1 is given by

$$\alpha_1 = \frac{R_{11} - R_{12}}{R_{11} + R_{12}}. \quad (2.16)$$

Similarly, the constituent three-pair series adaptor is as shown in Fig. 2.6

where the value of the digital multiplier α_2 is given by

$$\alpha_2 = \frac{R_{21}}{R_{22}}. \quad (2.17)$$

From Table 2.2 and Eqns. 2.13-2.17, one obtains the values for the multipliers

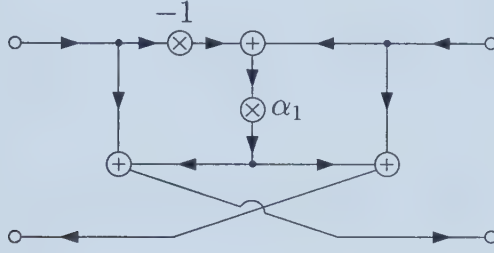


Figure 2.5: Two-pair parallel adaptor realization

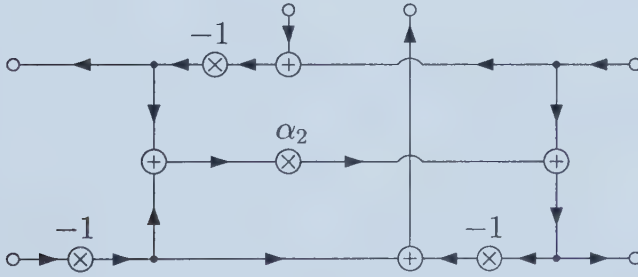


Figure 2.6: Three-pair series adaptor realization

α_1 and α_2 as given in Table 2.3.

There are two main parameters involved in the design of the first-order fan Bode-type VA WD equalizers, namely, the cut-off frequency ω_0 and the resistance \hat{R}_{1v} . By inspection of Table 2.3, it can be seen that the value of multiplier α_1 depends on both the frequency ω_0 and the variable \hat{R}_{1v} , but

Table 2.3: Multipliers α_1 and α_2 for first-order fan VA WD equalizers

Parameter	Equalizer Type	
	Low-Pass	High-Pass
α_1	$\frac{\hat{R}_{1v} - \frac{h+1}{h-1} - \frac{4}{(h-1)\omega_0 T}}{\hat{R}_{1v} + \frac{h+1}{h-1} + \frac{4}{(h-1)\omega_0 T}}$	$\frac{\hat{R}_{1v} - \frac{h+1}{h-1} - \frac{\omega_0 T}{h-1}}{\hat{R}_{1v} + \frac{h+1}{h-1} + \frac{\omega_0 T}{h-1}}$
α_2	$\frac{\frac{h+1}{h-1}}{\frac{h+1}{h-1} + \frac{4}{(h-1)\omega_0 T}}$	$\frac{\frac{h+1}{h-1}}{\frac{h+1}{h-1} + \frac{\omega_0 T}{(h-1)}}$

that the value of the multiplier α_2 depends on ω_0 *only*. Therefore, once the value of ω_0 has been fixed, the value of the multiplier α_2 becomes fixed. Then, the desired variations in \hat{R}_{1v} can be achieved by adjusting the value of the multiplier α_1 appropriately. This implies that the equalizer becomes adjustable with respect to \hat{R}_{1v} .

In some situations, it may be desirable to vary not only the variable resistance \hat{R}_{1v} , but also the cut-off frequency ω_0 . To achieve this, one can fix the value of the multiplier α_2 first, and then proceed to adjust the value of the multiplier α_1 .

2.2 Design of Second-Order Bump Bode-Type Variable-Amplitude Wave-Digital Equal- izers

For the design of second-order bump Bode-type VA WD equalizers, the continuous-time shaping transfer function $T_s(s)$ is chosen as [13]

$$T_s(s) = \frac{s^2 + \frac{\omega_p}{Q_p}s + w_p^2}{s^2 + h\frac{\omega_p}{Q_p}s + w_p^2}, \quad (2.18)$$

where the center frequency $\omega_p > 0$, the quality factor $Q_p > 0$, and the bump height h are design parameters. The substitution of Eqn. 2.18 into Eqn. 2.5 yields a normalized impedance function $\hat{Z}(s)$ of the form

$$\hat{Z}(s) = \frac{L_b}{R_n}s + \frac{1}{R_n C_b s} + \frac{R_{2b}}{R_n}. \quad (2.19)$$

Here,

$$\hat{L}_b = \frac{L_b}{R_n} = \frac{2Q_p}{(h-1)\omega_p} \quad (2.20)$$

is a normalized inductance,

$$\hat{C}_b = C_b R_n = \frac{(h-1)}{2\omega_p Q_p} \quad (2.21)$$

is a normalized capacitance, and

$$\hat{R}_{2b} = \frac{R_{2b}}{R_n} = \frac{h+1}{h-1} \quad (2.22)$$

is a normalized resistance. Then, the network in Fig. 2.1 can be represented as shown in Fig. 2.7. The WD realization of the network in Fig. 2.7 can be

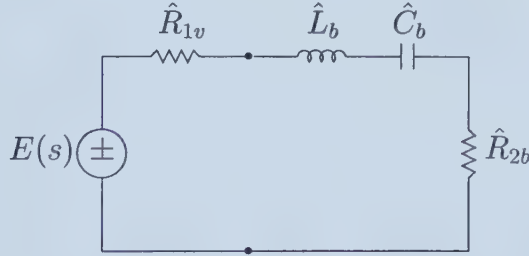


Figure 2.7: Analog prototype network for the second-order bump VA WD equalizers

achieved by following a procedure similar to that in the previous section. The resulting WD equalizer would then consist of one two-pair parallel adaptor and two three-pair series adaptors.

An alternative approach is adopted in the following, which is based on the use of two-pair unit-elements to realize the series connected inductor and capacitor in Figure 2.7 [19]. This leads to a reduction in the total number

of required adders by one and inverters by two without increasing the total number of required multipliers.

To arrive at the desired WD realization, the network in Fig. 2.7 is replaced by the network in Fig. 2.8 by substituting a capacitively-terminated unit-element for the series connected inductor and capacitor, and by incorporating the indicated two-port parallel and three-port series wire interconnections. As before, the use of the two-port parallel interconnection ① has the

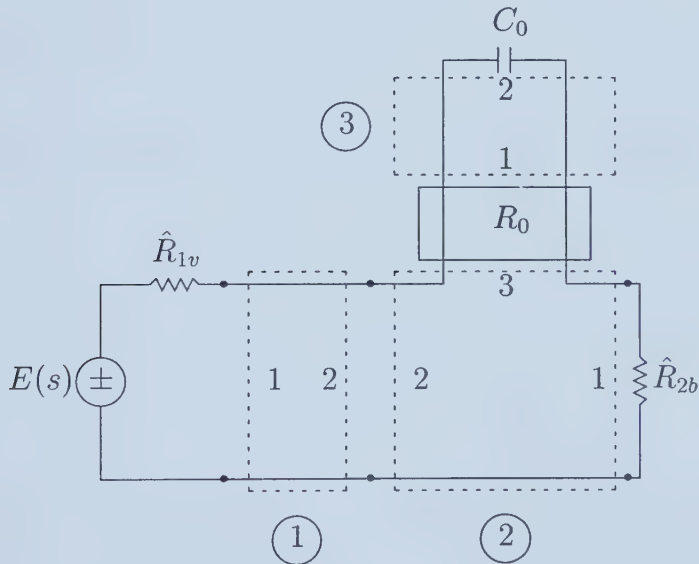


Figure 2.8: Identification of connections for the second-order bump VA WD equalizer realization

advantage of making the resulting WD realizations adjustable with respect to \hat{R}_{1v} without increasing the total number of digital multipliers required for the realization.

The characteristic impedance associated with the above unit-element is

given by

$$R_0 = \frac{4\hat{L}_b\hat{C}_b + T^2}{2T\hat{C}_b} \quad (2.23)$$

and the capacitor C_0 is obtained as

$$C_0 = \frac{4\hat{L}_b\hat{C}_b^2}{4\hat{L}_b\hat{C}_b + T^2}. \quad (2.24)$$

Then, the WD realization of the network in Fig. 2.8 can be obtained as shown in Fig. 2.9. By using Eqns. 2.19-2.22, the value of the digital multiplier for

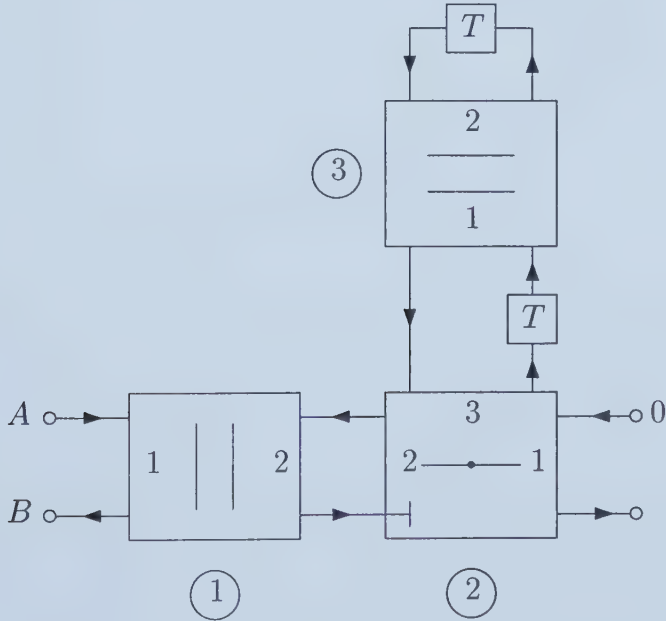


Figure 2.9: Second-order bump VA WD equalizer realization

two-port parallel adaptor ① is given by

$$\alpha_1 = \frac{\hat{R}_{1v} - \frac{h+1}{h-1} - \frac{Q_p(4+T^2\omega_p^2)}{T(h-1)\omega_p}}{\hat{R}_{1v} + \frac{h+1}{h-1} + \frac{Q_p(4+T^2\omega_p^2)}{T(h-1)\omega_p}}, \quad (2.25)$$

the value of the digital multiplier for the three-port series adaptor ② is given by

$$\alpha_2 = \frac{\frac{h+1}{h-1}}{\frac{h+1}{h-1} + \frac{Q_p(4+T^2\omega_p^2)}{T(h-1)\omega_p}}, \quad (2.26)$$

and the value of the multiplier for the two-port parallel adaptor ③ is given by

$$\alpha_3 = \frac{4 - T^2\omega_p^2}{4 + T^2\omega_p^2}. \quad (2.27)$$

By inspection of the digital multipliers α_1 , α_2 , and α_3 as given in Eqns. 2.25-2.27, it can be seen that multiplier α_1 is a function of the variable resistor \hat{R}_{1v} , but that the multipliers α_2 and α_3 are independent of the resistor \hat{R}_{1v} . Thus, the desired variations in \hat{R}_{1v} can be completely achieved directly through the variation of the value of the digital multiplier α_1 . This makes the equalizer adjustable with respect to \hat{R}_{1v} .

2.3 BIBO Stability of Bode-Type Variable-Amplitude Wave-Digital Equalizers

This section is concerned with the bounded-input bounded-output (BIBO) stability analysis of the above Bode-type VA WD equalizers under the following assumptions: (a) It is assumed that the VA WD equalizer operates under infinite-precision arithmetic, rendering the WD equalizer as linear, and, consequently, free from such finite-precision arithmetic effects as overflow saturation and limit cycle oscillations. (b) It is further assumed that the VA WD equalizer operates under “static” operating conditions. This implies that the variations of the variable digital multiplier occur slowly or only after the transients resulting from the “dynamic” variations of the variable multiplier have died out to negligible levels, allowing the WD equalizer to be considered essentially as shift-invariant.

Under the above conditions, it suffices to ensure the Bode-type VA WD equalizer is BIBO stable³ for all possible values of the variable multiplier α_1 . The investigation of BIBO stability can be carried out indirectly through the analysis of the analog prototype network in Fig. 2.1, or directly through the analysis of the corresponding VA WD equalizer. However, the BIBO

³Of course, when considering the stability features of an actual hardware implementation, one must take into account not only finite-precision arithmetic effects, but also “dynamic” changes in the variable multiplier. Discussions of these topics will be left to subsequent chapters.

stability of the prototype network is made complicated by the fact that the constituent variable resistance \hat{R}_{1v} may take on negative as well as positive values. Therefore, it is proposed to establish the BIBO stability directly by considering the WD equalizer proper.

As discussed in Section 2.1 and Section 2.2, the variation of the magnitude-frequency response of the Bode-type VA WD equalizers is controlled by the value of \hat{R}_{1v} , or, equivalently, by the value of the variable multiplier α_1 . However, as seen in Table 2.3 and Eqn. 2.25, α_1 is also a function of the values of the parameters Q , ω , h . Therefore, α_1 is confined to a fixed range of values. In the following subsections, it will be shown that the BIBO stability of the proposed VA WD equalizers is guaranteed for all in-range values of α_1 .

2.3.1 BIBO Stability of First-Order Fan WD Equalizers

In order to establish the BIBO stability of the first-order fan WD equalizers, consider the characteristic equation

$$Q(z) = z + c_0 \tag{2.28}$$

associated with the realization given in Fig. 2.4, where the coefficient c_0 is given by

$$c_0 = \pm(\alpha_1 - \alpha_1\alpha_2 + \alpha_2), \quad (2.29)$$

and where the upper sign in Eqn. 2.29 corresponds to lowpass fan equalizers and the lower sign corresponds to highpass fan equalizers.

For BIBO stability, the inequality

$$|c_0| < 1 \quad (2.30)$$

must hold for all possible α_1 and α_2 values, so that the root of Eqn. 2.28 lies strictly inside the unit-circle. But, Eqn. 2.30 is satisfied if and only if

$$\alpha_1 < 1 \quad (2.31a)$$

$$\alpha_1 > \frac{\alpha_2 + 1}{\alpha_2 - 1}, \quad (2.31b)$$

for all possible values of \hat{R}_{1v} .

In accordance with the definition of α_1 (c.f. row 1 of Table 2.3) and in accordance with the facts that $h > 1$ and $\omega_0 > 0$, one has

$$\alpha_1 < 0, \quad (2.32)$$

implying that Eqn. 2.31a is satisfied automatically. Furthermore, from the definitions of α_1 and α_2 as given in Table 2.3, it can be seen that they are of the general form

$$\alpha_1 = \frac{\hat{R}_{1v} - X - Y}{\hat{R}_{1v} + X + Y} \quad (2.33)$$

and

$$\alpha_2 = \frac{X}{X + Y}, \quad (2.34)$$

where X and Y are constants as given in Table 2.4. For $h > 1$ and $\omega_0 > 0$,

Table 2.4: Definition of X and Y for fan WD equalizers

Equalizer Type	X	Y
<i>Lowpass</i>	$\frac{h+1}{h-1}$	$\frac{4}{(h-1)\omega_0 T}$
<i>Highpass</i>	$\frac{h+1}{h-1}$	$\frac{\omega_0 T}{(h-1)}$

the variables X and Y will be constrained by the inequalities $X > 1$ and $Y > 0$. Then, from Eqn. 2.33 the minimum (most negative) value of α_1 occurs when $\hat{R}_{1v} = -1$. Thus, the condition in Eqn. 2.31b reduces to

$$-\frac{2X + Y}{Y} < \frac{1 + X + Y}{1 - X - Y} \quad (2.35)$$

or, equivalently, to

$$0 < (X + Y)(X - 1). \quad (2.36)$$

But, since $X > 1$ and $Y > 0$, Eqn. 2.36 will also be satisfied automatically.

In conclusion, Eqn. 2.31a and Eqn. 2.31b have been shown to be satisfied automatically, establishing the BIBO stability of the first-order fan WD equalizers for the entire range of α_1 values.

2.3.2 BIBO Stability of Second-Order Bump WD Equalizers

The characteristic equation for second-order bump WD equalizers is given by

$$Q(z) = z^2 + c_1z + c_0, \quad (2.37)$$

where the coefficients c_1 and c_0 are obtained from the realization given in Fig. 2.9 as

$$c_1 = -\alpha_1\alpha_2\alpha_3 + \alpha_1\alpha_3 + \alpha_2\alpha_3 - \alpha_3, \quad (2.38)$$

$$c_0 = -\alpha_1 + \alpha_1\alpha_2 - \alpha_2. \quad (2.39)$$

For BIBO stability, the inequalities

$$Q(1) > 0, \quad (2.40)$$

$$Q(-1) > 0, \quad (2.41)$$

$$|c_0| < 1, \quad (2.42)$$

must hold, so that the roots of Eqn. 2.37 lie strictly inside the unit-circle [20].

By applying Eqns. 2.38 and 2.39 to Eqn. 2.37, and by invoking the result in Eqn. 2.40 one obtains

$$(\alpha_2 - 1)(\alpha_3 - 1)(1 - \alpha_1) > 0. \quad (2.43)$$

By recalling the fact that $Q_p > 0$, $h > 1$, and $w_p > 0$, it is observed that α_1 , α_2 , and α_3 satisfy the following constraints

$$0 < \alpha_2 < 1, \quad (2.44)$$

$$-1 < \alpha_3 < 1, \quad (2.45)$$

$$\alpha_1 < 0. \quad (2.46)$$

By inspection of the inequality in Eqn. 2.43, and by taking into account Eqns. 2.44-2.46, it is observed that Eqn. 2.40 is satisfied automatically for

all possible values of α_1 , α_2 , and α_3 . Next, by substituting Eqns. 2.38 and 2.39 into Eqn. 2.37, and by invoking the result in Eqn. 2.41 one obtains

$$(\alpha_3 + 1)(1 - \alpha_2)(1 - \alpha_1) > 0 \quad (2.47)$$

Once again, by taking into account Eqns. 2.44-2.46, it is observed that Eqn. 2.41 will be satisfied for all possible α_1 , α_2 , and α_3 values. Finally, by applying Eqn. 2.39 to Eqn. 2.42 one obtains

$$| -\alpha_1 + \alpha_1\alpha_2 - \alpha_2 | < 1 \quad (2.48)$$

After some manipulations, the remaining condition for BIBO stability is obtained as

$$\frac{\alpha_2 + 1}{\alpha_2 - 1} < \alpha_1 < 1, \quad (2.49)$$

which is identical to that obtained for first-order fan equalizers as given in Eqn. 2.31a and Eqn. 2.31b. By comparing the general form of α_1 and α_2 for second-order bump VA WD equalizers in Eqns. 2.25 and 2.26 to that of first-order fan WD equalizers in Eqns. 2.33 and 2.34, it is observed that they share a common form. As it has already been established that this condition is satisfied for all possible α_1 and α_2 values for the fan digital equalizer,

the resulting bump WD equalizers are similarly BIBO stable over the entire in-range values of α_1 .

2.4 Application Examples

In this section, two examples are provided to illustrate the design of first-order fan and second-order bump Bode-type VA WD equalizers, followed by a brief discussion of the results.

As a first example, consider the design of first-order high-pass and low-pass fan Bode-type VA WD equalizers satisfying the specifications given in Table 2.5. Note that for a desired digital frequency Ω_0 , the corresponding analog frequency variable ω_0 is obtained in accordance with

$$\omega_0 = \frac{2}{T} \tan \frac{\Omega_0 T}{2}. \quad (2.50)$$

Table 2.5: Design specification for the first-order lowpass and highpass fan equalizers

Parameter	Value
<i>Fan Height</i>	$h = 5$ (14 dB)
<i>Sampling Period</i>	$T = \frac{1}{32000} s$
<i>Normalized Digital Cut-off Freq.</i>	$\frac{\Omega_0 T}{\pi} = 0.25$
<i>Pre-warped Analog Cut-off Freq.</i>	$\omega_0 = 2.6510 \times 10^4 \text{ rad.}$

The values of the multipliers α_1 and α_2 for five different values of the vari-

able resistor \hat{R}_{1v} are tabulated in Table 2.6 for a lowpass fan equalizer and in Table 2.7 for a highpass fan equalizer. Note that the variations in the variable resistor \hat{R}_{1v} are completely contained in the value of the multiplier α_1 . Therefore, once the values of \hat{R}_{1v} have been chosen, the value of the multiplier α_1 in the realization of the equalizers can be selected accordingly to produce the desired magnitude-frequency response. The resulting magnitude-frequency responses for the WD realizations are shown in Figs. 2.10 and 2.11 for lowpass and highpass equalizers, respectively.

Table 2.6: Multiplier values for the first-order lowpass fan equalizer

\hat{R}_{1v}	α_1
1.0	-4.604957×10^{-1}
0.5	-6.881925×10^{-1}
0.0	-1.0
-0.5	-1.453082
-1.0	-2.171573
$\alpha_2 = 5.540971 \times 10^{-1}$	

Table 2.7: Multiplier values for the first-order highpass fan equalizer

\hat{R}_{1v}	α_1
1.0	-2.612039×10^{-1}
0.5	-5.469182×10^{-1}
0.0	-1.0
-0.5	-1.828427
-1.0	-3.828427
$\alpha_2 = 8.786796 \times 10^{-1}$	

As a second example, consider the design of a second-order bump Bode-

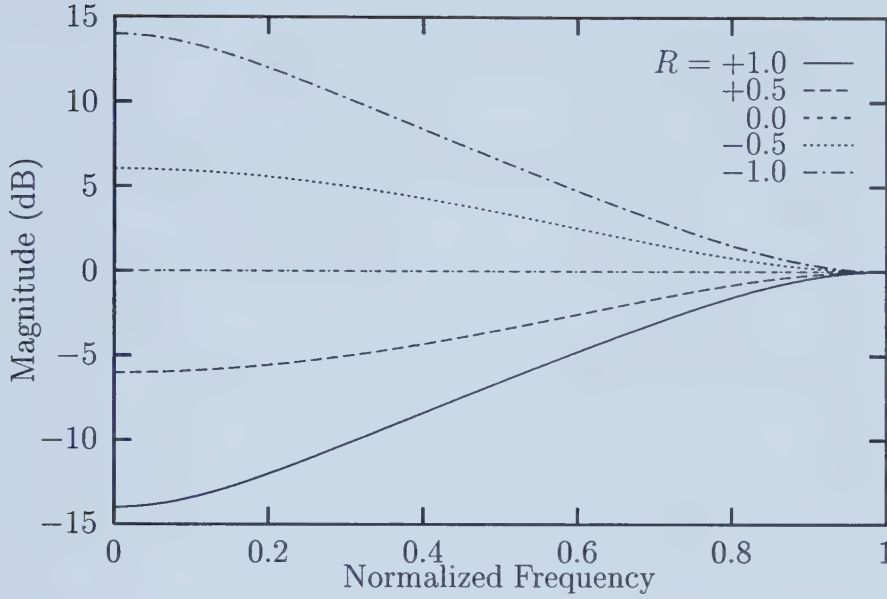


Figure 2.10: Magnitude-frequency response characteristics for the first-order lowpass fan equalizer

type VA WD equalizer satisfying the specifications in Table 2.8. The values

Table 2.8: Design specification for the second-order bump equalizer

Parameter	Value
<i>Bump Height</i>	$h = 5$ (14 dB)
<i>Quality Factor</i>	$Q_p = 2.5$
<i>Sampling Period</i>	$T = \frac{1}{32000} s$
<i>Normalized Digital Center Freq.</i>	$\frac{\Omega_0 T}{\pi} = 0.4$
<i>Pre-warped Analog Center Freq.</i>	$\omega_p = 4.6499 \times 10^4 \text{ rad.}$

of the multipliers α_1 , α_2 , and α_3 are tabulated in Table 2.9 using the same set of values for the variable \hat{R}_{1v} as in the previous example. The corresponding magnitude responses for the above WD realization are shown in Fig. 2.12.

It is interesting to note that in the above fan or bump Bode-type VA WD equalizers, although the value of α_1 varies with \hat{R}_{1v} , the values of α_2

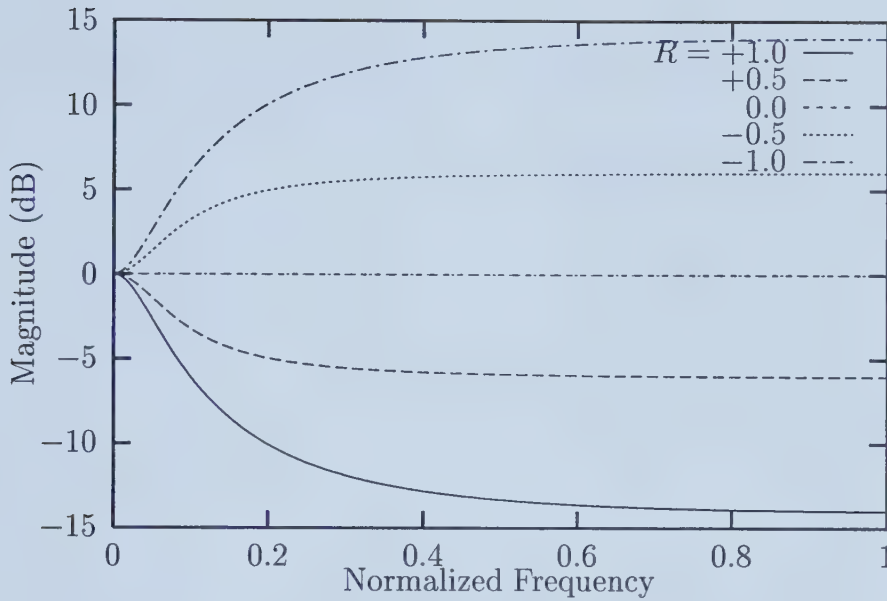


Figure 2.11: Magnitude-frequency response characteristics for the first-order highpass equalizer

and α_3 remain constant. Furthermore, it is interesting to note that the arithmetic variations (around 0) in \hat{R}_{1v} cause geometric variations (around 1) in α_1 . Finally, it is interesting to note that these responses are arithmetically symmetric (around 0 dB) for geometrically symmetric α_1 values. Therefore, not only does the digital multiplier α_1 provide independent adjustments of the magnitude-frequency responses of the proposed VA WD equalizers, but also the resulting variations in the magnitude-frequency response are mirror images of each other about 0 dB (c.f. Figs. 2.10, 2.11, and 2.12). The latter is the most outstanding practical feature of Bode-type VA equalizers (analog or digital), and is otherwise very difficult (if not impossible) to secure by using other types of variable-amplitude digital equalizers.

Table 2.9: Multiplier values for the second-order bump equalizer

$\hat{\mathbf{R}}_{1v}$	α_1
1.0	-6.100343×10^{-1}
0.5	-7.839545×10^{-1}
0.0	-1.0
-0.5	-1.275584
-1.0	-1.639252
$\alpha_2 = 3.633144 \times 10^{-1}$	
$\alpha_3 = 3.090170 \times 10^{-1}$	

2.5 Conclusions

This chapter has presented a synthesis technique for the design of first- and second-order Bode-type VA WD equalizers. The proposed first-order equalizer consists of one unit-delay and two digital multipliers and produces a fan-shaped magnitude-frequency response, while the proposed second-order equalizer consists of two unit-delays and three digital multipliers and produces a bump-shaped magnitude-frequency response. The salient feature of the resulting WD equalizers is that only one single variable digital multiplier is required to control the fan amplitude in the first-order equalizer and the bump amplitude in the second-order equalizer without changing their other important magnitude-frequency response characteristics (e.g. the cut-off frequency in the fan equalizer and the center frequency and quality factor in the bump equalizer). Moreover, these equalizers remain BIBO stable (under infinite-precision arithmetic) for all possible values of the variable multiplier.

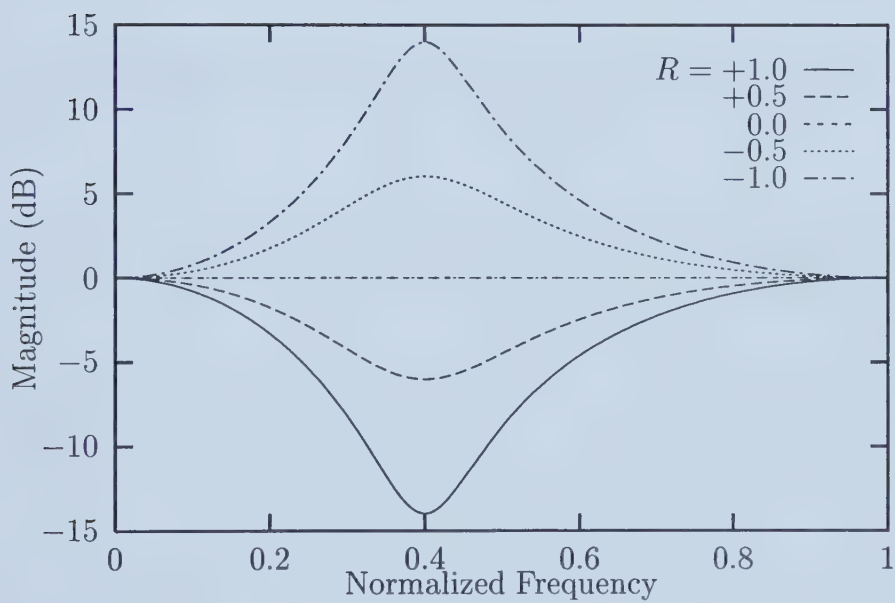


Figure 2.12: Magnitude-frequency response characteristics for the second-order bump equalizer

Chapter 3

Realizability Conditions for Bode-Type Variable-Amplitude Digital Equalizers

In the previous chapter, Bode-type variable-amplitude (VA) digital equalizers were designed based on a corresponding analog prototype VA equalizer. This chapter presents a novel approach to the direct discrete-time z -domain design [23] and enumeration [24–26] of Bode-type VA digital equalizers. The salient features of the proposed approach are threefold: (1) it does not make any recourse to the concept of a continuous-time s -domain prototype analog network or its transfer function, (2) it ensures that the frequency response of the resulting VA digital equalizers can be varied from that of an shaping

transfer function, to its inverse for arbitrary shaping transfer functions, and, (3) it only requires a single variable digital multiplier (of course, in addition to the required usual fixed digital multipliers).

A set of three realizability conditions is developed for the design of the above Bode-type VA digital equalizers. In the case of the corresponding second-order Bode-type VA digital equalizers, these realizability conditions are supplemented through the development of a corresponding BIBO stability condition. The results thus obtained are then applied to the design and enumeration of two classes of second-order bump VA digital equalizers, one class including digital equalizers operating under infinite-precision arithmetic and the other including digital equalizers operating under finite-precision arithmetic operations.

3.1 Background

The transfer function of a Bode-type VA digital equalizer is of the general form

$$T_v(z) = \frac{1 + xT_s(z)}{x + T_s(z)}, \quad (3.1)$$

where z represents the discrete-time complex frequency variable, and where x represents a variable digital multiplier.

For a full scale symmetrical variation of the logarithmic magnitude-frequency response $\ln |T_v(e^{j\omega})|$ associated with the transfer function $T_v(z)$ from $\ln |T_s(e^{j\omega})|$ to $-\ln |T_s(e^{j\omega})|$, it is required to vary the value of digital multiplier x from 0 to $+\infty$, or equivalently from 0 to $-\infty$, where ω represents the discrete-time real frequency variable. However, in the practical design of Bode-type VA digital equalizers, it may be desirable to confine the variation of the variable multiplier x to a specified limited range of values. This can be achieved by replacing the multiplier x by a generic multiplier v in accordance with the bilinear variable transformation

$$x = \frac{(V_I - v)(V_o - V_F)}{(v - V_F)(V_I - V_o)}, \quad (3.2)$$

where V_I , V_o , and V_F are design parameters that define the range of values for the variable multiplier v variations. Then, the variation of v from V_I (via V_o) to V_F , results in the variation of x from 0 (via 1) to ∞ . By substituting for x from Eqn. 3.2 into Eqn. 3.1, and by simplifying the result, one obtains¹

$$T_v(z) = \frac{\frac{V_I(V_o - V_F)T_s(z) + V_F(V_o - V_I)}{(V_I - V_o)T_s(z) + (V_F - V_o)} + \frac{(V_F - V_o)T_s(z) + (V_I - V_o)}{(V_I - V_o)T_s(z) + (V_F - V_o)}v}{v + \frac{V_F(V_o - V_I)T_s(z) + V_I(V_o - V_F)}{(V_I - V_o)T_s(z) + (V_F - V_o)}}. \quad (3.3)$$

In this way, by varying the value of the digital multiplier v from V_I (via V_o)

¹Note that the majority of the equations in this thesis have been developed and/or verified using Maple Release V.

to V_F , the transfer function $T_v(z)$ varies from $T_s^{-1}(z)$ (via 1) to $T_s(z)$, as desired.

By performing a power series expansion of the logarithm of $T_v(e^{j\omega})$ given in Eqn. 3.3, and by applying the real part operator to the result, one obtains

$$\begin{aligned} \ln |T_v(e^{j\omega})| = & f(v) \ln |T_s(e^{j\omega})| + f_3(v) \Re\{\ln^3 T_s(e^{j\omega})\} \\ & + f_5(v) \Re\{\ln^5 T_s(e^{j\omega})\} + \dots, \end{aligned} \quad (3.4)$$

where

$$f(v) = \frac{V_o(V_I - V_F) + v(V_F - V_I)}{V_I(V_o - 2V_F + v) + V_o(V_F - 2v) + vV_F}. \quad (3.5)$$

By inspection of Eqn. 3.4, it can be seen that Eqn. 3.3 generates not only the term $f(v) \ln |T_s(e^{j\omega})|$ as required in the ideal magnitude-frequency response characteristic given in Eqn. 1.6, but also additional terms that may be considered as approximation error terms. These error terms are functions of the magnitude-frequency and phase-frequency responses associated with $T_s(e^{j\omega})$ as well as being functions of the value of the multiplier v .

3.2 Realizability Conditions for Bode-Type Variable-Amplitude Digital Equalizers

The transfer function $T_v(z)$ of a Bode-type VA digital equalizer can be realized as the transfer function $T_v(z) = \frac{Y(z)}{X(z)}$ of the network N shown in Figure 3.1, where $X(z)$ and $Y(z)$ represent the input and output signals associated with N , respectively. In order to facilitate the realization of the VA digital equalizer, the variable digital multiplier v is extracted from the network N to define the network N_1 as indicated in Figure 3.1. Here, $X_v(z)$ and $Y_v(z)$ represent the input and output signals associated with the multiplier v , respectively.

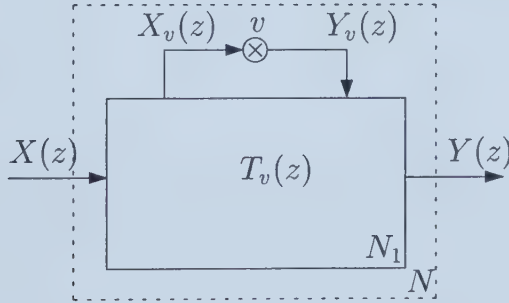


Figure 3.1: Schematic diagram representing a Bode-type VA digital equalizer

The network N_1 in Figure 3.1 can be characterized in terms of its transfer matrix representation in accordance with

$$\begin{bmatrix} Y(z) \\ X_v(z) \end{bmatrix} = \begin{bmatrix} t_{11}(z) & t_{12}(z) \\ t_{21}(z) & t_{22}(z) \end{bmatrix} \begin{bmatrix} X(z) \\ Y_v(z) \end{bmatrix}, \quad (3.6)$$

where the parameters $t_{ij}(z)$ ($i, j = 1, 2$) are elements of the transfer matrix.

In addition,

$$Y_v(z) = vX_v(z). \quad (3.7)$$

In this way, by invoking Eqn. 3.7 in Eqn. 3.6, and by manipulating the result, one can obtain the transfer function $T_v(z)$ in the form

$$T_v(z) = \frac{-\frac{t_{11}(z)}{t_{22}(z)} + \frac{t_{11}(z)t_{22}(z) - t_{12}(z)t_{21}(z)}{t_{22}(z)}v}{v - \frac{1}{t_{22}(z)}}. \quad (3.8)$$

By matching the general form of the transfer function $T_v(z)$ as given in Eqn. 3.8 to the actual form as given in Eqn. 3.3, one arrives at the following three design equations

$$\frac{(V_F - V_o)T_s(z) + (V_I - V_o)}{(V_I - V_o)T_s(z) + (V_F - V_o)} = \frac{t_{11}(z)t_{22}(z) - t_{12}(z)t_{21}(z)}{t_{22}(z)}, \quad (3.9)$$

$$\frac{(V_IV_o - V_IV_F)T_s(z) + (V_FV_o - V_IV_F)}{(V_I - V_o)T_s(z) + (V_F - V_o)} = \frac{-t_{11}(z)}{t_{22}(z)}, \quad (3.10)$$

$$\frac{(V_FV_o - V_FV_I)T_s(z) + (V_IV_o - V_IV_F)}{(V_I - V_o)T_s(z) + (V_F - V_o)} = \frac{-1}{t_{22}(z)}. \quad (3.11)$$

Through inspection of Eqn. 3.11, it is observed that $t_{22}(z)$ can be determined in terms of $T_s(z)$, and vice versa, $T_s(z)$ can be determined in terms of $t_{22}(z)$ in accordance with

$$T_s(z) = \frac{(V_I V_F - V_o V_I)t_{22}(z) + (V_o - V_F)}{(V_F V_o - V_F V_I)t_{22}(z) + (V_I - V_o)}. \quad (3.12)$$

Realizability Condition 1

From Eqn. 3.12, if the shaping transfer function $T_s(z)$ is of order n , then the transfer matrix parameter $t_{22}(z)$ must be also of order n , and of the general form

$$t_{22}(z) = \frac{a_0 + a_1 z^{-1} + a_2 z^{-2} + \dots + a_n z^{-n}}{1 + b_1 z^{-1} + b_2 z^{-2} + \dots + b_n z^{-n}}. \quad (3.13)$$

In accordance with Eqn. 3.6, it can be seen that the parameter $t_{22}(z)$ signifies the signal transmission from the output of the digital multiplier v to its input through the network N_1 . Therefore, it becomes evident that in order to avoid the creation of delay-free loops through the multiplier v , one must also have the following realizability condition

$$a_0 = 0. \quad (\text{R.C. 1})$$

By using Eqn. 3.12, one can eliminate $T_s(z)$ from Eqns. 3.9 and 3.10, result-

ing in the following general realizability conditions for the transfer matrix parameters $t_{ij}(z)$.

Realizability Condition 2

$$t_{11}(z) = \frac{t_{22}(z)(2V_IV_FV_o - V_IV_o^2 - V_FV_o^2) - V_IV_F + V_o^2}{V_IV_o - V_IV_F - V_o^2 + V_FV_o}, \quad (\text{R.C. 2})$$

Realizability Condition 3

$$t_{12}(z)t_{21}(z) = \frac{-t_{22}(z)F_1 - t_{22}(z)^2F_2 + V_I - 2V_o + V_F}{V_IV_o - V_IV_F - V_o^2 + V_FV_o}, \quad (\text{R.C. 3})$$

where

$$\begin{aligned} F_1 &= 2V_IV_F - 2V_o^2, \\ F_2 &= V_o^2V_F - 2V_IV_FV_o + V_IV_o^2. \end{aligned}$$

From realizability conditions R.C. 2 and R.C. 3, it can be seen that the choice of values for V_I , V_o and V_F directly affects the transfer matrix parameters $t_{11}(z)$, $t_{12}(z)$, and $t_{21}(z)$. Ideally, these values are chosen such that

conditions R.C. 2 and R.C. 3 are easily satisfied without the need for fixed digital multipliers or multiple separate realizations of the transfer function $t_{22}(z)$ within the resulting digital equalizer proper. However, choices solely based on these criteria may lead to impractical values for V_I , V_o , and V_F when considering a corresponding hardware implementation of the VA digital equalizer.

3.3 Design of Bode-Type Variable-Amplitude Digital Equalizers

In the practical design of Bode-type VA digital equalizers, the shaping transfer function $T_s(z)$ is usually specified at the outset in the form

$$T_s(z) = \frac{A_0 + A_1 z^{-1} + A_2 z^{-2} + \dots + A_n z^{-n}}{1 + B_1 z^{-1} + B_2 z^{-2} + \dots + B_n z^{-n}}, \quad (3.14)$$

where the coefficients A_i and B_i form the specifications. By substituting the general form of $t_{22}(z)$ from Eqn. 3.13 (subject to the satisfaction of the realizability condition R.C. 1) into Eqn. 3.12, and by comparing the result to Eqn. 3.14, one arrives at the following constraint among the parameters

V_I , V_o , and V_F

$$\frac{V_o - V_F}{V_I - V_o} = A_0. \quad (3.15)$$

From Eqn. 3.15, it can be observed that there is an inter-relationship between the value of the specified coefficient A_0 on the one hand, and the actual values of V_I , V_o , and V_F on the other. Therefore, one must first choose the values of V_I , V_o , and V_F such that Eqn. 3.15 is satisfied. It is interesting to note that in accordance with the realizability conditions R.C. 2 and R.C. 3, the resulting values for V_I , V_o , and V_F may adversely affect the realizability conditions associated with the VA digital equalizer, and, ultimately, the cost of the corresponding hardware implementation of the equalizer²

In accordance with Eqn. 3.11,

$$t_{22}(z) = \frac{(V_I - V_o)T_s(z) + (V_F - V_o)}{(V_F V_I - V_F V_o)T_s(z) + (V_F V_I - V_I V_o)}. \quad (3.16)$$

By substituting for $T_s(z)$ from Eqn. 3.14 in Eqn. 3.16, and by comparing the coefficients of the like powers of z^{-1} in the numerator and denominator of

²Again, in the next chapter, a design technique for general-order Bode-type VA digital equalizers will be presented that bypasses the constraint given by Eqn. 3.15.

the resulting equation to those of $t_{22}(z)$ in Eqn. 3.13, one obtains

$$a_i = \frac{A_i(V_o - V_I) + B_i(V_o - V_F)}{V_F^2 - V_I V_F + V_I V_o - V_o V_F}, \quad (3.17)$$

$$b_i = \frac{A_i(V_F V_o - V_I V_F) + B_i(V_I V_o - V_I V_F)}{V_F^2 - V_I V_F + V_I V_o - V_o V_F}. \quad (3.18)$$

In this way, one can complete the realization of the above VA digital equalizers by using realizability conditions R.C. 2 and R.C. 3 along with equations 3.15, 3.17 and 3.18.

3.4 BIBO Stability Condition for Second-Order Bode-Type Variable-Amplitude Digital Equalizers

In this section, a BIBO stability condition is developed for the special case of second-order VA digital equalizers. The resulting BIBO stability condition provides the range of values for the variable digital multiplier v for which the VA digital equalizer will be BIBO stable in terms of the specified shaping transfer function $T_s(z)$.

By using Jury's stability criterion [20], the BIBO stability of a second-order Bode-type VA digital equalizer can be investigated by examining its

characteristic equation

$$Q(z) = c_2 z^2 + c_1 z + c_0. \quad (3.19)$$

By invoking Eqns. 3.14 and 3.15 in Eqn. 3.3, the coefficients c_i are obtained as

$$c_2 = A_0(V_F - V_I), \quad (3.20)$$

$$c_1 = (V_F - v)A_1 + (v - V_I)A_0B_1, \quad (3.21)$$

$$c_0 = (V_F - v)A_2 + (v - V_I)A_0B_2. \quad (3.22)$$

Then, the necessary and sufficient conditions for the VA digital equalizer to be BIBO stable are

$$|c_0| < c_2, \quad (3.23)$$

$$Q(1) > 0, \quad (3.24)$$

$$Q(-1) > 0. \quad (3.25)$$

In accordance with these conditions, one arrives at the final realizability condition

$$V_L < v < V_U \quad (\text{R.C. 4})$$

where

$$V_U = \min \begin{cases} V_A & \text{if } A_0 B_2 > A_2, \\ V_B & \text{if } A_0 B_2 < A_2, \\ \infty & \text{if } A_0 B_2 = A_2, \\ V_C & \text{if } A_0(B_1 + B_2) < (A_1 + A_2), \\ V_D & \text{if } A_0(B_2 - B_1) < (A_2 - A_1), \\ \infty & \text{if } A_0(B_2 \pm B_1) = (A_2 \pm A_1), \end{cases} \quad (3.26)$$

where

$$V_L = \max \begin{cases} V_B & \text{if } A_0 B_2 > A_2, \\ V_A & \text{if } A_0 B_2 < A_2, \\ -\infty & \text{if } A_0 B_2 = A_2, \\ V_C & \text{if } A_0(B_1 + B_2) > (A_1 + A_2), \\ V_D & \text{if } A_0(B_2 - B_1) > (A_2 - A_1), \\ -\infty & \text{if } A_0(B_2 \pm B_1) = (A_2 \pm A_1), \end{cases} \quad (3.27)$$

and where

$$\begin{aligned}
V_A &= \frac{V_I(A_0B_2 - A_0) + V_F(A_0 - A_2)}{A_0B_2 - A_2}, \\
V_B &= \frac{V_I(A_0B_2 + A_0) - V_F(A_0 + A_2)}{A_0B_2 - A_2}, \\
V_C &= \frac{A_0V_I(1 + B_1 + B_2) - V_F(A_0 + A_1 + A_2)}{A_0(B_1 + B_2) - (A_1 + A_2)}, \\
V_D &= \frac{A_0V_I(1 - B_1 + B_2) - V_F(A_0 - A_1 + A_2)}{A_0(B_2 - B_1) - (A_2 - A_1)}.
\end{aligned} \tag{3.28}$$

It should be pointed out that depending on the actual values of the specified coefficients A_i and B_i , the permitted range of variations for the variable multiplier v may be smaller than the full scale range as defined by V_I and V_F . Consequently, the corresponding VA digital equalizer would be prevented from realizing a full-scale symmetric variation from $T_s^{-1}(z)$ to $T_s(z)$.

3.5 Computational Design of Bode-Type Variable-Amplitude Digital Equalizers by Enumeration

In this section, the Realizability Conditions R.C. 1 - R.C. 3 are exploited and applied to the computational design of second-order Bode-type VA bump dig-

ital equalizers by enumeration. Two classes of bump VA digital equalizers are identified, one of which consists of distinct digital equalizers assuming infinite-precision internal arithmetic operations, while the other consists of distinct digital equalizers assuming finite-precision internal arithmetic operations. The latter digital equalizers are suitable for an actual hardware implementation for real-time digital graphic equalizer applications.

The above bump VA digital equalizers are assumed to consist of one variable digital multiplier v , two fixed multipliers α_2 and α_3 , and two unit-delays, only, implying a shaping transfer function $T_s(z)$ of the general form³

$$T_s(z) = \frac{(\alpha_2 - 1)\alpha_3 z^{-1} + (1 - \alpha_2)z^{-2}}{1 + (\alpha_2 - 1)\alpha_3 z^{-1} - \alpha_2 z^{-2}}. \quad (3.29)$$

Clearly, the numerator polynomial of the transfer function $T_s(z)$ in Eqn. 3.29 is devoid of a z^0 term. This can be achieved, e.g. by choosing $V_I = -\infty$, $V_o = -1$, and $V_F = 0$. Then, by substituting these values of V_I , V_o , and V_F into Eqn. 3.16, one obtains

$$t_{22}(z) = T_s(z). \quad (3.30)$$

³It can be easily shown that the shaping transfer function $T_s(z)$ for all of the above Bode-type VA digital equalizers take on the same form. This fact has already been exploited in the previous chapter for identifying $T_s(z)$ in Eqn. 3.29 as the shaping transfer function of the Bode-type bump VA WD digital equalizers.

Moreover, in accordance with realizability conditions R.C. 2 and R.C. 3, one gets

$$t_{11}(z) = t_{22}(z), \quad (3.31)$$

$$t_{12}(z)t_{21}(z) = t_{22}^2(z) - 1. \quad (3.32)$$

The Bode-type bump VA digital equalizers conforming to Eqns. 3.30, 3.31, and 3.32 can be derived by extracting the multipliers α_2 and α_3 and unit-delays from the network N_1 in Figure 3.1 to form a network N_2 as shown in Figure 3.2. The network N_2 in Figure 3.2 consists of 36 symbolic transmittances a_{ij} connecting the input ports I_i to the output ports O_j (for $i, j = 1, 2, \dots, 6$), and taking +1, 0, or -1 as their numeric values.

Through a symbolic analysis of the network in Figure 3.2 (e.g. by using the classical technique in [27]) the transfer matrix parameters $t_{ij}(z)$ can be determined in terms of the symbolic transmittances a_{ij} . Then, by replacing the symbolic transmittance a_{ij} exhaustively by their corresponding numeric values of +1, 0, or -1 , one obtains 3^{36} sets of transfer matrix parameters $t_{11}(z)$, $t_{12}(z)$, $t_{21}(z)$, and $t_{22}(z)$. By using Realizability Conditions 1-3, one can break up the problem into smaller and more manageable sub-problems and automatically eliminate invalid cases from the search space. Subsequently, each valid subset of transfer matrix parameters $t_{11}(z)$, $t_{12}(z)$,

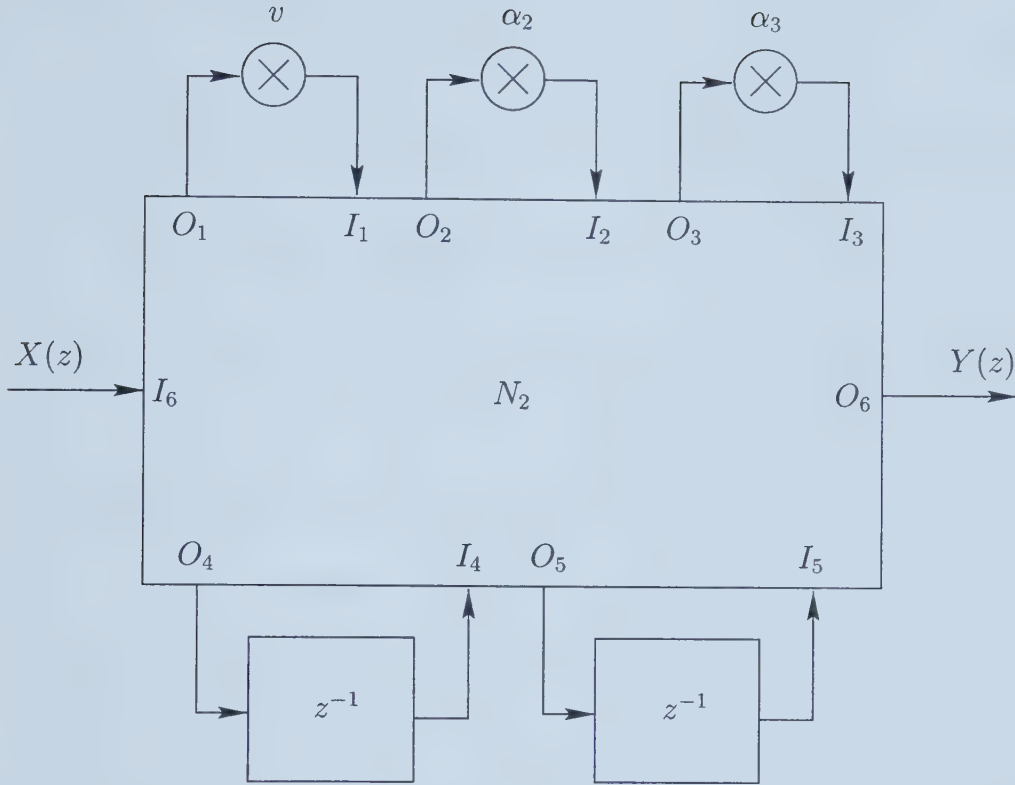


Figure 3.2: Network N_2 obtained by extracting multipliers α_2 and α_3 , and the two unit-delays from network N_1

$t_{21}(z)$, and $t_{22}(z)$ is examined against the realizability conditions R.C. 1, R.C. 2, and R.C. 3 (c.f. Eqns. 3.30, 3.31, and 3.32) for the identification of the numeric values for the transmittance a_{ij} . By adopting this exhaustive enumeration technique, a class of 8704 Bode-type bump VA digital equalizers have been identified.

The above 8704 Bode-type bump VA digital equalizers can be examined further for the identification of distinct bump VA digital equalizers both for infinite-precision as well as finite-precision internal arithmetic operations as

discussed in the following two subsections.

3.5.1 A Class of Infinite-Precision Bode-Type Variable-Amplitude Digital Equalizers

Under the assumption of infinite-precision internal arithmetic operations, a set of distinct Bode-type bump VA digital equalizers can be obtained by considering the loops formed within the digital equalizer proper via the transmittances a_{ij} . Consequently, the digital equalizers which contain identical loops of all orders are considered as a single distinct equalizer. In this way, a class of 14 distinct bump VA digital equalizers have been obtained.

The nonzero transmittance a_{ij} for each of the above 14 VA digital equalizers are as given in Table 3.1 for positive-valued a_{ij} 's and as given in Table 3.2 for negative-valued a_{ij} 's.

By matching the numeric values of transmittances a_{ij} 's in Tables 3.1 and 3.2 to the VA digital equalizer schematic diagram in Figure 2.9, it can be shown that the digital equalizer numbered as 1 is identical to the Bode-type variable-amplitude wave-digital equalizer derived in the previous chapter. By way of an example, the digital equalizer numbered as 4 in Tables 3.1 and 3.2 is as shown in the schematic diagram in Figure 3.3.

Table 3.1: Positive-valued transmittances a_{ij} for infinite-precision Bode-type bump digital equalizers

Equalizer #	Positive-Valued Transmittances
1	$a_{15}, a_{25}, a_{34}, a_{41}, a_{42}, a_{43}, a_{46}, a_{54}, a_{61}, a_{65}$
2	$a_{15}, a_{25}, a_{31}, a_{34}, a_{36}, a_{41}, a_{42}, a_{43}, a_{46}, a_{51}, a_{54}, a_{56}, a_{61}, a_{65}$
3	$a_{25}, a_{31}, a_{34}, a_{42}, a_{43}, a_{46}, a_{51}, a_{54}, a_{61}, a_{64}, a_{65}$
4	$a_{14}, a_{24}, a_{34}, a_{35}, a_{43}, a_{45}, a_{51}, a_{52}, a_{56}, a_{61}, a_{64}$
5	$a_{14}, a_{15}, a_{24}, a_{34}, a_{35}, a_{43}, a_{45}, a_{51}, a_{52}, a_{56}, a_{61}, a_{64}, a_{65}$
6	$a_{31}, a_{34}, a_{35}, a_{43}, a_{46}, a_{51}, a_{52}, a_{61}, a_{64}, a_{65}$
7	$a_{25}, a_{31}, a_{34}, a_{42}, a_{43}, a_{51}, a_{52}, a_{61}, a_{64}$
8	$a_{15}, a_{25}, a_{34}, a_{41}, a_{42}, a_{43}, a_{46}, a_{51}, a_{52}, a_{56}, a_{61}, a_{65}$
9	$a_{14}, a_{24}, a_{34}, a_{42}, a_{43}, a_{45}, a_{51}, a_{52}, a_{56}, a_{61}, a_{64}$
10	$a_{14}, a_{24}, a_{34}, a_{41}, a_{42}, a_{43}, a_{45}, a_{51}, a_{52}, a_{61}, a_{62}, a_{63}, a_{65}$
11	$a_{13}, a_{25}, a_{32}, a_{34}, a_{42}, a_{43}, a_{51}, a_{52}, a_{61}, a_{64}$
12	$a_{13}, a_{14}, a_{24}, a_{34}, a_{42}, a_{43}, a_{45}, a_{51}, a_{52}, a_{56}, a_{61}, a_{63}, a_{64}$
13	$a_{15}, a_{25}, a_{34}, a_{35}, a_{41}, a_{42}, a_{43}, a_{46}, a_{54}, a_{55}, a_{61}, a_{65}$
14	$a_{15}, a_{25}, a_{34}, a_{35}, a_{41}, a_{42}, a_{46}, a_{53}, a_{54}, a_{55}, a_{61}, a_{65}$

3.5.2 A Class of Finite-Precision Bode-Type Variable-Amplitude Digital Equalizers

In the enumeration of Bode-type bump VA digital equalizers under finite-precision arithmetic, the order of internal multiplication operations in the digital equalizer becomes important, rendering the considerations in subsection 3.5.1 that led to the identification of VA digital equalizers under infinite-precision arithmetic inadequate. In the following, a new class of VA digital equalizers is identified such that the requirements for stability under finite-precision arithmetic is distinct for each member of the class.

In an actual hardware implementation of Bode-type VA digital equalizers,

Table 3.2: Negative-valued transmittances a_{ij} for infinite-precision Bode-type bump digital equalizers

Equalizer #	Negative-Valued Transmittances
1	$a_{12}, a_{13}, a_{16}, a_{23}, a_{62}, a_{63}$
2	$a_{14}, a_{16}, a_{23}, a_{64}$
3	$a_{14}, a_{15}, a_{16}, a_{23}, a_{36}, a_{41}, a_{56}$
4	$a_{12}, a_{13}, a_{16}, a_{23}, a_{62}, a_{63}$
5	$a_{16}, a_{23}, a_{31}, a_{36}, a_{41}, a_{46}$
6	$a_{14}, a_{15}, a_{16}, a_{23}, a_{24}, a_{36}, a_{41}, a_{45}, a_{56}$
7	$a_{14}, a_{16}, a_{23}, a_{24}, a_{36}, a_{45}, a_{56}$
8	$a_{12}, a_{13}, a_{14}, a_{16}, a_{23}, a_{24}, a_{45}, a_{62}, a_{63}, a_{64}$
9	$a_{16}, a_{23}, a_{25}, a_{31}, a_{36}$
10	$a_{12}, a_{13}, a_{15}, a_{16}, a_{23}, a_{25}, a_{46}, a_{56}, a_{64}$
11	$a_{14}, a_{16}, a_{24}, a_{35}, a_{45}, a_{56}, a_{63}$
12	$a_{16}, a_{25}, a_{32}, a_{35}$
13	$a_{12}, a_{13}, a_{16}, a_{23}, a_{44}, a_{45}, a_{62}, a_{63}$
14	$a_{12}, a_{16}, a_{31}, a_{32}, a_{36}, a_{44}, a_{45}, a_{62}$

one must account for the non-ideal effects of internal finite-precision arithmetic operations including overflow saturation and limit-cycles. Of course, one must also take into account the dynamic variations of the variable digital multiplier. This section carries out an investigation of the “static” BIBO stability of these digital equalizers under finite-precision arithmetic and under the assumption that the variations of the variable multiplier occur slowly or only after the constituent transients have died down to a negligible level. This allows the equalizer to be considered as essentially shift-invariant. Under such circumstances, it suffices to ensure the equalizer is BIBO stable for all possible values of the variable multiplier and to ensure that the equalizer is free from overflow saturation and limit-cycle oscillations under finite-precision

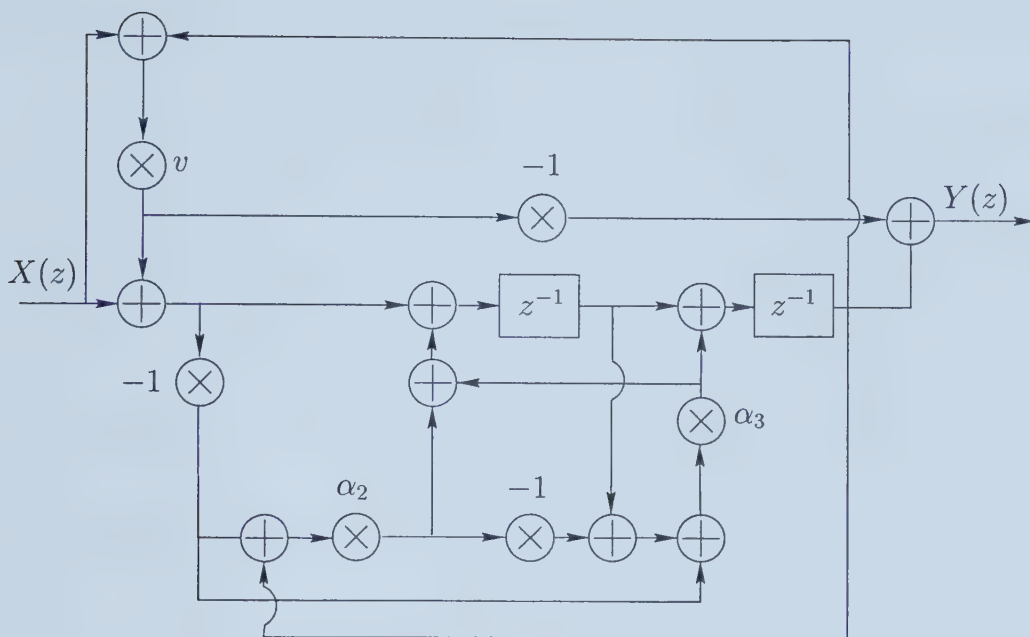


Figure 3.3: One of the 14 new Bode-type VA bump digital equalizers

arithmetic.

In order to counteract the detrimental effects of finite-precision internal signal wordlengths in an actual hardware implementation of the VA digital equalizer, the internal signal words are augmented with upper “guard bits” to offset signal overflow and with lower “guard bits” to restrict limit-cycle oscillations to amplitudes of at most a half-bit [28]. The L_1 -norm is used to determine the growth of internal signals in calculating the required number of guard bits. The L_1 -norm was chosen (as opposed to other less conservative norms) due to the fact, (a) that it *guarantees* that signal overflow will not occur, and (b) that it *guarantees* that the limit-cycle oscillations will have amplitudes of at most a half a bit. This is critical when one considers the

high signal-to-noise ratios inherent in digital audio applications.

Under the assumption of two's complement arithmetic operations, the number of upper guard bits is identified by using the L_1 -norm to determine the growth of the signal from the digital equalizer input to the inputs of the constituent multipliers. For a bump VA digital equalizer with three digital multipliers, the number of the required upper guard bits is obtained in accordance with

$$UGB = \lceil \log_2 [\max(\|h_v(n)\|_1, \|h_{\alpha_2}(n)\|_1, \|h_{\alpha_3}(n)\|_1)] \rceil, \quad (3.33)$$

where $h_v(n)$, $h_{\alpha_2}(n)$, and $h_{\alpha_3}(n)$ are the unit-impulse responses from the equalizer input to the inputs of the multipliers v , α_2 , and α_3 , respectively, and where

$$\|h_v(n)\|_1 = \sum_{n=0}^{\infty} |h_v(n)| \quad (3.34)$$

$$\|h_{\alpha_2}(n)\|_1 = \sum_{n=0}^{\infty} |h_{\alpha_2}(n)| \quad (3.35)$$

$$\|h_{\alpha_3}(n)\|_1 = \sum_{n=0}^{\infty} |h_{\alpha_3}(n)| \quad (3.36)$$

for causal digital equalizers. Similarly, the number of the required lower guard bits is determined by using the L_1 -norms to determine the growth

of the signal from the outputs of the constituent multipliers to the digital equalizer output. In this way, the number of the required lower guard bits is obtained in accordance with

$$LGB = \lceil \log_2[\|g_v(n)\|_1 + \|g_{\alpha_2}(n)\|_1 + \|g_{\alpha_3}(n)\|_1] \rceil, \quad (3.37)$$

where $g_v(n)$, $g_{\alpha_2}(n)$, and $g_{\alpha_3}(n)$ represent the unit-impulse responses from the output of multipliers v , α_2 , and α_3 to the equalizer output, respectively, and where

$$\|g_v(n)\|_1 = \sum_{n=0}^{\infty} |g_v(n)| \quad (3.38)$$

$$\|g_{\alpha_2}(n)\|_1 = \sum_{n=0}^{\infty} |g_{\alpha_2}(n)| \quad (3.39)$$

$$\|g_{\alpha_3}(n)\|_1 = \sum_{n=0}^{\infty} |g_{\alpha_3}(n)|. \quad (3.40)$$

In accordance with the previous subsection, one can identify a class of 8704 realizable bump VA digital equalizers that satisfy R.C. 1, R.C. 2, and R.C. 3. In the case of infinite-precision arithmetic, these 8704 equalizers can be narrowed down to 14 distinct equalizers by imposing a requirement that the corresponding internal loops of all orders be distinct. This was achieved without any consideration of the precedence relationships between the various multipliers within the internal loops. In the case of the desired class of

distinct finite-precision VA digital equalizers, on the other hand, the precedence relationships between the various multipliers within the internal loops have important bearings on the finite-precision operation of the equalizer. Therefore, it is proposed that the guard-bit requirements for each member of the VA digital equalizer class be distinct.

From Eqns. 3.33 and 3.37, it can be seen that a unique combination of the L_1 -norms will give rise to a distinct guard bit requirement (prior to applying the ceiling function). In this way, a unique combination of the unit-impulse responses $h_v(n)$, $h_{\alpha_2}(n)$, $h_{\alpha_3}(n)$, $g_v(n)$, $g_{\alpha_2}(n)$, and $g_{\alpha_3}(n)$ or their corresponding z -transforms $H_v(z)$, $H_{\alpha_2}(z)$, $H_{\alpha_3}(z)$, $G_v(z)$, $G_{\alpha_2}(z)$, and $G_{\alpha_3}(z)$ can be used to identify distinct equalizers.

The transfer functions $H_v(z)$, $H_{\alpha_2}(z)$, $H_{\alpha_3}(z)$, $G_v(z)$, $G_{\alpha_2}(z)$, and $G_{\alpha_3}(z)$ have a common denominator polynomial given by

$$D(z) = 1 + (-v\alpha_2\alpha_3 + v\alpha_3 + \alpha_2\alpha_3 - \alpha_3)z^{-1} + (-v + v\alpha_2 - \alpha_2)z^{-2}. \quad (3.41)$$

Consequently, in order to obtain a unique guard bit requirement, one must determine the unique combinations of the of the numerator polynomials of the transfer functions $H_v(z)$, $H_{\alpha_2}(z)$, $H_{\alpha_3}(z)$, $G_v(z)$, $G_{\alpha_2}(z)$, and $G_{\alpha_3}(z)$. In this way, a class of 40 distinct bump VA digital equalizers has been identified.

The nonzero transmittance a_{ij} for each of these 40 VA digital equalizers are as given in Table 3.4 for positive-valued a_{ij} 's and as given in Table 3.5 for negative-valued a_{ij} 's.

3.6 Selection of Bode-Type Bump Variable-Amplitude Digital Equalizer with Minimal Internal Signal Wordlength

In this section, a technique is developed for the selection of a digital equalizer from the class of 40 distinct finite-precision Bode-type bump VA digital equalizers subject to a minimal number of internal signal guard bits and subject to satisfying the design specifications for the center frequency ω_p , the quality factor Q_p , and the maximum magnitude h of the equalizer.

Definition of the Objective Functions

The total number of internal signal guard bits required for an equalizer to be free from overflow saturation and limit-cycle oscillations is the sum of the guard bits in Eqns. 3.33 and 3.37. Therefore, the problem under consideration amounts to the identification of the equalizer(s) that require the

minimum number of internal signal guard bits using

$$OBJ_1 = UGB + LGB, \quad (3.42)$$

as the objective function. Usually, one or more VA digital equalizer yield the same value for the objective function in Eqn. 3.42. In order to differentiate between these digital equalizers, a relative comparison can be made by removing the ceiling function from Eqns. 3.33 and 3.37 to obtain

$$OBJ_2 = w_1 \log_2[\max(\|h_v(n)\|_1, \|h_\alpha(n)\|_1, \|h_\beta(n)\|_1)] \\ + w_2 \log_2[\|g_v(n)\|_1 + \|g_\alpha(n)\|_1 + \|g_\beta(n)\|_1], \quad (3.43)$$

where w_1 and w_2 are weighting factors between 0 and 1. Therefore, one must first select the digital equalizers that minimize object function OBJ_1 , and then choose the optimum equalizer from the resulting set of digital equalizers that minimizes the objective function OBJ_2 .

Analytic Upper Bound for L_1 -Norm

The L_1 -norms in the above objective function can be found by approximating the infinite sum in Eqn. 3.36 by a finite sum. Alternatively, one can use an analytic upper bound for the infinite sum as adopted in the present

subsection.

Let $H(z)$ represent a general second-order z-domain transfer function of the form

$$H(z) = \frac{n_0 + n_1 z^{-1} + n_2 z^{-2}}{(1 - \lambda_1 z^{-1})(1 - \lambda_2 z^{-1})}, \quad (3.44)$$

where λ_1 and λ_2 are the finite poles of $H(z)$. If $\lambda_1 \neq \lambda_2$, then the unit-impulse response $h(n)$ associated with a transfer function $H(z)$ can be obtained as

$$h(n) = C_0 \delta(n) + C_1 \lambda_1^n u(n) + C_2 \lambda_2^n u(n), \quad (3.45)$$

where

$$C_0 = \frac{n_2}{\lambda_1 \lambda_2} \quad (3.46)$$

$$C_1 = \frac{n_1 \lambda_1 + \lambda_1^2 n_0 + n_2}{\lambda_1 (\lambda_1 - \lambda_2)} \quad (3.47)$$

$$C_2 = \frac{\lambda_2 n_1 + \lambda_2^2 n_0 + n_2}{\lambda_2 (\lambda_2 - \lambda_1)}. \quad (3.48)$$

Moreover, let $\|h(n)\|_1$ represent the L_1 -norm of the unit-impulse response $h(n)$ given by

$$\|h(n)\|_1 = \sum_{n=0}^{\infty} |h(n)| \quad (3.49)$$

Then, one can obtain an upper bound on the L_1 -norm $\|h(n)\|_1$ in accordance with

$$\|h(n)\|_1 \leq |C_0| + \frac{|C_1|}{1 - |\lambda_1|} + \frac{|C_2|}{1 - |\lambda_2|}. \quad (3.50)$$

Similarly, if $\lambda_2 = \lambda_1 = \lambda$ then one obtains

$$\|h(n)\|_1 \leq |D_0| + \frac{|D_1|}{1 - |\lambda|} + \frac{|D_2|}{(1 - |\lambda|)^2}, \quad (3.51)$$

where

$$D_0 = \frac{n_2}{\lambda^2} \quad (3.52)$$

$$D_1 = \frac{-n_1\lambda - 2n_2}{\lambda^2} \quad (3.53)$$

$$D_2 = \frac{\lambda n_1 + \lambda^2 n_0 + n_2}{\lambda^2}. \quad (3.54)$$

In this way, one can substitute Eqns. 3.50 and 3.51 into Eqns 3.33 and 3.37 in order to obtain the analytic upper bound on the required number of upper and lower guard bits.

Effect of Changing Multiplier Values

The calculation of the number of guard bits required to counteract the detrimental effects of finite-precision internal signal wordlengths is made compli-

cated by the fact that the bump amplitude is a function of the value of the variable digital multiplier v . Consequently, during the real-time operation of the VA digital equalizer, the digital multiplier v can take on different values, resulting in different values for the objective functions $OBJ1$ and $OBJ2$. To determine the total internal signal guard bit requirements, one can exhaustively evaluate $OBJ1$ and $OBJ2$ for all possible values of the variable multiplier and select the worst case. Alternatively, one can predict the worst case of when the value of the variable multiplier will result in the largest number of guard bits. The latter approach is discussed in the following.

Consider the coefficient of z^{-2} in Eqn. 3.41 as given by

$$-v + v\alpha_2 - \alpha_2 = v(\alpha_2 - 1) - \alpha_2, \quad (3.55)$$

which is the product of the two poles of all internal transfer functions. For practical values of $h > 1$, $Q > 0$, and $w_p > 0$, the coefficients v and α are constrained by $v < 0$ and $0 < \alpha_2 < 1$. Therefore, it can be seen from Eqn. 3.55 that one or both of the poles moves toward the unit circle as $|v|$ increases. This also corresponds to an increase in the bump amplitude of the digital equalizer. Therefore, the guard bit requirements are evaluated and compared at the coefficient values when $|v|$ is at its maximum. Furthermore, if a single equalizer is to be used for a number of different sets of values for

h and Q , the specifications with the largest values of h and Q will typically have the largest guard bit requirements and should be used for comparison purposes.

3.6.1 Application Example

In this section, an application example is given to illustrate the procedure for selecting an optimum equalizer for a given set of design parameters.

Consider the selection of an equalizer from the class of 40 bump equalizers that provides the optimum finite-precision performance for the following specifications: $h = 4$, $Q = 4$, $F_s = 32000$ Hz, and $F_p = 8000$ Hz. By evaluating the objective functions OBJ_1 and OBJ_2 with $w_1 = w_2 = 1$, and by using the analytic upper bounds discussed above, one obtains the guard-bit requirements as shown in Figure 3.4. Evidently, it can be seen that equalizers 11 and 20 require the minimum number of nine guard bits for these specifications. Furthermore, by comparing the values of objective function OBJ_2 for these two equalizers, one can see that equalizer 20 is the optimum choice. The corresponding transfer functions for this equalizer are given in Table 3.3. Note that the nine guard bits required for this example is an upper bound which guarantees that the equalizer is free from overflow saturation and limit cycle oscillations. Numerical analysis gives rise to smaller guard bit requirements, but the results no longer guarantee overflow-free and limit-

Table 3.3: Multiplier transfer functions for equalizer 20

Location	Numerator Polynomial
$H_v(z)$	$-1 + z^{-2}$
$G_v(z)$	$1 + 2\alpha_3(\alpha_2 - 1)z^{-1} + (1 - 2\alpha_2)z^{-2}$
$H_{\alpha_2}(z)$	$\alpha_3(v - 1)z^{-1} + (-v + 1)z^{-2}$
$G_{\alpha_2}(z)$	$-(v + 1) + (v + 1)z^{-2}$
$H_{\alpha_3}(z)$	$(v - 1) - (v - 1)z^{-1}$
$G_{\alpha_3}(z)$	$(-v\alpha_2 + v - \alpha_2 + 1)z^{-1} + (-v\alpha_2 + v - \alpha_2 + 1)z^{-2}$

cycle restricted operation due to the approximation of an infinite sum with a finite sum.

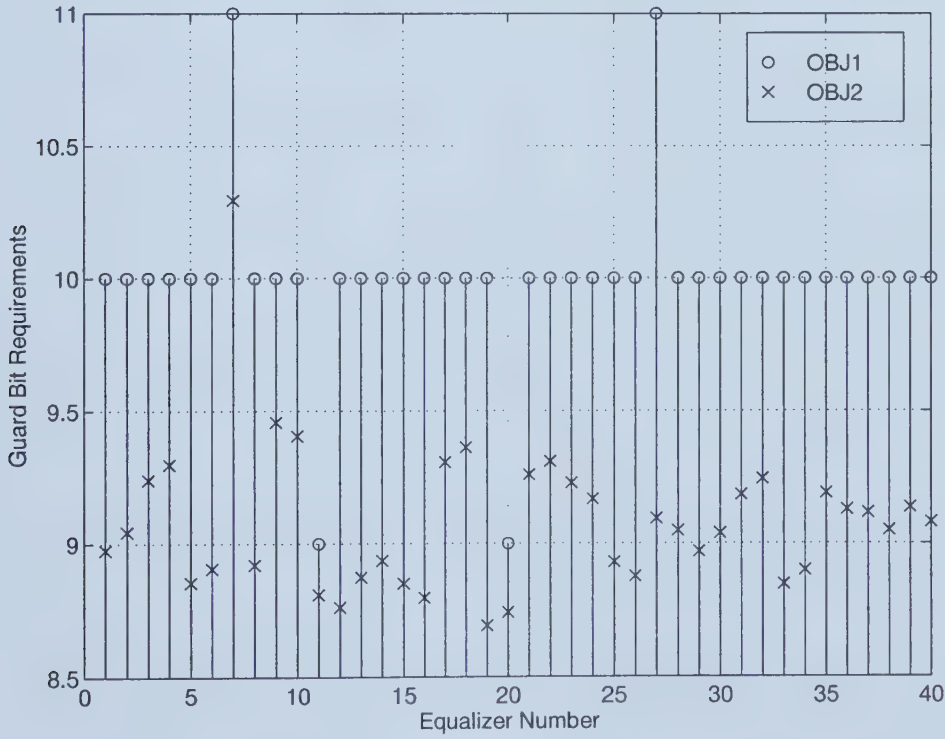


Figure 3.4: Objective function values for the finite-precision class of 40 digital equalizers

3.7 Conclusions

This chapter has presented a novel approach to the direct discrete-time z -domain design and enumeration of Bode-type VA digital equalizers. The salient features of the proposed approach are: (1) it does not make any recourse to the concept of a continuous-time s -domain prototype analog network or its transfer function, (2) it ensures that the frequency response of the resulting VA digital equalizers can be varied from that of a shaping transfer function, to its inverse for arbitrary shaping transfer functions, and (3) it requires a single variable digital multiplier (of course, in addition to the required usual fixed digital multipliers) only. This approach has been applied to the design and enumeration of two classes of second-order bump VA digital equalizers, one class including digital equalizers operating under infinite-precision arithmetic and the other including digital equalizers operating under finite-precision arithmetic operations. For the case of finite-precision arithmetic operations, a technique was developed for the selection of a digital equalizer from the corresponding VA digital equalizer class such that internal signal guard bits are minimized for a given set of design specifications.

Table 3.4: Positive-valued finite-precision bump Bode-type VA digital equalizers class interconnections

Member	Positive Nonzero Transmittances
1	$a_{15}, a_{25}, a_{34}, a_{41}, a_{42}, a_{43}, a_{46}, a_{54}, a_{61}, a_{65}$
2	$a_{15}, a_{16}, a_{25}, a_{34}, a_{41}, a_{42}, a_{43}, a_{46}, a_{54}, a_{65}$
3	$a_{15}, a_{25}, a_{34}, a_{41}, a_{42}, a_{43}, a_{46}, a_{54}, a_{61}, a_{65}$
4	$a_{15}, a_{16}, a_{25}, a_{34}, a_{41}, a_{42}, a_{43}, a_{46}, a_{54}, a_{65}$
5	$a_{15}, a_{25}, a_{31}, a_{34}, a_{36}, a_{41}, a_{42}, a_{43}, a_{46}, a_{51}, a_{54}, a_{56}, a_{61}, a_{65}$
6	$a_{15}, a_{16}, a_{25}, a_{31}, a_{34}, a_{36}, a_{41}, a_{42}, a_{43}, a_{46}, a_{51}, a_{54}, a_{56}, a_{65}$
7	$a_{25}, a_{31}, a_{34}, a_{42}, a_{43}, a_{46}, a_{51}, a_{54}, a_{61}, a_{64}, a_{65}$
8	$a_{16}, a_{25}, a_{31}, a_{34}, a_{42}, a_{43}, a_{46}, a_{51}, a_{54}, a_{64}, a_{65}$
9	$a_{31}, a_{32}, a_{34}, a_{43}, a_{51}, a_{52}, a_{61}, a_{62}, a_{64}$
10	$a_{16}, a_{31}, a_{32}, a_{34}, a_{43}, a_{51}, a_{52}, a_{62}, a_{64}$
11	$a_{26}, a_{31}, a_{32}, a_{34}, a_{43}, a_{51}, a_{52}, a_{61}, a_{64}$
12	$a_{16}, a_{26}, a_{31}, a_{32}, a_{34}, a_{43}, a_{51}, a_{52}, a_{64}$
13	$a_{15}, a_{32}, a_{34}, a_{41}, a_{43}, a_{46}, a_{51}, a_{52}, a_{56}, a_{61}, a_{65}$
14	$a_{15}, a_{16}, a_{32}, a_{34}, a_{41}, a_{43}, a_{46}, a_{51}, a_{52}, a_{56}, a_{65}$
15	$a_{13}, a_{32}, a_{34}, a_{43}, a_{46}, a_{51}, a_{52}, a_{61}, a_{64}, a_{65}$
16	$a_{13}, a_{16}, a_{32}, a_{34}, a_{43}, a_{46}, a_{51}, a_{52}, a_{64}, a_{65}$
17	$a_{14}, a_{24}, a_{34}, a_{35}, a_{43}, a_{45}, a_{51}, a_{52}, a_{56}, a_{61}, a_{64}$
18	$a_{14}, a_{16}, a_{24}, a_{34}, a_{35}, a_{43}, a_{45}, a_{51}, a_{52}, a_{56}, a_{64}$
19	$a_{14}, a_{24}, a_{34}, a_{35}, a_{43}, a_{45}, a_{51}, a_{52}, a_{56}, a_{61}, a_{64}$
20	$a_{14}, a_{16}, a_{24}, a_{34}, a_{35}, a_{43}, a_{45}, a_{51}, a_{52}, a_{56}, a_{64}$
21	$a_{14}, a_{15}, a_{24}, a_{34}, a_{35}, a_{43}, a_{45}, a_{51}, a_{52}, a_{56}, a_{61}, a_{64}, a_{65}$
22	$a_{14}, a_{15}, a_{16}, a_{24}, a_{34}, a_{35}, a_{43}, a_{45}, a_{51}, a_{52}, a_{56}, a_{64}, a_{65}$
23	$a_{34}, a_{35}, a_{43}, a_{51}, a_{52}, a_{61}, a_{62}, a_{63}, a_{64}$
24	$a_{16}, a_{34}, a_{35}, a_{43}, a_{51}, a_{52}, a_{62}, a_{63}, a_{64}$
25	$a_{26}, a_{34}, a_{35}, a_{43}, a_{51}, a_{52}, a_{61}, a_{63}, a_{64}$
26	$a_{16}, a_{26}, a_{34}, a_{35}, a_{43}, a_{51}, a_{52}, a_{63}, a_{64}$
27	$a_{31}, a_{34}, a_{35}, a_{43}, a_{46}, a_{51}, a_{52}, a_{61}, a_{64}, a_{65}$
28	$a_{16}, a_{31}, a_{34}, a_{35}, a_{43}, a_{46}, a_{51}, a_{52}, a_{64}, a_{65}$
29	$a_{15}, a_{25}, a_{32}, a_{34}, a_{41}, a_{42}, a_{43}, a_{46}, a_{52}, a_{54}, a_{61}, a_{65}$
30	$a_{15}, a_{16}, a_{25}, a_{32}, a_{34}, a_{41}, a_{42}, a_{43}, a_{46}, a_{52}, a_{54}, a_{65}$
31	$a_{15}, a_{25}, a_{31}, a_{32}, a_{34}, a_{36}, a_{41}, a_{42}, a_{43}, a_{46}, a_{51}, a_{52}, a_{54}, a_{56}, a_{61}, a_{65}$
32	$a_{15}, a_{16}, a_{25}, a_{31}, a_{32}, a_{34}, a_{36}, a_{41}, a_{42}, a_{43}, a_{46}, a_{51}, a_{52}, a_{54}, a_{56}, a_{65}$
33	$a_{15}, a_{25}, a_{31}, a_{32}, a_{34}, a_{36}, a_{41}, a_{42}, a_{43}, a_{46}, a_{51}, a_{52}, a_{54}, a_{56}, a_{61}, a_{65}$
34	$a_{15}, a_{16}, a_{25}, a_{31}, a_{32}, a_{34}, a_{36}, a_{41}, a_{42}, a_{43}, a_{46}, a_{51}, a_{52}, a_{54}, a_{56}, a_{65}$
35	$a_{24}, a_{34}, a_{41}, a_{42}, a_{43}, a_{52}, a_{61}, a_{63}, a_{65}$
36	$a_{16}, a_{24}, a_{34}, a_{41}, a_{42}, a_{43}, a_{52}, a_{63}, a_{65}$
37	$a_{14}, a_{24}, a_{34}, a_{36}, a_{41}, a_{42}, a_{43}, a_{51}, a_{52}, a_{61}, a_{62}, a_{65}$
38	$a_{14}, a_{16}, a_{24}, a_{34}, a_{36}, a_{41}, a_{42}, a_{43}, a_{51}, a_{52}, a_{62}, a_{65}$
39	$a_{14}, a_{24}, a_{26}, a_{34}, a_{36}, a_{41}, a_{42}, a_{43}, a_{51}, a_{52}, a_{61}, a_{65}$
40	$a_{14}, a_{16}, a_{24}, a_{26}, a_{34}, a_{36}, a_{41}, a_{42}, a_{43}, a_{51}, a_{52}, a_{65}$

Table 3.5: Negative-valued finite-precision bump Bode-type VA digital equalizers class interconnections

Member	Negative Nonzero Transmittances
1	$a_{12}, a_{13}, a_{16}, a_{23}, a_{62}, a_{63}$
2	$a_{12}, a_{13}, a_{23}, a_{61}, a_{62}, a_{63}$
3	$a_{13}, a_{16}, a_{21}, a_{23}, a_{26}, a_{63}$
4	$a_{13}, a_{21}, a_{23}, a_{26}, a_{61}, a_{63}$
5	$a_{14}, a_{16}, a_{23}, a_{64}$
6	$a_{14}, a_{23}, a_{61}, a_{64}$
7	$a_{14}, a_{15}, a_{16}, a_{23}, a_{36}, a_{41}, a_{56}$
8	$a_{14}, a_{15}, a_{23}, a_{36}, a_{41}, a_{56}, a_{61}$
9	$a_{12}, a_{14}, a_{16}, a_{24}, a_{36}, a_{45}, a_{56}$
10	$a_{12}, a_{14}, a_{24}, a_{36}, a_{45}, a_{56}, a_{61}$
11	$a_{14}, a_{16}, a_{21}, a_{24}, a_{36}, a_{45}, a_{56}$
12	$a_{14}, a_{21}, a_{24}, a_{36}, a_{45}, a_{56}, a_{61}$
13	$a_{13}, a_{14}, a_{16}, a_{24}, a_{45}, a_{63}, a_{64}$
14	$a_{13}, a_{14}, a_{24}, a_{45}, a_{61}, a_{63}, a_{64}$
15	$a_{14}, a_{15}, a_{16}, a_{24}, a_{41}, a_{45}, a_{56}, a_{63}$
16	$a_{14}, a_{15}, a_{24}, a_{41}, a_{45}, a_{56}, a_{61}, a_{63}$
17	$a_{12}, a_{13}, a_{16}, a_{23}, a_{62}, a_{63}$
18	$a_{12}, a_{13}, a_{23}, a_{61}, a_{62}, a_{63}$
19	$a_{13}, a_{16}, a_{21}, a_{23}, a_{26}, a_{63}$
20	$a_{13}, a_{21}, a_{23}, a_{26}, a_{61}, a_{63}$
21	$a_{16}, a_{23}, a_{31}, a_{36}, a_{41}, a_{46}$
22	$a_{23}, a_{31}, a_{36}, a_{41}, a_{46}, a_{61}$
23	$a_{12}, a_{13}, a_{14}, a_{16}, a_{23}, a_{24}, a_{45}, a_{56}$
24	$a_{12}, a_{13}, a_{14}, a_{23}, a_{24}, a_{45}, a_{56}, a_{61}$
25	$a_{13}, a_{14}, a_{16}, a_{21}, a_{23}, a_{24}, a_{45}, a_{56}$
26	$a_{13}, a_{14}, a_{21}, a_{23}, a_{24}, a_{45}, a_{56}, a_{61}$
27	$a_{14}, a_{15}, a_{16}, a_{23}, a_{24}, a_{36}, a_{41}, a_{45}, a_{56}$
28	$a_{14}, a_{15}, a_{23}, a_{24}, a_{36}, a_{41}, a_{45}, a_{56}, a_{61}$
29	$a_{13}, a_{16}, a_{24}, a_{63}$
30	$a_{13}, a_{24}, a_{61}, a_{63}$
31	$a_{12}, a_{14}, a_{16}, a_{24}, a_{62}, a_{64}$
32	$a_{12}, a_{14}, a_{24}, a_{61}, a_{62}, a_{64}$
33	$a_{14}, a_{16}, a_{21}, a_{24}, a_{26}, a_{64}$
34	$a_{14}, a_{21}, a_{24}, a_{26}, a_{61}, a_{64}$
35	$a_{13}, a_{15}, a_{16}, a_{25}, a_{32}, a_{46}, a_{54}$
36	$a_{13}, a_{15}, a_{25}, a_{32}, a_{46}, a_{54}, a_{61}$
37	$a_{12}, a_{15}, a_{16}, a_{25}, a_{31}, a_{32}, a_{46}, a_{54}, a_{56}, a_{64}$
38	$a_{12}, a_{15}, a_{25}, a_{31}, a_{32}, a_{46}, a_{54}, a_{56}, a_{61}, a_{64}$
39	$a_{15}, a_{16}, a_{21}, a_{25}, a_{31}, a_{32}, a_{46}, a_{54}, a_{56}, a_{64}$
40	$a_{15}, a_{21}, a_{25}, a_{31}, a_{32}, a_{46}, a_{54}, a_{56}, a_{61}, a_{64}$

Chapter 4

Design of General-Order

Bode-Type Variable-Amplitude

Digital Equalizers

4.1 Introduction

In the previous chapter, a novel technique was developed for the direct discrete-time z -domain design and enumeration of Bode-type variable-amplitude (VA) digital equalizers. This technique resulted in VA digital equalizers realizing overall magnitude-frequency response characteristics which can be varied from that of a specified shaping transfer function to its inverse by varying the value of a single variable digital multiplier only. In this technique,

the specified shaping transfer function placed a constraint on the admissible range of values for the variable digital multiplier.

The present chapter is concerned with the development of a new approach [29] for the design of arbitrary-order Bode-type VA digital equalizers which eliminates the above constraint between the range of variable digital multiplier values and the shaping transfer function. This approach is based on replacing the conventional shaping transfer function with an effective shaping transfer function. The main salient feature of this approach is that it leads to a substantial simplification in the realizability conditions associated with the VA digital equalizer, and, in turn, leads to a reduction in the cost of the corresponding hardware implementation of the digital equalizer.

In Section 4.2, a theoretical background is presented. In Section 4.3, a new design technique is developed for general-order Bode-type VA digital equalizers. Section 4.4 is concerned with the development of shaping transfer function approximations [30] for the resulting Bode-type VA digital equalizers. Section 4.5 is concerned with the development a BIBO stability condition [31] for general-order Bode-type VA digital equalizers. Finally, in Section 4.6, the proposed technique is illustrated through its application to the design of a fourth-order Bode-type variable-amplitude digital equalizer.

4.2 Effective Shaping Transfer Function

As indicated in the previous chapter, a conventional VA digital equalizer realizes transfer a function of the form

$$T_v(z) = \frac{1 + xT_s(z)}{x + T_s(z)}, \quad (4.1)$$

where x plays the role of a variable digital multiplier. However, this transfer function does not lend itself to a finite-precision implementation in hardware due to the fact that for $T_v(z) = T_s^{-1}(z)$ or $T_v(z) = T_s(z)$ one must allow $x = 0$ or $x = \infty$ (both of which are impractical¹).

In order to restrict the variation of the variable digital multiplier x to a prespecified practical range of values, a bilinear variable transformation was employed to obtain a new VA digital equalizer transfer function of the form

$$T_v(z) = \frac{\frac{V_I(V_o - V_F)T_s(z) + V_F(V_o - V_I)}{(V_I - V_o)T_s(z) + (V_F - V_o)} + \frac{(V_F - V_o)T_s(z) + (V_I - V_o)}{(V_I - V_o)T_s(z) + (V_F - V_o)}v}{v + \frac{V_F(V_o - V_I)T_s(z) + V_I(V_o - V_F)}{(V_I - V_o)T_s(z) + (V_F - V_o)}}, \quad (4.2)$$

where v plays the role of a new variable digital multiplier. From Eqn. 4.2, it can be seen that the variation of the digital multiplier v from V_I (via V_o) to V_F results in a corresponding variation of the transfer function $T_v(z)$ from $T_s^{-1}(z)$ (via 1) to $T_s(z)$, as desired. However, as shown in the previous chapter, in

¹The value 0 is impractical if it is desired to minimize the ratio between the extreme values of the variable digital multiplier x .

order to realize a VA digital equalizer with a specific shaping transfer function $T_s(z)$, a constraint must be imposed on the choice of values for V_I , V_o , and V_F (c.f. Eqn. 3.15). The resulting values for V_I , V_o , and V_F may adversely affect the realizability conditions associated with the digital equalizer, and, ultimately, the cost of the corresponding hardware implementation of the equalizer.

In the following, a novel approach is presented for the design of general-order Bode-type VA digital equalizers which eliminates the above constraint on the choice of values for V_I , V_o , and V_F . This is achieved through the use of an effective shaping transfer function $T_{se}(z)$ instead of the conventional shaping transfer function $T_s(z)$. This results in VA digital equalizers realizing transfer functions $T_v(z)$ which can be varied from $T_{se}^{-1}(z)$ to $T_{se}(z)$ by varying the value of the variable digital multiplier v over an effective range of values from V_{Ie} to V_{Fe} . In this way, one can eliminate the direct relationship between the range of values for the variable digital multiplier v and the shaping transfer function $T_s(z)$. This results in a smaller effective range of values for the digital multiplier v as compared to the range that would have otherwise been necessary if the design had been carried out in terms of the conventional shaping transfer function $T_s(z)$.

4.3 Development of the New Design Technique

The transfer function $T_v(z)$ can be expressed in terms of the transfer matrix parameter $t_{22}(z)$ by substituting the realizability conditions R.C. 2 and R.C. 3 into Eqn. 3.8, and by simplifying the result to obtain

$$T_v(z) = \frac{V_1 t_{22}(z) + V_2}{V_3 t_{22}(z) + V_4} \quad (4.3)$$

where

$$V_1 = 2V_I V_o V_F - V_I V_o^2 + v V_o^2 - V_F V_o^2 - v V_I V_F \quad (4.4)$$

$$V_2 = v V_I + v V_F - V_I V_F + V_o^2 - 2v V_o \quad (4.5)$$

$$V_3 = v V_I V_F - V_I V_o v - V_F V_o v + v V_o^2 \quad (4.6)$$

$$V_4 = V_I V_o - V_I V_F + V_F V_o - V_o^2. \quad (4.7)$$

By substituting Eqn. 3.13 into Eqn. 4.3, and by invoking the realizability condition R.C. 1 in the result, one obtains

$$T_v(z) = \frac{\frac{V_2}{V_4} + (\frac{V_1}{V_4} a_1 + \frac{V_2}{V_4} b_1) z^{-1} + \dots + (\frac{V_1}{V_4} a_n + \frac{V_2}{V_4} b_n) z^{-n}}{1 + (\frac{V_3}{V_4} a_1 + b_1) z^{-1} + \dots + (\frac{V_3}{V_4} a_n + b_n) z^{-n}}, \quad (4.8)$$

which places in evidence the direct relationship between the coefficients of $T_v(z)$ and the coefficients of $t_{22}(z)$.

Let the effective shaping transfer function $T_{se}(z)$ be of the general form

$$T_{se}(z) = \frac{N(z)}{D(z)} = \frac{\alpha_0 + \alpha_1 z^{-1} + \dots + \alpha_n z^{-n}}{1 + \beta_1 z^{-1} + \dots + \beta_n z^{-n}}. \quad (4.9)$$

If $T_v(z) = T_{se}(z)$ for a certain value v , say V_{Fe} , then by equating the coefficients of like powers of z in Eqns. 4.8 and 4.9, one can obtain the value V_{Fe} and the value of the coefficients of the transfer matrix parameter $t_{22}(z)$ in accordance with

$$V_{Fe} = \frac{-V_I V_F + V_o^2 + \alpha_0 (V_I V_F - V_I V_o - V_F V_o + V_o^2)}{2V_o - V_I - V_F}, \quad (4.10)$$

$$a_i = \frac{-V_4(V_4\alpha_i - \beta_i V_2)}{V_2 V_3 - V_1 V_4}, \quad (4.11)$$

$$b_i = \frac{V_4(V_3\alpha_i - V_1\beta_i)}{V_2 V_3 - V_1 V_4}, \quad (4.12)$$

where $i = 1, 2, \dots, n$. For V_{Fe} to be of finite value, it can be seen from Eqn. 4.10 that one must ensure that

$$V_I + V_F - 2V_o \neq 0. \quad (4.13)$$

It is important to point out that this is the only constraint imposed on the values of V_I , V_o , and V_F , and that unlike the design technique presented in the previous chapter, it does not depend on the transfer functions $T_{se}(z)$ or $T_s(z)$. In order to obtain the corresponding value of V_{Ie} , one must solve the equation

$$f(V_{Fe}) = -f(V_{Ie}), \quad (4.14)$$

where $f(v)$ is given by

$$f(v) = \frac{V_o(V_I - V_F) + v(V_F - V_I)}{V_I(V_o - 2V_F + v) + V_o(V_F - 2v) + vV_F} \quad (4.15)$$

(c.f. Eqn. 3.5). Then, by invoking Eqn. 4.15 in Eqn. 4.14 one can obtain²

$$V_{Ie} = -\frac{-2V_IV_oV_F + V_IV_FV_{Fe} + V_IV_o^2 - V_{Fe}V_o^2 + V_FV_o^2}{V_IV_F - V_{Fe}V_I - V_o^2 + 2V_{Fe}V_o - V_{Fe}V_F}. \quad (4.16)$$

Consequently, as v is varied from V_{Fe} (via V_o) to V_{Ie} , the transfer function $T_v(z)$ varies from $T_{se}(z)$ (via 1) to $T_{se}^{-1}(z)$, as desired. In this way, it is possible to define the permissible range of values for the variable digital multiplier v (as given by V_I and V_F) such that the realizability conditions

²If $V_{Ie} > V_{Fe}$, then one must simply swap the values of V_{Fe} and V_{Ie} . If $V_{Fe} > V_F$ or $V_{Ie} < V_I$, then different values should be assigned V_F and V_I .

are simplified, while still obtaining the desired response characteristics over an *effective* range of values for the digital multiplier v as given by V_{Fe} and V_{Ie} . This effective range that is always smaller than the hitherto range and proves more practical for a corresponding hardware realization of the VA digital equalizer.

4.4 Design of General-Order Bode-type VA digital equalizer Shaping Transfer Functions

In the design of Bode-type variable-amplitude digital equalizers, the constituent effective shaping transfer function is frequently required to satisfy certain prescribed magnitude-frequency response characteristics. These characteristics include: a “passband”³ with a prespecified maximum gain h , a “stopband” with unity gain, and a single prespecified gain p at the passband edge(s) (where $h > p > 1$).

When designing the above transfer functions, one may adopt to employ optimization techniques (such as [34–36]) or analytic approximations tech-

³In what follows, the term *passband* is used to denote the frequency band of interest throughout which the magnitude-frequency response is to be amplified or attenuated, while the term *stopband* is used to refer to the band of frequencies for which the magnitude-frequency response is left unchanged.

niques. This section presents a novel approximation technique for the analytic design of general-order shaping transfer functions $T_{se}(z)$ with maximally flat or equiripple lowpass, highpass, or bandpass magnitude-frequency response characteristics. This is achieved by first deriving a corresponding normalized prototype lowpass shaping transfer function, and then by applying a lowpass-to-lowpass, lowpass-to-highpass, or lowpass-to-bandpass frequency transformation to obtain the desired (denormalized) shaping transfer function. These shaping transfer functions can be employed in the design of variable-amplitude digital equalizers having magnitude-frequency responses with sharp transition bands and reduced inter-band interference in the corresponding digital graphic equalizers. In Section 4.4.1, Feldtkeller's equation is modified for the design of normalized prototype lowpass shaping transfer functions satisfying the above magnitude-frequency response characteristics. In Section 4.4.2, the result thus obtained is exploited and applied to the derivation of normalized prototype shaping transfer functions with maximally flat passband magnitude-frequency response characteristics. Similarly, in Sections 4.4.3 and 4.4.4, prototype shaping transfer functions with equiripple passband and stopband magnitude-frequency response characteristics are derived. Depending on the application, one may use equiripple approximations in order to obtain a sharper transition from the passband to the stopband in the magnitude-frequency response.

4.4.1 Design of Normalized Prototype Lowpass Shaping Transfer Functions

The classical approximation techniques for the design of continuous-time s -domain normalized prototype transfer functions $H(s)$ are based on Feldtkeller's equation [37]

$$|H(j\Omega)|^2 = \frac{1}{1 + |K(j\Omega)|^2}, \quad (4.17)$$

where $s = j\Omega$ is the complex frequency variable (Ω is the corresponding real-frequency variable). In this way, $|H(j\Omega)|^2$ varies between 0 and 1 as $|K(j\Omega)|^2$ varies between 0 and ∞ , where the actual form of $|K(j\Omega)|^2$ is determined by the particular approximation to be used. By replacing $j\Omega$ by s , and by analytic continuation, one can rewrite Eqn. 4.17 in the form

$$H(s)H(-s) = \frac{1}{1 + K(s)K(-s)}. \quad (4.18)$$

In accordance with Eqn. 4.18, $H(s)$ may be determined by selecting those poles and zeros of $H(s)H(-s)$ which are located in the left half s -plane.

The design of z -domain shaping transfer functions can be accomplished

in a similar way by modifying Eqn. 4.17 in accordance with

$$|T_{se}(e^{j\omega})|^2 = \frac{h^2 + |K(e^{j\omega})|^2}{1 + |K(e^{j\omega})|^2}, \quad (4.19)$$

where ω has been defined above. In this way, $|T_{se}(e^{j\omega})|^2$ varies between h^2 and 1 when $|K(e^{j\omega})|^2$ varies between 0 and ∞ (as desired). The general forms of the discrete-time terms $|K(e^{j\omega})|^2$ are developed from the corresponding continuous-time terms $|K(j\Omega)|^2$ by employing the bilinear frequency transformation

$$\Omega = \tan \frac{\omega}{2}. \quad (4.20)$$

The following sections are concerned with the derivation of denormalized shaping transfer functions $T_s(z)$ having maximally flat or equiripple lowpass, highpass, and bandpass magnitude-frequency response characteristics. This can be achieved by deriving a corresponding normalized prototype lowpass shaping transfer function satisfying the magnitude-frequency response characteristics shown in Figure 4.1: a passband with a prespecified maximum gain h , a stopband with unity gain, and a prespecified gain p at $\omega = 1$. Then, through the application of the frequency transformation technique in [19] to the resulting transfer function, one can obtain the desired denormalized

lowpass, highpass, and bandpass shaping transfer functions $T_{se}(z)$.

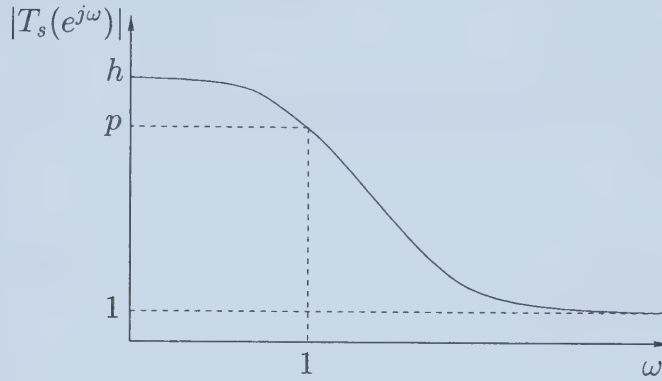


Figure 4.1: Normalized magnitude-frequency response

4.4.2 Derivation of Shaping Transfer Functions with Maximally Flat Passbands

In the classical Butterworth normalized prototype transfer function approximation, $|K(j\Omega)|^2$ is of the form

$$|K(j\Omega)|^2 = a_N \omega^{2N}, \quad (4.21)$$

where N is the order of $H(s)$, and where the parameter a_N is used to define the passband gain at $\Omega = 1$. By substituting for Ω from Eqn. 4.20 into Eqn. 4.21, one obtains

$$|K(e^{j\omega})|^2 = a_N \tan^{2N} \frac{\omega}{2}. \quad (4.22)$$

Then, by substituting Eqn. 4.22 into Eqn. 4.19, one gets

$$|T_{se}(e^{j\omega})|^2 = \frac{h^2 + a_N \tan^{2N}(\frac{\omega}{2})}{1 + a_N \tan^{2N}(\frac{\omega}{2})}. \quad (4.23)$$

It can be easily shown that the resulting prototype transfer function $T_{se}(e^{j\omega})$ in Eqn. 4.23 exhibits the desired maximally flat magnitude-frequency response characteristic, i.e. (a) ideal transmission occurs at $\omega = 0$ (e.g. $|T_{se}(1)|^2 = h^2$ or $|K(1)|^2 = 0$) and (b) the first $2N - 1$ derivatives of the transmission error

$$\Delta(\omega) = h^2 - |T_s(e^{j\omega})|^2 = \frac{(1 - h^2)|K(e^{j\omega})|^2}{1 + |K(e^{j\omega})|^2} \quad (4.24)$$

with respect to ω are equal to zero at $\omega = 0$.

As in the continuous-time case, the parameter a_N is used to set the pass-band gain at $\omega = 1$. By inspection of Figure 4.1, it can be seen that one should have $|T_{se}(e^{j1})| = p$, or, equivalently,

$$|T_{se}(e^{j1})|^2 = p^2. \quad (4.25)$$

Therefore, by substituting Eqn. 4.23 into Eqn. 4.25, and by solving for the

parameter a_N , one obtains

$$a_N = \frac{h^2 - p^2}{\tan^{2N}(1/2)(p^2 - 1)}. \quad (4.26)$$

By invoking Euler's equations into Eqn. 4.23, one can obtain an alternate form of $|T_s(e^{j\omega})|^2$ in terms of $e^{j\omega}$ in accordance with

$$|T_{se}(e^{j\omega})|^2 = \frac{\binom{2N}{N}F_1(h^2) + \sum_{k=1}^N \binom{2N}{N-k}F_2(h^2) \{e^{-j\omega k} + e^{j\omega k}\}}{\binom{2N}{N}F_1(1) + \sum_{k=1}^N \binom{2N}{N-k}F_2(1) \{e^{-j\omega k} + e^{j\omega k}\}}, \quad (4.27)$$

where

$$F_1(x) = (x + a_N), \quad (4.28)$$

$$F_2(x) = [x + (-1)^{2N-k}a_N]. \quad (4.29)$$

Then, through analytic continuation, one can obtain $T_{se}(z)T_{se}(z^{-1})$ from $|T_{se}(e^{j\omega})|^2$ in Eqn. 4.27. Finally, $T_{se}(z)$ is obtained by selecting the poles and zeros of $T_{se}(z)T_{se}(z^{-1})$ located inside the unit-circle.

Alternatively, by solving for the roots of the numerator and denominator of Eqn. 4.23 to obtain the zeros z_k and poles p_k (for $k = 1 \dots N$), $T_s(z)$ can be defined in accordance with

$$T_{se}(z) = T_0 \frac{\prod_{k=1}^N (z - z_k)}{\prod_{k=1}^N (z - p_k)}, \quad (4.30)$$

where

$$z_k = \frac{1 + e^{j\frac{(2k+N-1)\pi}{2N}} h^{\frac{1}{N}} a_N^{\frac{-1}{2N}}}{1 - e^{j\frac{(2k+N-1)\pi}{2N}} h^{\frac{1}{N}} a_N^{\frac{-1}{2N}}} \quad (4.31)$$

and

$$p_k = \frac{1 + e^{j\frac{(2k+N-1)\pi}{2N}} a_N^{\frac{-1}{2N}}}{1 - e^{j\frac{(2k+N-1)\pi}{2N}} a_N^{\frac{-1}{2N}}}. \quad (4.32)$$

From Eqn. 4.27, the constant parameter T_0 can be obtained as

$$T_0 = \sqrt{\frac{K_n}{K_d}}, \quad (4.33)$$

where

$$K_n = (h^2 + (-1)^N a_N) \prod_{k=1}^N p_k \quad (4.34)$$

and

$$K_d = (1 + (-1)^N a_N) \prod_{k=1}^N z_k. \quad (4.35)$$

4.4.3 Derivation of Shaping Transfer Functions with Equiripple Passbands

In the classical Chebyshev normalized prototype transfer function approximation, $|K(j\Omega)|^2$ is of the form [37]

$$|K(j\Omega)|^2 = a_N C_N^2(\Omega), \quad (4.36)$$

where

$$C_N(\Omega) = \cos [N \cos^{-1} \Omega]. \quad (4.37)$$

For the purposes of the following derivations, it is important to note that $C_N(1) = 1$ for all N .

By substituting for Ω from Eqn. 4.20 into Eqn. 4.36, one obtains

$$|K(e^{j\omega})|^2 = a_N C_N^2(\omega), \quad (4.38)$$

where

$$C_N(\omega) = \cos \left[N \cos^{-1} \left(\alpha \tan \left(\frac{\omega}{2} \right) \right) \right], \quad (4.39)$$

and where

$$\alpha = \frac{1}{\tan(1/2)} \quad (4.40)$$

so that the property $C_N(1) = 1$ is preserved. By using trigonometric identities, $C_N(\omega)$ can be expressed as a polynomial in ω and calculated using the recurrence relationships given in the following

$$C_0(\omega) = 1 \quad (4.41)$$

$$C_1(\omega) = \alpha \tan\left(\frac{\omega}{2}\right) \quad (4.42)$$

$$C_N(\omega) = 2\alpha \tan\left(\frac{\omega}{2}\right) C_{N-1}(\omega) - C_{N-2}(\omega). \quad (4.43)$$

In this way, $C_N^2(\omega)$ will be of the general form

$$C_N^2(\omega) = \sum_{k=0}^N c_{2k} \alpha^{2k} \tan^{2k}\left(\frac{\omega}{2}\right). \quad (4.44)$$

By substituting Eqn. 4.38 into Eqn. 4.19, one obtains

$$|T_{se}(e^{j\omega})|^2 = \frac{h^2 + a_N C_N^2(\omega)}{1 + a_N C_N^2(\omega)}. \quad (4.45)$$

Once again, it is required that $|T_s(e^{j1})| = p$ (c.f. Figure 4.1). Therefore, by substituting Eqn. 4.45 into Eqn. 4.25, and by solving for the parameter a_N ,

one obtains

$$a_N = \frac{h^2 - p^2}{p^2 - 1}. \quad (4.46)$$

Again, from Eqn. 4.45, an alternate form of $|T_{se}(e^{j\omega})|^2$ can be obtained in terms of $e^{j\omega}$ in accordance with

$$|T_{se}(e^{j\omega})|^2 = \frac{h^2 F_3(2)^N + a_N \sum_{k=0}^N c_{2k} (-1)^k \alpha^{2k} F_3(2)^k F_3(-2)^{N-k}}{F_3(2)^N + a_N \sum_{k=0}^N c_{2k} (-1)^k \alpha^{2k} F_3(2)^k F_3(-2)^{N-k}}, \quad (4.47)$$

where

$$F_3(x) = e^{j\omega} - x + e^{-j\omega}. \quad (4.48)$$

Then, one can obtain $T_{se}(z)T_{se}(z^{-1})$ from $|T_{se}(e^{j\omega})|^2$ in Eqn. 4.47 through analytic continuation. Finally, $T_{se}(z)$ is obtained by selecting the poles and zeros of $T_{se}(z)T_{se}(z^{-1})$ located inside the unit-circle.

Alternatively, by solving for the roots of the numerator and denominator of Eqn. 4.45 to obtain the zeros z_k and poles p_k (for $k = 1 \dots N$), $T_{se}(z)$ can

be defined in accordance with Eqn. 4.30, where

$$p_k = \frac{1 + F_4(k, 1)}{1 - F_4(k, 1)} \quad (4.49)$$

$$z_k = \frac{1 + F_4(k, h^2)}{1 - F_4(k, h^2)}, \quad (4.50)$$

and where

$$F_4(k, x) = \frac{j}{\alpha} \cos \left[\frac{\cos^{-1} \left(\frac{-(2x+a_N)}{a_N} \right) + 2\pi(k-1)}{2N} \right]. \quad (4.51)$$

From Eqn. 4.47, the constant parameter T_0 can be obtained as given in Eqn. 4.33, where

$$K_n = \frac{h^2 + a_N \sum_{k=0}^N c_{2k} (-1)^k \alpha^{2k}}{\prod_{k=1}^N z_k} \quad (4.52)$$

$$K_d = \frac{1 + a_N \sum_{k=0}^N c_{2k} (-1)^k \alpha^{2k}}{\prod_{k=1}^N p_k} \quad (4.53)$$

4.4.4 Derivation of Shaping Transfer Functions with Equiripple Stopbands

The discrete-time Inverse Chebyshev shaping transfer function approximation can be obtained by performing an inversion and frequency translation

of $|K(e^{j\omega})|^2$ in Eqn. 4.38 in accordance with

$$|K(e^{j\omega})|^2 = \frac{a_N}{C_N^2(\pi - \omega)}, \quad (4.54)$$

where $C_N^2(\omega)$ is as defined in Eqn. 4.39, and where the parameter α is defined in accordance with

$$\alpha = \frac{2}{\tan\left(\frac{\pi-1}{2}\right)}. \quad (4.55)$$

By substituting Eqn. 4.54 into Eqn. 4.19, one obtains

$$|T_s(e^{j\omega})|^2 = \frac{h^2 C_N^2(\pi - \omega) + a_N}{C_N^2(\pi - \omega) + a_N}. \quad (4.56)$$

As before, it is required that $|T_{se}(e^{j1})| = p$. Therefore, by substituting Eqn. 4.56 into Eqn. 4.25 and by solving for the parameter a_N , one obtains

$$a_N = \frac{\cos^2[N \cos^{-1}(2)](h^2 - p^2)}{p^2 - 1} \quad (4.57)$$

An alternate form of $|T_{se}(e^{j\omega})|^2$ can be derived in terms of $e^{j\omega}$ from Eqn. 4.45 in accordance with

$$|T_{se}(e^{j\omega})|^2 = \frac{h^2 \sum_{k=0}^N c_{2k}(-1)^k \alpha^{2k} F_5(-2)^k F_5(2)^{N-k} + a_N F_5(2)}{\sum_{k=0}^N c_{2k}(-1)^k \alpha^{2k} F_5(-2)^k F_5(2)^{N-k} + a_N F_5(2)}, \quad (4.58)$$

where

$$F_5(x) = -e^{-j\omega} + x - e^{j\omega}. \quad (4.59)$$

Then, by employing analytic continuation, $T_{se}(z)T_{se}(z^{-1})$ can be obtained from Eqn. 4.58. Finally, by selecting the poles and zeros inside the unit-circle, one can obtain $T_{se}(z)$.

Alternatively, by solving for the roots of the numerator and denominator of Eqn. 4.45 to obtain the zeros z_k and poles p_k (for $k = 1...N$), $T_{se}(z)$ can be defined in accordance with Eqn. 4.30, where

$$p_k = \frac{F_6(k, 1) - 1}{F_6(k, 1) + 1} \quad (4.60)$$

$$z_k = \frac{F_6(k, h^2) - 1}{F_6(k, h^2) + 1}, \quad (4.61)$$

and where

$$F_6(k, x) = \frac{j}{\alpha} \cos \left[\frac{\cos^{-1} \left(\frac{-2a_N - x}{x} \right) - 2\pi k}{2N} \right]. \quad (4.62)$$

4.5 BIBO Stability of Bode-type VA digital equalizers

In this section, a BIBO stability condition is developed for general-order Bode-type VA digital equalizers. This BIBO stability condition imposes constraints on the shaping transfer function of the Bode-type VA digital equalizer such that the Bode-type VA digital equalizer is guaranteed to be BIBO stable over the entire permissible range of values of the variable multiplier v (as opposed to the BIBO stability condition in Chapter 3 for second-order Bode-type VA digital equalizers which, when given the shaping transfer function $T_s(z)$, defines the range of the variable multiplier v over which the Bode-type VA digital equalizer is BIBO stable). As in Chapter 3, the following discussions will consider the Bode-type VA digital equalizer to be essentially shift-invariant.

In Section 4.5.1, it is shown that the variation of the variable multiplier v in Eqn. 4.2 over the full range $V_I \rightarrow V_F$ or the smaller effective range $V_{Ie} \rightarrow V_{Fe}$, is equivalent to varying the variable multiplier x in Eqn. 4.1 from $0 \rightarrow \infty$. In this way, one must only consider the BIBO stability of the single Bode-type VA digital equalizer transfer function given in Eqn. 4.1. In Section 4.5.2, this result is used to develop a BIBO stability condition for general-order Bode-type VA digital equalizers.

4.5.1 Theoretical Background

As derived in Chapter 3, the transfer function of a Bode-type VA digital equalizer with a variable multiplier v that varies over a specified range of values (given by V_I , V_o , and V_F) is given by Eqn. 3.3, where

$$T_v(z) = T_s^{-1} \rightarrow 1 \rightarrow T_s(z) \quad \text{as} \quad v = V_I \rightarrow V_o \rightarrow V_F. \quad (4.63)$$

This equation was obtained by applying the bilinear variable transformation in Eqn. 3.2 to Eqn. 3.1. Obviously, by applying the corresponding reverse variable transformation

$$v = \frac{x(V_IV_F - V_FV_o) + V_IV_o - V_FV_I}{x(V_I - V_o) + V_o - V_F} \quad (4.64)$$

one obtains Bode's original approximation

$$T_v(z) = \frac{1 + xT_s(z)}{x + T_s(z)}, \quad (4.65)$$

where x varies from 0 to ∞ . In this way, if $T_v(z)$ in Eqn. 4.65 is BIBO stable for $x \in (0, \infty)$, then $T_v(z)$ in Eqn. 3.3 will also be BIBO stable for $v \in (V_I, V_F)$. Therefore, one must only consider the BIBO stability of Eqn. 4.65.

In Section 4.3, an alternate technique was developed for the design of

general-order Bode-type VA digital equalizers with transfer functions given by Eqn. 3.3, but where the variable multiplier v varies over a smaller effective range $v \in (V_{Ie}, V_{Fe})$, and where

$$T_v(z) = T_{se}^{-1} \rightarrow 1 \rightarrow T_{se}(z) \quad \text{as } v = V_{Ie} \rightarrow V_o \rightarrow V_{Fe}. \quad (4.66)$$

In what follows, it will be shown that BIBO stability of the resulting Bode-type VA digital equalizers can also be investigated by only considering the BIBO stability of Eqn. 4.65 (with $T_s(z) = T_{se}(z)$).

By simplification of Eqn. 3.3, one obtains

$$T_v(z) = \frac{1 + \frac{(V_I - v)(V_o - V_F)}{(v - V_F)(V_I - V_o)} T_s(z)}{\frac{(V_I - v)(V_o - V_F)}{(v - V_F)(V_I - V_o)} + T_s(z)}. \quad (4.67)$$

In the design technique presented in Section 4.3, the transfer matrix parameter $t_{22}(z)$ and the parameter V_{Fe} were defined such that $T_v(z) = T_{se}(z)$ for $v = V_{Fe}$. Therefore, by substituting $v = V_{Fe}$ in Eqn. 4.67, and by equating the resulting to $T_{se}(z)$, one obtains

$$\frac{1 + \frac{(V_I - V_{Fe})(V_o - V_F)}{(V_{Fe} - V_F)(V_I - V_o)} T_s(z)}{\frac{(V_I - V_{Fe})(V_o - V_F)}{(V_{Fe} - V_F)(V_I - V_o)} + T_s(z)} = T_{se}(z). \quad (4.68)$$

By modifying Eqn. 4.64, one can obtain the bilinear variable transforma-

tion

$$v = \frac{xV_{Fe}(V_{Ie} - V_o) + V_{Ie}(V_o - V_{Fe})}{x(V_{Ie} - V_o) + V_o - V_{Fe}}. \quad (4.69)$$

In this way, as x varies from 0 (via 1) to ∞ , v varies from V_{Ie} (via V_o) to V_{Fe} . By applying the transformation in Eqn. 4.69 to Eqn. 4.67, and by substituting Eqn. 4.16 into the result, one obtains

$$T_v(z) = \frac{[F_1 + F_2T_s(z)] + x[F_2 + F_1T_s(z)]}{[F_2 + F_1T_s(z)] + x[F_1 + F_2T_s(z)]}, \quad (4.70)$$

where

$$F_1 = (V_I - V_{Fe})(V_o - V_F), \quad (4.71)$$

$$F_2 = (V_F - V_{Fe})(V_o - V_I). \quad (4.72)$$

But, from Eqn. 4.68

$$\frac{1 + \frac{F_1}{F_2}T_s(z)}{\frac{F_1}{F_2} + T_s(z)} = T_{se}(z). \quad (4.73)$$

Therefore, by substituting Eqn. 4.73 into Eqn. 4.70 one obtains

$$T_v(z) = \frac{1 + xT_{se}(z)}{x + T_{se}(z)}. \quad (4.74)$$

In this way, if $T_v(z)$ in Eqn. 4.74 is BIBO stable for $x \in (0, \infty)$, then $T_v(z)$ in Eqn. 3.3 will also be BIBO stable for $v \in (V_{Ie}, V_{Fe})$.

4.5.2 Development of BIBO Stability Condition

In this section, a condition for the BIBO stability of Bode-type VA digital equalizers will be established for arbitrary values of V_F , V_o , V_I , V_{Ie} , and V_{Fe} by considering the general case of the transfer function given in Eqn. 4.74. It will be shown that if $T_{se}(z)$ is a minimum-phase transfer function, then the corresponding Bode-type VA digital equalizer will be BIBO stable for $x \in (0, \infty)$ provided that the phase of $T_{se}(z)$ satisfies a certain condition.

The BIBO stability of the transfer function given in Eqn. 4.74 can be investigated by examining the roots of the characteristic equation

$$Q(z) = N(z) + xD(z) = 0, \quad (4.75)$$

where $N(z)$ and $D(z)$ are as defined in Eqn. 4.9. For the purposes of this section, it is assumed that $T_{se}(z)$ is minimum-phase transfer function, i.e. the roots of $N(z)$ and $D(z)$ are located inside the unit-circle.

By following the same mathematical steps as in the development of Kharitonov's stability theorem [38], if $Q(z)$ is degree-invariant, then the roots of $Q(z)$ will vary continuously along a constant number of root-locus branches.

From Eqn. 4.75, it can be seen that $Q(z)$ will be degree-invariant if

$$\alpha_0 + x \neq 0. \quad (4.76)$$

By taking into account that $x \in (0, \infty)$, Eqn. 4.76 can be simplified to

$$\alpha_0 > 0. \quad (4.77)$$

In practical design situations, Eqn. 4.77 can be easily satisfied.

From Eqn. 4.75, it can be seen that for the extreme values of $x = 0$ and $x = \infty$, the roots of $Q(z)$ will be located inside the unit-circle. Therefore, if $T_{se}(z)$ satisfies Eqn. 4.77, then the transfer function $T_v(z)$ in Eqn. 4.74 will become BIBO unstable if, and only if, one or more of the root-locus branches associated with $Q(z)$ intersects the unit-circle, i.e. if

$$x + T_{se}(e^{j\omega}) = 0. \quad (4.78)$$

Since x is assumed to be a real quantity, Eqn. 4.78 can be recast as

$$\Im \{T_{se}(e^{j\omega})\} = 0 \text{ and } x + \Re \{T_{se}(e^{j\omega})\} = 0. \quad (4.79)$$

In this way, the conditions for guaranteed BIBO stability for $x \in (0, \infty)$ can

be obtained in accordance with

$$\text{If } \Im \{T_{se}(e^{j\omega})\} = 0, \text{ then} \quad (4.80)$$

$$\Re \{T_{se}(e^{j\omega})\} > 0. \quad (4.81)$$

The conditions in Eqns. 4.80 and 4.81 can be simplified by considering the general form of $T_{se}(e^{j\omega})$ given by

$$\begin{aligned} T_{se}(e^{j\omega}) &= M(\omega)e^{j\Theta(\omega)} \\ &= M(\omega) [\cos(\Theta(\omega)) + j \sin(\Theta(\omega))], \end{aligned} \quad (4.82)$$

where $M(\omega)$ and $\Theta(\omega)$ are the magnitude-frequency and phase-frequency responses associated with $T_{se}(z)$, and where [39]

$$-\pi < \Theta(\omega) \leq \pi. \quad (4.83)$$

From Eqn. 4.82, the real and imaginary parts of $T_{se}(e^{j\omega})$ can be expressed in accordance with

$$\Re \{T_{se}(e^{j\omega})\} = M(\omega) \cos(\Theta(\omega)) \quad (4.84)$$

$$\Im \{T_{se}(e^{j\omega})\} = M(\omega) \sin(\Theta(\omega)). \quad (4.85)$$

Since $T_{se}(z)$ is assumed to be a minimum-phase transfer function, the magnitude-frequency response $M(\omega)$ is strictly positive⁴ in accordance with

$$M(\omega) > 0. \quad (4.86)$$

Therefore, from Eqn. 4.85, it can be seen that if the condition in Eqn. 4.80 is satisfied (i.e. $\Im\{T_{se}(e^{j\omega})\} = 0$), then

$$\sin(\Theta(\omega)) = 0, \quad (4.87)$$

or equivalently

$$\Theta(\omega) = 0 \text{ or } \pi. \quad (4.88)$$

If $\Theta(\omega) = 0$, then from Eqn. 4.84

$$\Re\{T_{se}(e^{j\omega})\} = M(\omega). \quad (4.89)$$

By comparing Eqn. 4.89 and Eqn. 4.81, and by taking into account the relationship in Eqn. 4.86, it can be seen that the BIBO stability conditions in Eqns. 4.80 and 4.81 are always satisfied. On the other hand, if $\Theta(\omega) = \pi$,

⁴i.e. $M(\omega)$ cannot become zero.

then from Eqn. 4.84

$$\Re \{T_{se}(e^{j\omega})\} = -M(\omega). \quad (4.90)$$

In the same way, by comparing Eqn. 4.89 and Eqn. 4.81, and by taking into account the relationship in Eqn. 4.86, it can be seen that the BIBO stability conditions in Eqns. 4.80 and 4.81 are always violated. Therefore, if $T_{se}(z)$ is a minimum-phase transfer function, and if $T_v(z)$ is degree-invariant, then the corresponding Bode-type VA digital equalizer is guaranteed to be BIBO for $x \in (0, \infty)$ if

$$\boxed{\Theta(\omega) \neq \pi \quad \text{for all } \omega}. \quad (4.91)$$

Note that as shown in Section 4.5.1, this result can be applied to Bode-type VA digital equalizers with $v \in (V_I, V_F)$ or $v \in (V_{Ie}, V_{Fe})$.

4.6 Application Example

This section is concerned with the application of the proposed design technique to the design of a fourth order Bode-type variable amplitude digital equalizer.

By using the derivations in Section 4.4, one can obtain suitable general-

order normalized lowpass shaping transfer function candidates for the design of Bode-type variable-amplitude digital equalizers. As an example, the magnitude-frequency response characteristics of fourth-order normalized maximally flat, Chebyshev, and inverse Chebyshev lowpass (fan) shaping transfer functions for $h = 4$ and $p = 3.5$ are shown in Figure 4.2.

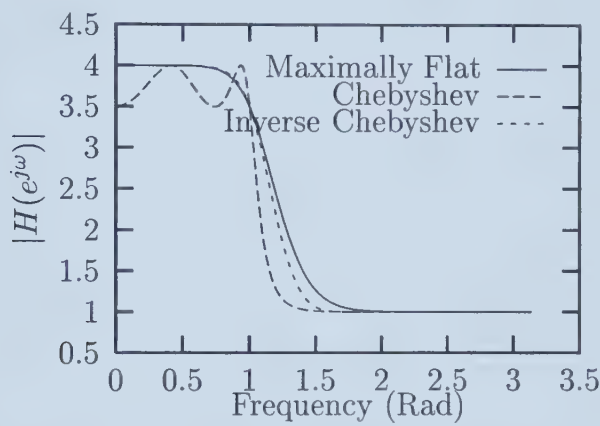


Figure 4.2: Normalized prototype magnitude-frequency responses

For the purposes of this application example, $T_{se}(z)$ is obtained by applying a lowpass-to-bandpass transformation [19] to the fourth-order maximally flat shaping transfer function given in Figure 4.2 in accordance with Table 4.1. A plot of the magnitude-frequency and phase-frequency responses of $T_{se}(z)$

Table 4.1: Coefficient values for $T_{se}(z)$

i	α_i	β_i
0	1.1866409	1
1	-0.6203626	-0.5739552
2	1.6576517	1.7355932
3	-0.04347331	-0.4811405
4	0.5959603	0.7046597

is given in Figures 4.3 and 4.4. Note that $T_{se}(z)$ is a minimum-phase transfer function. Note further that the phase-frequency response of $T_{se}(z)$ shown in Figure 4.4 satisfies the BIBO stability condition in Eqn. 4.91. Therefore, the resulting Bode-type VA digital equalizer is guaranteed to be BIBO stable for $v \in (V_{Ie}, V_{Fe})$.

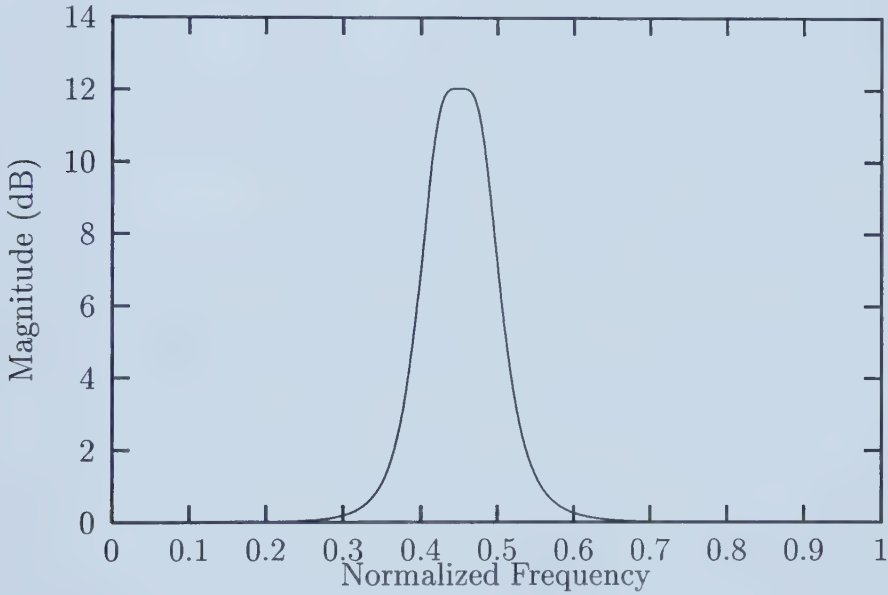


Figure 4.3: Magnitude-frequency response of $T_{se}(z)$

In accordance with the discussions in Section 4.3, the values of V_I , V_o , and V_F are chosen as (c.f. Eqn. 4.13)

$$V_I = -\infty, \quad V_o = -1, \quad \text{and} \quad V_F = 0. \quad (4.92)$$

Then, by substituting Eqn. 4.92 into conditions R.C. 2 and R.C. 3, one

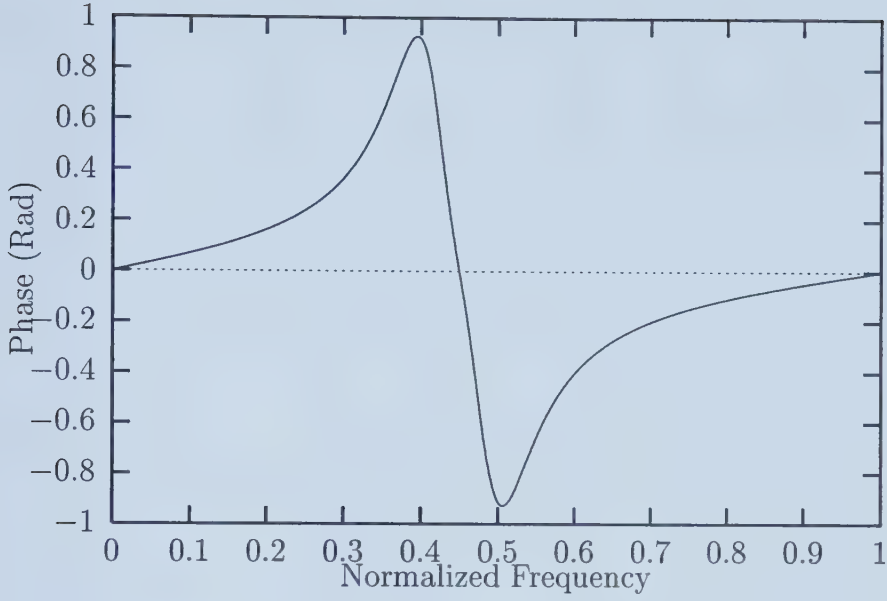


Figure 4.4: Phase-frequency response of $T_{se}(z)$

obtains the following realizability conditions

$$t_{11}(z) = t_{22}(z) \quad (4.93)$$

$$t_{12}(z)t_{21}(z) = t_{22}^2(z) - 1. \quad (4.94)$$

Consequently, Eqn. 4.94 can be easily factored into the following

$$t_{12}(z) = t_{22}(z) - 1 \quad (4.95)$$

$$t_{21}(z) = t_{22}(z) + 1. \quad (4.96)$$

To proceed further, one can realize the equalizer in terms of the transfer matrix parameter $t_{22}(z)$ using conditions R.C. 1, R.C. 2 and R.C. 3. A pos-

sible realization of the digital equalizer can be obtained as shown in Fig. 4.5, where, for simplicity, $t_{22}(z)$ has been implemented using a Direct Form II realization.

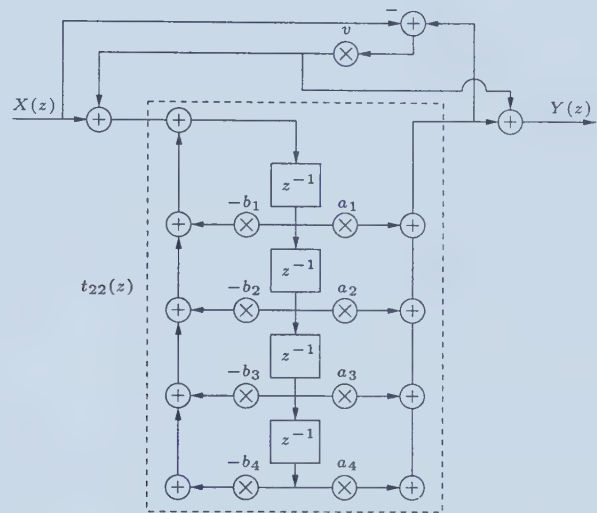


Figure 4.5: Fourth-order bump digital equalizer

In the conventional approach to the design of Bode-type digital equalizers, $T_s(z) = T_{se}(z)$, which would require the variable multiplier v to vary over the range specified in Eqn. 4.92 in order to obtain the desired variations in $T_v(z)$. However, if $T_v(z)$ is designed in accordance with the design technique given in Section 4.3, then $T_v(z)$ varies from $T_{se}^{-1}(z)$ to $T_{se}(z)$ as v varies over a smaller *effective* range⁵. This effective range can be determined by

⁵Of course, v can still be varied from V_I to V_F . However, since $T_s(z) \neq T_{se}(z)$, one will not obtain the desired magnitude-frequency response characteristic.

substituting Eqn. 4.92 into Eqns. 4.10 and 4.16 to obtain

$$V_{Fe} = -\alpha_0 = -0.8427149 \quad (4.97)$$

$$V_{Ie} = \frac{1}{V_{Fe}} = -\frac{1}{\alpha_0} = -1.1866409 \quad (4.98)$$

The intermediate values for v can be chosen between V_{Fe} and V_o , and between V_{Ie} and V_o to obtain the desired frequency response characteristic. Therefore, it can be seen that it is only necessary to vary v over a small practical range of values in order to obtain the desired symmetrical variation in the magnitude-frequency response of the equalizer.

Finally, by invoking Eqn. 4.92 in Eqns. 4.11 and 4.12, one obtains

$$a_i = \frac{\alpha_0 \beta_i - \alpha_i}{\alpha_0^2 - 1} \quad (4.99)$$

$$b_i = \frac{\alpha_0 \alpha_i - \beta_i}{\alpha_0^2 - 1}. \quad (4.100)$$

Then, the coefficients of $t_{22}(z)$ can be obtained from the specified coefficients of $T_{se}(z)$ (Table 4.1) as given in Table 4.2. The magnitude-frequency response

Table 4.2: Multiplier coefficient values for $t_{22}(z)$

i	a_i	b_i
1	-0.1487716	-0.3974167
2	0.9847043	0.5671028
3	-0.3337474	-0.0851022
4	0.5886006	0.0062022

of the resulting equalizer is obtained by Matlab/Simulink simulation as shown in Fig. 4.6. A plot of the poles of $T_v(z)$ as v is varied from V_{Ie} to V_{Fe} is given in Figure 4.7. As seen in Figure 4.7, the digital equalizer is BIBO stable for all values of the variable multiplier v in the range $v \in (V_{Ie}, V_{Fe})$.

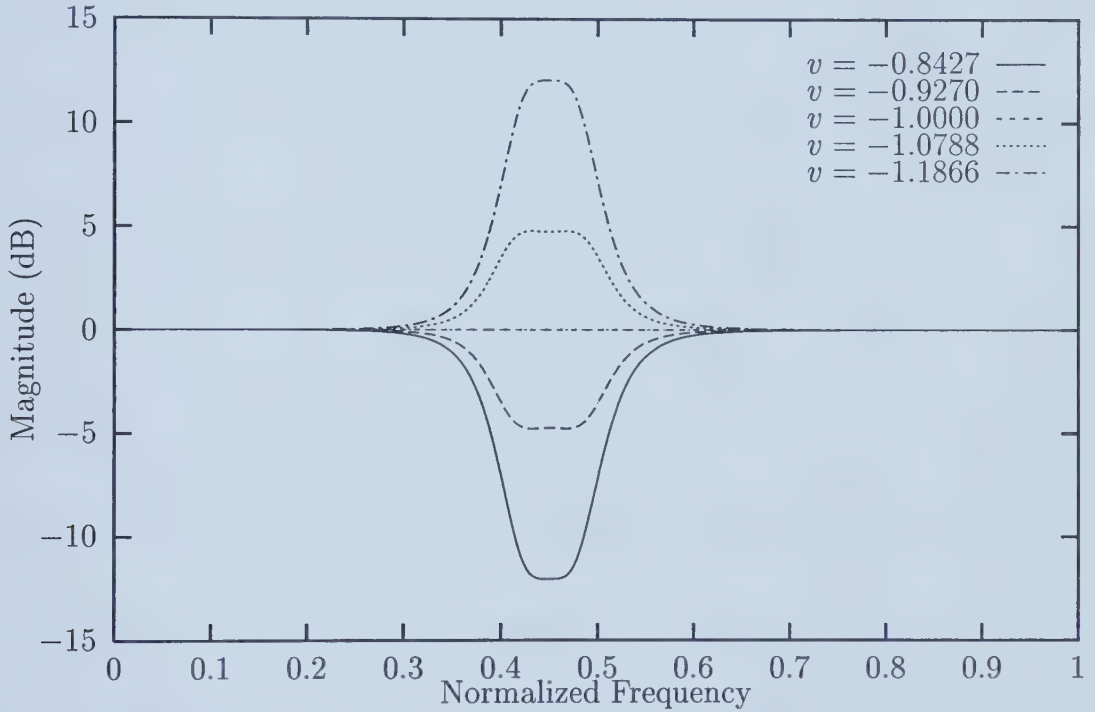


Figure 4.6: Magnitude-frequency response of digital equalizer

4.7 Conclusions

This chapter has presented a new approach to the design of arbitrary-order Bode-type VA digital equalizers. This approach eliminates the constraint between the range of variable digital multiplier values by replacing the conven-

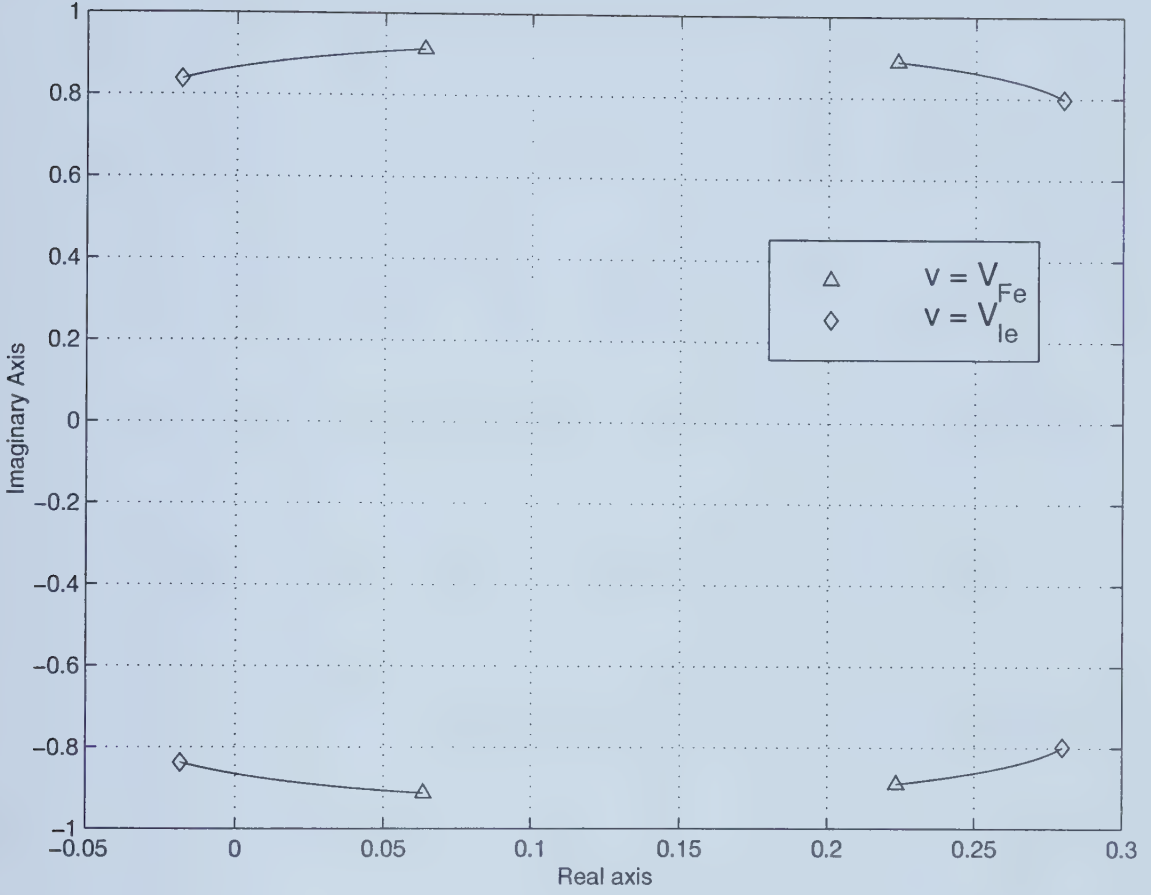


Figure 4.7: Plot of poles of $T_v(z)$ for $v \in (V_{Le}, V_{Fe})$

tional shaping transfer function by an effective shaping transfer function. The main salient feature of this approach is that it leads to a substantial simplification in the realizability conditions associated with the VA digital equalizer, and, in turn, leads to a reduction in the cost of the corresponding hardware implementation of the digital equalizer. In addition, a novel approximation technique was presented for the design of general-order shaping transfer functions with maximally flat or equiripple lowpass, highpass, or bandpass magnitude-frequency response characteristics. This was achieved by first de-

ring a corresponding normalized prototype lowpass shaping transfer function, and then by applying a lowpass-to-lowpass, lowpass-to-highpass, or lowpass-to-bandpass frequency transformation to obtain the desired (denormalized) shaping transfer function. These shaping transfer functions can be employed in the design of VA digital equalizers having magnitude-frequency responses with sharp transition bands and reduced inter-band interference in the corresponding digital graphic equalizers. Finally, the theoretical basis of Kharitonov's stability theorem was used for the development of a novel BIBO stability condition for general-order Bode-type VA digital equalizers. The results of this chapter can be easily applied to the design of high-quality digital graphic equalizers.

Chapter 5

Implementation Issues for Bode-type VA Digital Equalizers with Time-Varying Coefficients

5.1 Introduction

The BIBO stability of Bode-type variable-amplitude (VA) digital equalizers was investigated in Chapters 3 and 4 from a “static” point of view only, namely under the assumption that the variations of the variable digital multiplier occur slowly or only after the output signal transients have died down

to a negligible level. In this case, the VA digital equalizer can be considered essentially as shift-invariant.

The present chapter, on the other hand, is concerned with the effect of the “dynamic” variations of the variable digital multiplier on the stability¹ and the transient signal behaviour of Bode-type VA digital equalizers. Such variations of the variable digital multiplier render the the VA digital equalizer proper as shift-variant. In this way, the state-space representation [19, 40] of the digital equalizer will be of the general form

$$\mathbf{q}(n+1) = \mathbf{A}(n)\mathbf{q}(n) + \mathbf{b}(n)x(n) \quad (5.1)$$

$$y(n) = \mathbf{c}'(n)\mathbf{q}(n) + d(n)x(n), \quad (5.2)$$

where

$$\mathbf{A}(n) = \begin{bmatrix} a_{11}(n) & a_{12}(n) & \cdots & a_{1N}(n) \\ a_{21}(n) & a_{22}(n) & \cdots & a_{2N}(n) \\ \vdots & \vdots & \vdots & \vdots \\ a_{N1}(n) & a_{N2}(n) & \cdots & a_{NN}(n) \end{bmatrix}, \quad (5.3)$$

¹The stability under consideration is essentially BIBO stability but under the assumption that the digital equalizer is considered as shift variant.

$$\mathbf{b}(n) = \begin{bmatrix} b_1(n) \\ b_2(n) \\ \vdots \\ b_N(n) \end{bmatrix}, \quad (5.4)$$

$$\mathbf{c}'(n) = \begin{bmatrix} c_1(n) & c_2(n) & \cdots & c_N(n) \end{bmatrix}, \quad (5.5)$$

$$d(n) = d_0(n), \quad (5.6)$$

$$\mathbf{q}(n) = \begin{bmatrix} q_1(n) & q_2(n) & \cdots & q_N(n) \end{bmatrix}', \quad (5.7)$$

where $q(n)$ represents the state vector, where N is the number of the constituent unit-delays, and where the superscript $'$ denotes the operation of matrix transposition.

In Section 5.2, it is shown that the state-space representation of a Bode-type VA digital equalizer consisting of a dynamically-varying variable digital multiplier can be decomposed into a series of shift-invariant state-space representations. This fact is then exploited to investigate the stability of the

VA digital equalizer for two different cases, including the case corresponding to infinite precision arithmetic and that corresponding to finite-precision arithmetic hardware implementations of the digital equalizer. Section 5.3 is concerned with the transient behavior of VA digital equalizers in the presence of a dynamically-varying variable digital multiplier. By using the state-space representation of the digital equalizer together with the Cayley-Hamilton theorem [43], an analytical approach is developed for the estimation of the time required for the transients in the digital equalizer output signal to reduce to a specified level. An example is given in Section 5.4 to illustrate the application of the proposed results to the stability of a fourth-order Bode-type VA digital equalizer.

5.2 Stability Analysis of Bode-type VA Digital Equalizers Consisting of a Dynamically-Varying Variable Digital Multiplier

5.2.1 Stability under Infinite-Precision Arithmetic

This section is concerned with the investigation of the stability of a Bode-type VA digital equalizer consisting of a single dynamically-varying variable digital multiplier for an infinite-precision arithmetic implementation environment.

Let $t = t_0$ represent the time instant at which the variable digital multiplier v takes on a value v_0 ², and let t_i (for $i \geq 1$) represent the time instants at which the digital multiplier v undergoes dynamic changes from v_{i-1} to v_i . Moreover, let

$$n_i = \left\lfloor \frac{t_i}{T} \right\rfloor, \quad (5.8)$$

where $\lfloor \cdot \rfloor$ is the floor operator, and where T denotes the sample period. Finally, let the consideration of the changes made to the variable digital multiplier v at time instant t_i be deferred until the completion of the processing of the digital equalizer input signal $x(n_i)$ ³. Then, for $v = v_i$ (or, equivalently, for $n_i + 1 \leq n \leq n_{i+1}$), the shift-variant state-space representation of the digital equalizer as given in Eqns. 5.1 and 5.2 can be decomposed into a series of shift-invariant state-space representations in accordance with

$$\mathbf{q}(n+1) = \mathbf{A}_{n_i+1} \mathbf{q}(n) + \mathbf{b}_{n_i+1} x(n) \quad (5.9)$$

$$y(n) = \mathbf{c}'_{n_i+1} \mathbf{q}(n) + d_{n_i+1} x(n), \quad (5.10)$$

²Basically, v_0 represents the initial value of the variable digital multiplier v

³In this way, the change made to the value of the variable digital multiplier v at the time instant t_i is taken into consideration for the processing of the digital equalizer input signal sample $x(n_i + 1)$

where

$$\mathbf{A}_{n_i+1} = \mathbf{A}(n_i + 1), \quad (5.11)$$

$$\mathbf{b}_{n_i+1} = \mathbf{b}(n_i + 1), \quad (5.12)$$

$$\mathbf{c}'_{n_i+1} = \mathbf{c}'(n_i + 1), \quad (5.13)$$

$$d_{n_i+1} = d(n_i + 1), \quad (5.14)$$

are as obtained from Eqns. 5.3, 5.4, 5.5, and 5.6, respectively. In this way, from Eqns. 5.9 and 5.10 one can obtain the output signal sample $y(n)$ in accordance with

$$y(n) = y_{zi}(n) + y_{zs}(n) \quad \text{for } n_i + 1 \leq n \leq n_{i+1}, i > 1, \quad (5.15)$$

where

$$y_{zi}(n) = \mathbf{c}'_{n_i+1} \mathbf{A}_{n_i+1}^{n-n_i+1} \mathbf{q}(n_i) \quad (5.16)$$

$$y_{zs}(n) = \mathbf{c}'_{n_i+1} \sum_{k=n_i+1}^{n-1} \mathbf{A}_{n_i+1}^{n-1-k} \mathbf{b}_{n_i+1} x(k) + d_{n_i+1} x(n), \quad (5.17)$$

and where $\mathbf{q}(n_i)$ represents the state vector after the completion of the processing of input signal sample $x(n_i)$.

From Eqns. 5.15, 5.16, and 5.17, it can be seen that for the values of the sample index in the interval $n_i + 1 \leq n \leq n_{i+1}$, the Bode-type VA digital equalizer can be considered, essentially, as a linear shift-invariant digital equalizer but with a non-zero initial state vector. Consequently, one can consider the operation of a Bode-type VA digital equalizer consisting of a dynamically-varying variable digital multiplier as a series of linear shift-invariant digital equalizers whose initial state vector values are the final state values of the digital equalizer processed during the previous time interval.

In accordance with the BIBO stability condition developed in the previous chapter, if a general-order VA digital equalizer satisfies the BIBO stability condition given in Eqn. 4.91, then the roots of its characteristic equation are guaranteed to be located inside the unit-circle in the z -plane for all permissible values of the variable digital multiplier v . Consequently, since the roots of the characteristic equation are located inside the unit-circle in the z -plane,

the VA digital equalizer will be not only BIBO stable, but also zero-input stable as well as asymptotically stable [41]. Therefore, under the assumption of infinite-precision arithmetic, and under the assumption that changes in value v_i of the variable digital multiplier v (made at time instants t_i) are deferred until the processing of the input signal sample $x(n_i)$ is completed, the Bode-type VA digital equalizer will remain stable.

5.2.2 Stability under Finite-precision Arithmetic

In the practical implementations of Bode-type VA digital equalizers, the values of the constituent internal signals as well as those of the constituent digital multipliers must be represented in finite-precision. The theoretical analysis of the stability of Bode-type VA digital equalizers with finite-precision internal signals is beyond the scope of this thesis. However, through detailed empirical investigations as well as actual microprocessor hardware implementations of these VA digital equalizers, it has become evident that through the allocation of signal guard bits, the resulting VA digital equalizers will still remain stable when the value of the variable digital multiplier undergoes dynamic changes.

Under the assumption of finite-precision digital multiplier values and infinite-precision internal signals, one can still consider the operation of a Bode-type VA digital equalizer consisting of a single dynamically-varying

variable digital multiplier as a series of linear shift-invariant digital equalizers as discussed in the previous section. However, one must still ensure, (a) that the resulting finite-precision digital multiplier values satisfy the BIBO stability condition developed in Chapter 4, and (b) that the finite-precision counterpart \hat{v} of the variable multiplier v conforms to the permissible range of values for the digital multiplier v in accordance with $\hat{v} \in (V_{Ie}, V_{Fe})$. In this way, if both (a) and (b) are satisfied, then the Bode-type VA digital equalizer will remain stable.

5.3 Analysis of the Transient Behavior of Bode-type VA Digital Equalizers Consisting of a Dynamically-Varying Variable Digital Multiplier

The dynamic variation of the variable digital multiplier in a Bode-type VA digital equalizer will produce unwanted and unavoidable detrimental transient effects in the VA digital equalizer output signal, leading to what is often referred to as “zipper noise”. The zipper noise may become audible when large dynamic changes are made to the value of the variable digital multiplier v , or if a number of dynamic changes are made in quick succession (with time

instants t_i being in close proximity of one another) without allowing the VA digital equalizer to settle down to its steady-state regime.

In order to limit the magnitude of the transients caused by dynamic changes in the variable digital multiplier value, one can use a large number of incremental steps [42] between the desired variable digital multiplier v values in accordance with

$$v = v_i, v_i + \Delta, v_i + 2\Delta, \dots, v_{i+1}, \quad (5.18)$$

where Δ is an incremental step size. In [42], the time-interval t_Δ between the incremental steps was considered from a perceptual point-of-view. In this section, a mathematical approach is developed to estimate the required sample time n_Δ between the incremental steps so as to limit the magnitude of the transients in the output signal to a specified level.

From Eqns. 5.15, 5.16 and 5.17, it can be seen that the output signal $y(n)$ consists of terms of the general form

$$g(n) = F_1 \mathbf{A}^n F_2 \quad (5.19)$$

which essentially represent the output signal transients to be minimized.

From [39], $\mathbf{A}^n \rightarrow 0$ as $n \rightarrow \infty$ if the eigenvalues of \mathbf{A} are located inside

the unit-circle. For a canonical Bode-type VA digital equalizer, i.e. for a VA digital equalizer where the number of the constituent unit-delays equals the order of the digital equalizer, the eigenvalues of \mathbf{A} are the roots of the corresponding characteristic equation. Therefore, for a BIBO stable Bode-type VA digital equalizer, the output signal transients $g(n) \rightarrow 0$ as $n \rightarrow \infty$.

In the following, an analytical expression is developed for the approximation of the time interval n_D (in samples) required for the output signal transients $g(n)$ to reduce to a fraction a of their initial value.

From the Cayley-Hamilton theorem,

$$f(A) = \sum_{k=1}^n f(\lambda_k) \mathbf{E}_k, \quad (5.20)$$

where λ_k (for $k = 1, 2, \dots, N$) are the eigenvalues of \mathbf{A} , where

$$\mathbf{E}_k = e_k(\mathbf{A}), \quad (5.21)$$

and where

$$e_k(z) = \prod_{\substack{j=1 \\ j \neq k}}^n \frac{z - \lambda_j}{\lambda_k - \lambda_j}. \quad (5.22)$$

In this way, one can obtain an expression for \mathbf{A}^n in terms of its eigenvalues

λ_k in accordance with

$$\mathbf{A}^n = \sum_{k=1}^N \lambda_k^n \mathbf{E}_k. \quad (5.23)$$

By substituting Eqn. 5.23 into Eqn. 5.19, and by simplifying the result one obtains

$$g(n) = \sum_{k=1}^N \lambda_k^n c_k, \quad (5.24)$$

where c_k is a constant defined in accordance with

$$c_k = F_1 E_k F_2. \quad (5.25)$$

As discussed above, for a BIBO stable Bode-type VA digital equalizer, $|\lambda_k| < 1$. Therefore, the terms λ_k^n will decay rapidly. This decay rate can be determined (approximately) by examining the largest eigenvalue

$$\lambda_{max} = \max \{ \lambda_k | k = 1, 2, \dots, N \}. \quad (5.26)$$

In this way, the time for $g(n)$ to decay to a fraction a of its original value

can be approximated in accordance with

$$n_{\Delta} = \log_{|\lambda_{max}|} a \quad \text{for } 0 < a < 1. \quad (5.27)$$

In a practical implementation of Bode-type VA digital equalizers, the digital multiplier v will take on a finite number of values (usually stored in memory). Therefore, one must only evaluate Eqn. 5.27 for the corresponding finite number of values for λ_{max} and use the largest value of n_{Δ} as the time interval between changes to the value of the variable multiplier. In addition, depending on the actual value of $|\lambda_{max}|$, it may not be necessary to implement incremental transition steps in practical implementations of Bode-type VA digital equalizers. Due to the sampling rates of high-quality audio products (e.g. 44.1 KHz and 48 KHz), it may be impossible for the user to make changes faster than n_{Δ} sample periods. In such cases, if the user interface of the Bode-type VA digital equalizer does not allow abrupt changes to the value of the variable multiplier (e.g. 1 dB steps only), the Bode-type VA digital equalizer should be relatively immune to "zipper noise".

5.4 Application Example

Let us consider the application of the above results to investigation of the stability and output signal transients associated with the fourth-order VA

digital equalizer introduced in Section 4.6. By using Matlab/Simulink simulations, the values of the variable digital multiplier v were chosen between V_{Ie} and V_{Fe} accordingly, such that the peak amplitude of the effective shaping transfer function varied from -12 dB to $+12$ dB in 1 dB steps. The resulting values for v are given in Table 5.1. The investigation of the stability and output signal transients are included in the following two subsections.

Table 5.1: Coefficient values for variable multiplier v

Magnitude (dB)	v
-12	-0.84309
-11	-0.85237
-10	-0.86240
-9	-0.87315
-8	-0.88461
-7	-0.89683
-6	-0.90977
-5	-0.92341
-4	-0.93769
-3	-0.95255
-2	-0.96796
-1	-0.98383
0	-1.00000
1	-1.01654
2	-1.03321
3	-1.04992
4	-1.06659
5	-1.08305
6	-1.09930
7	-1.11513
8	-1.13054
9	-1.14540
10	-1.15964
11	-1.17324
12	-1.18617

5.4.1 Investigation of Dynamic Stability

To investigate the stability of the above Bode-type VA digital equalizer in the case of dynamically-varying variable digital multiplier v , the input signal $x(n)$ was chosen as a sinusoid of frequency $\omega = 0.45\pi$ which corresponds to the center frequency of the Bode-type VA digital equalizer. Moreover, the value v_i of the variable digital multiplier was set randomly at random time instants t_i . This led to typical simulation results as shown in Figure 5.1, where the dashed lines represent the in-between sample times when the changes in the variable digital multiplier v take place. As observed from Figure 5.1, the Bode-type VA digital equalizer remains stable (as expected).

5.4.2 Investigation of Output Signal Transients

As discussed in Section 5.3, dynamic changes made to the value of the variable digital multiplier v can introduce detrimental output signal transients. A typical output signal $y(n)$ produced by the Bode-type VA digital equalizer is shown in Figure 5.2 when the VA digital equalizer is excited by a sinusoidal input signal $x(n)$, and when the values of the digital multiplier v are changed from V_{Ie} to V_{Fe} in 1 sample time. Evidently, the output signal $y(n)$ exhibits noticeable transients after the value of v is changed.

In order to minimize the output signal transients, one can assign incre-

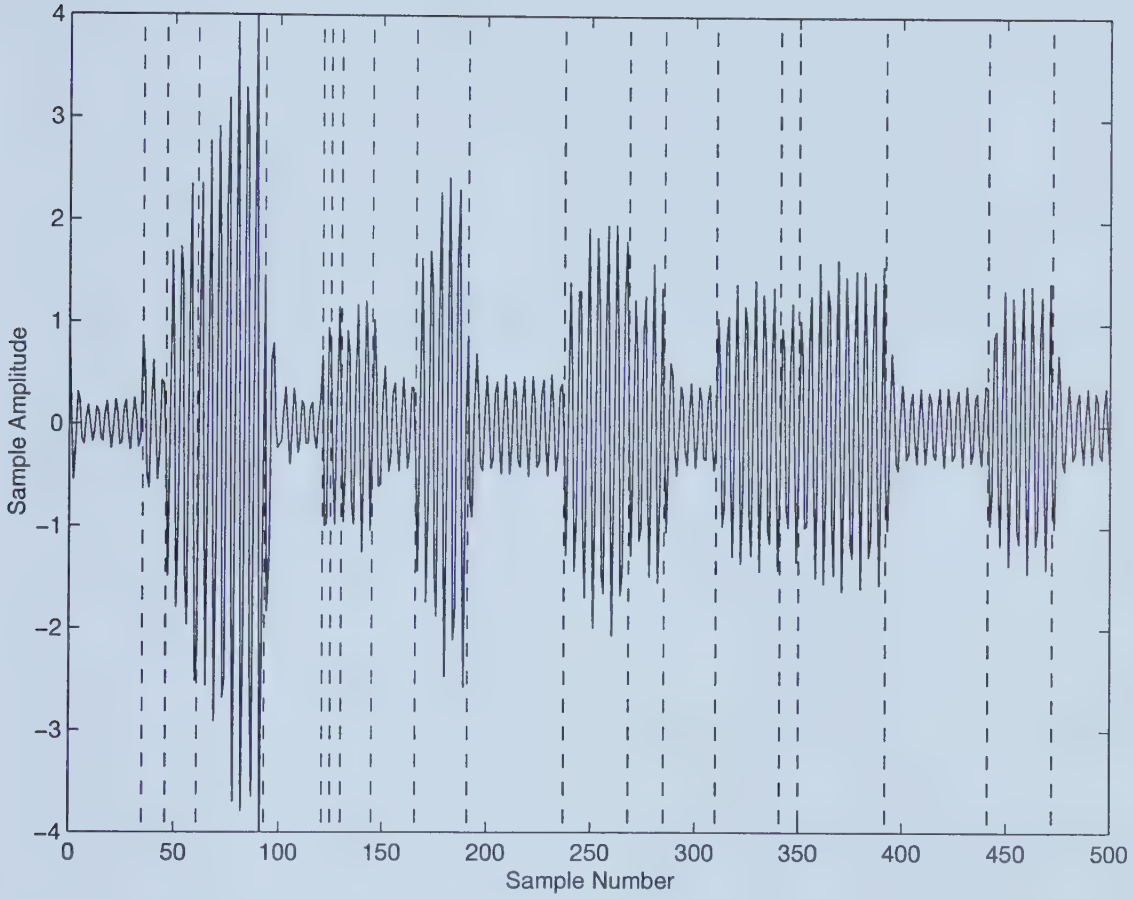


Figure 5.1: Time-domain response of 4th-order Bode-type VA digital equalizer

mental values between V_{Ie} and V_{Fe} to the variable digital multiplier v as discussed in Section 5.3. Moreover, the time interval between incremental steps can be determined by using Eqn. 5.27. By using the values for the variable digital multiplier v as given in Table 5.1, the largest value of $|\lambda_{max}|$ is found to be .91725. If it is required that the output transients be reduced to $a = 0.05$ (i.e. 5 percent) of their initial value, then from Eqn. 5.27 the

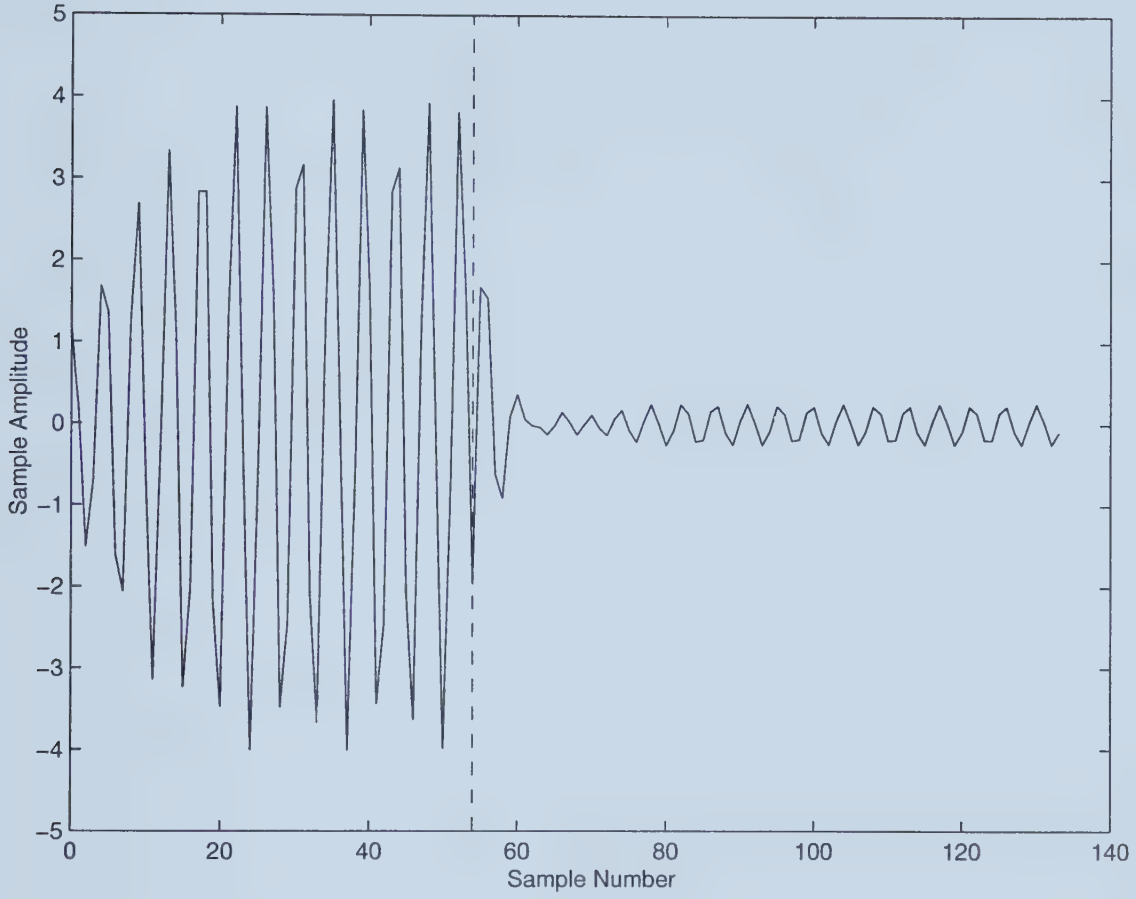


Figure 5.2: Transient output signal

required delay (in samples) is given by

$$n_{\Delta} = \lceil \log_{|\lambda_L|} 0.05 \rceil = 35, \quad (5.28)$$

where $\lceil \cdot \rceil$ is the ceiling operator. This value of n_{Δ} can be verified by examining the decay of the transient response of the Bode-type VA digital equalizer considering a non-zero initial state, as shown in Figure 5.3.

Simulation results for a change in v from V_{Ie} to V_{Fe} using transition steps

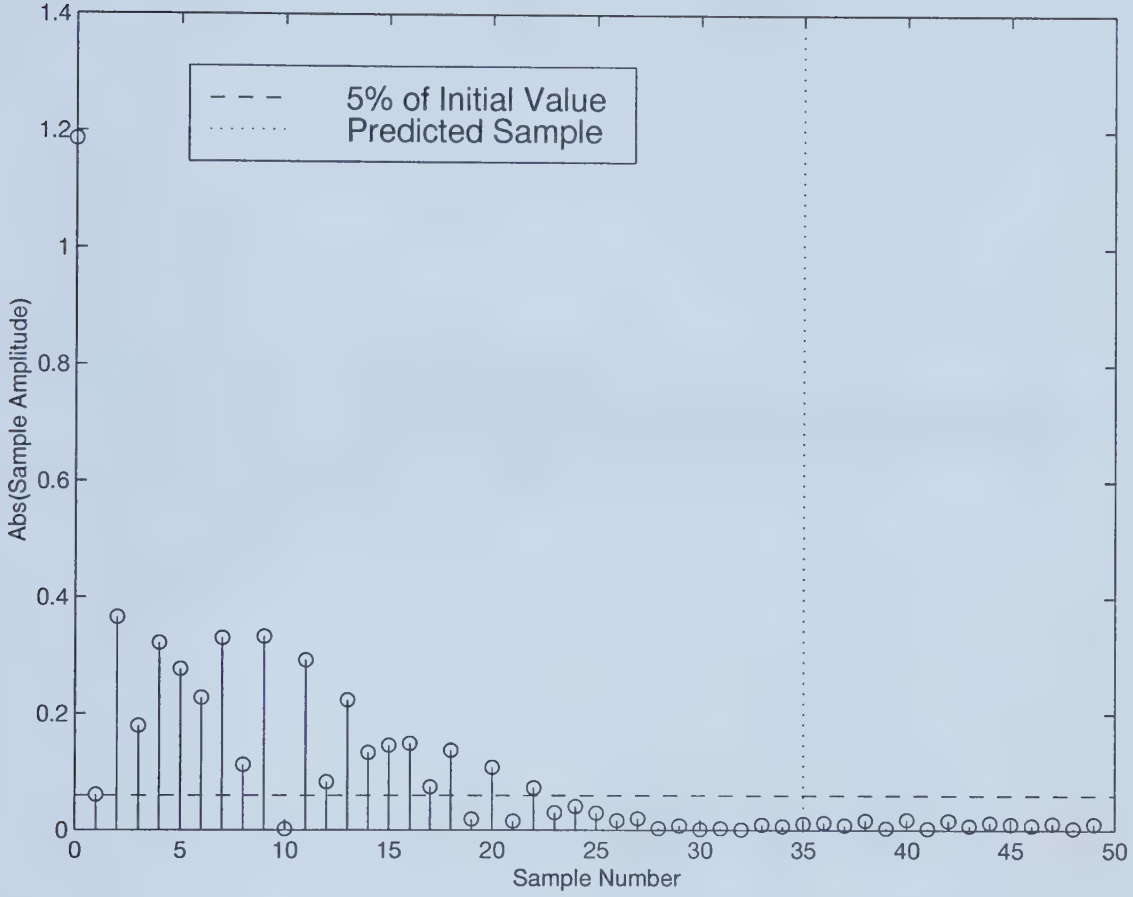


Figure 5.3: Illustration of settling-time verification

separated by $n_{\Delta} = 35$ samples is given in Figure 5.4. Note that transitions between $v_i = V_{Ie}$, $v_i + \Delta$, $v_i + 2\Delta$, \dots , $v_{i+1} = V_{Fe}$, occur much more smoothly as shown in Figure 5.5 (c.f. Figure 5.2). Assuming a sampling frequency of 48 KHz, the actual time between transition steps would be 0.729 ms. Therefore, the worst-case transition time for a change from $v = V_{Ie}$ to $v = V_{Fe}$ in this example (25 total steps) would be 18.2 ms.

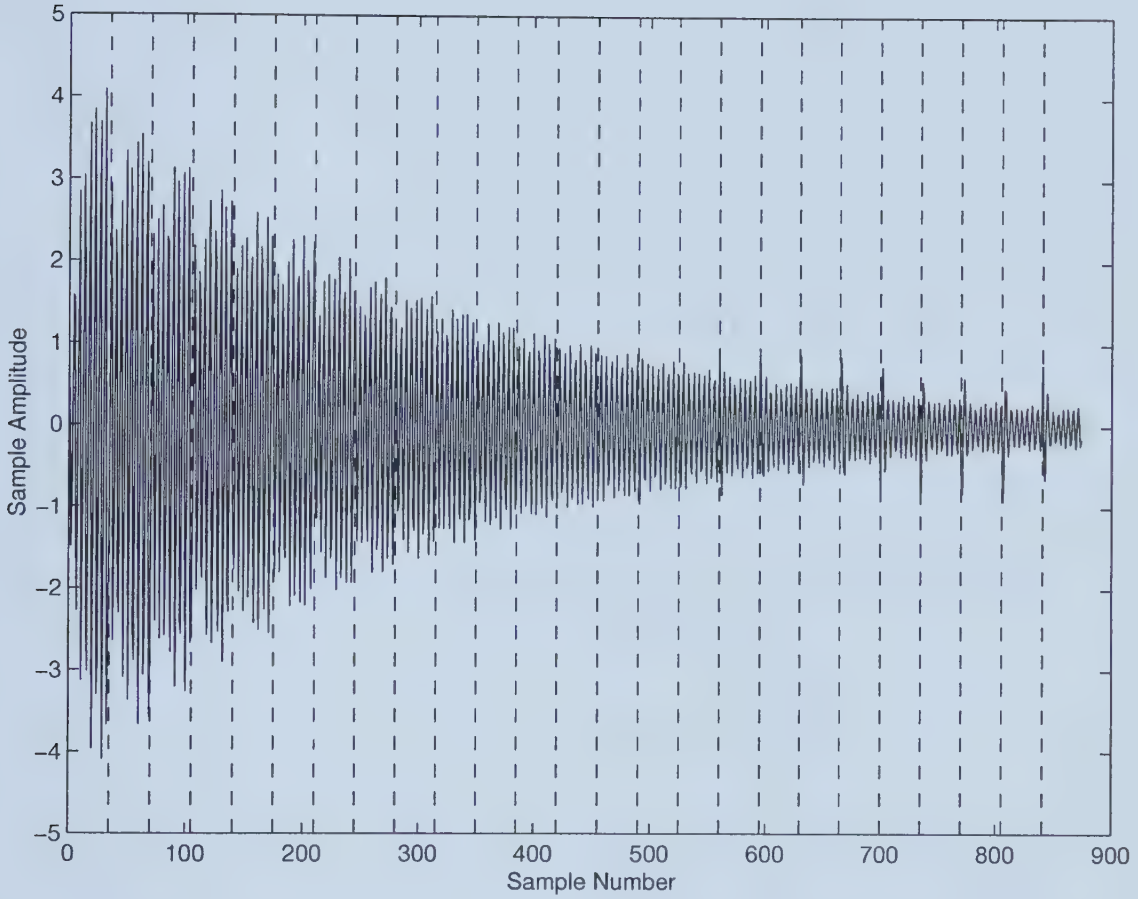


Figure 5.4: Illustration of incremental transition steps

5.5 Conclusions

This chapter has been concerned with the effect of the “dynamic” variations of the variable digital multiplier on the stability and the transient signal behaviour of Bode-type VA digital equalizers. It was shown that the state-space representation of a Bode-type VA digital equalizer consisting of a dynamically-varying variable digital multiplier can be decomposed into a series of shift-invariant state-space representations. This fact was subsequently

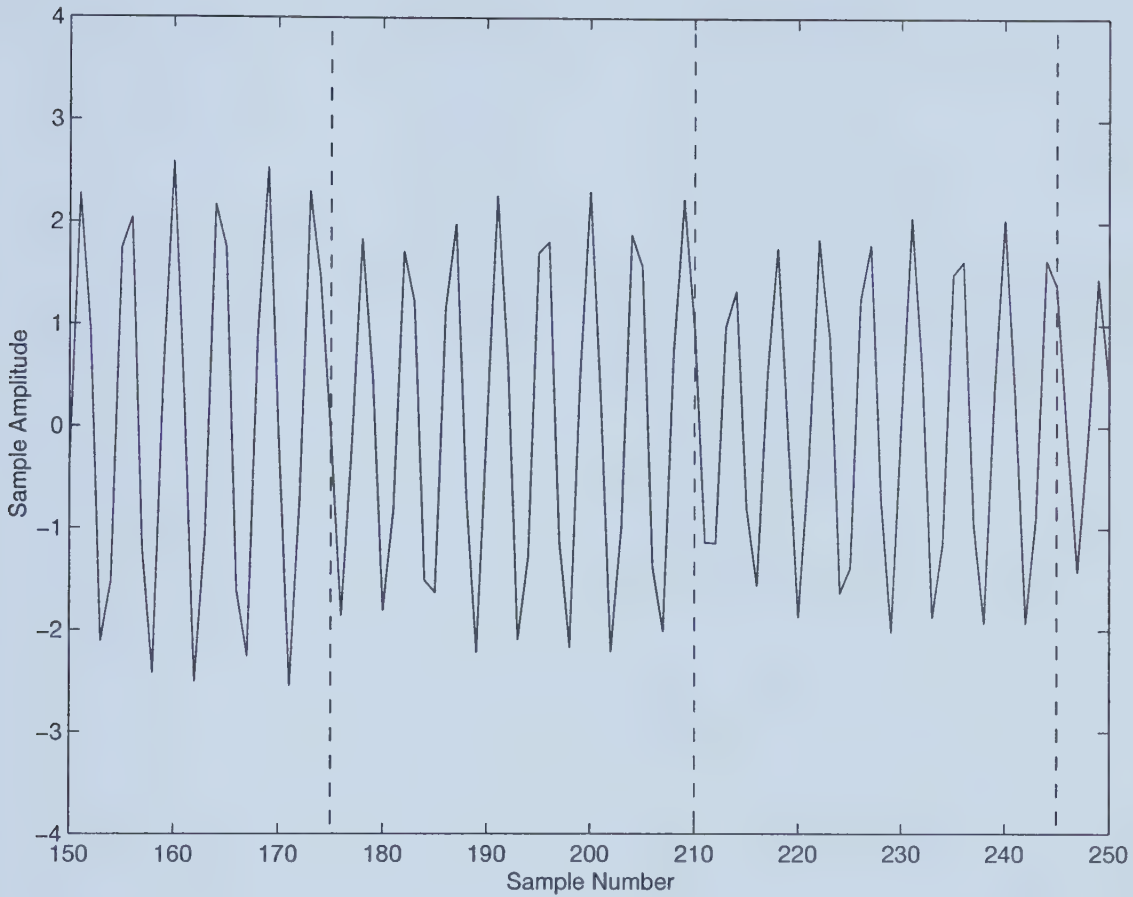


Figure 5.5: Illustration of transitions between incremental steps

exploited for the investigation of the stability of the VA digital equalizer for two different cases, including the case corresponding to infinite precision arithmetic and that corresponding to finite-precision arithmetic hardware implementations of the digital equalizer. In addition, the transient behavior of VA digital equalizers in the presence of a dynamically-varying variable digital multiplier was investigated. By using the state-space representation of the digital equalizer together with Cayley-Hamilton theorem, an analytical approach was developed for the estimation of the time required for the tran-

sients in the output signal produced by the VA digital equalizer to reduce to a specified level.

Chapter 6

Implementation of a Real-Time Multi-Band Digital Graphic Equalizer

6.1 Introduction

In Chapters 3 and 4, the theoretical basis was presented for the design of Bode-type variable-amplitude (VA) digital equalizers using a set of realizability conditions as well as the design of their corresponding effective shaping transfer functions. In the present chapter, these realizability conditions and effective shaping transfer functions are exploited and applied to the design and implementation of a real-time stereo 4-band digital graphic equalizer.

This digital graphic equalizer consists of two subsystems as shown in Figure 6.1: (a) a graphical user interface (GUI) subsystem implemented on an IBM PC (or compatible) running the Microsoft Win32 operating system, and (b) a digital equalizer (DE) subsystem running on a Motorola DSP56002EVM microprocessor board. The GUI subsystem facilitates real-time changes to the values of the variable digital multipliers by the user via a set of 9 sliders (8 band controls and 1 volume control). The DE subsystem, using the resulting variable digital multiplier values, performs CD-quality equalization of a 2-channel (stereo) audio input signal using eight second-order Bode-type VA digital equalizer sections (4 Bode-type VA digital equalizer sections per channel). Value changes are transmitted between subsystems via a parallel interface.

In Section 6.2, a general overview of the DSP56002EVM microprocessor system is given. Section 6.3 is concerned with the design and Motorola DSP56002 implementation of the second-order Bode-type VA digital equalizer sections that form the basis of the DE subsystem. Section 6.4 is concerned with the parallel interface between the two subsystems. Finally, in Section 6.4, the GUI subsystem is presented.

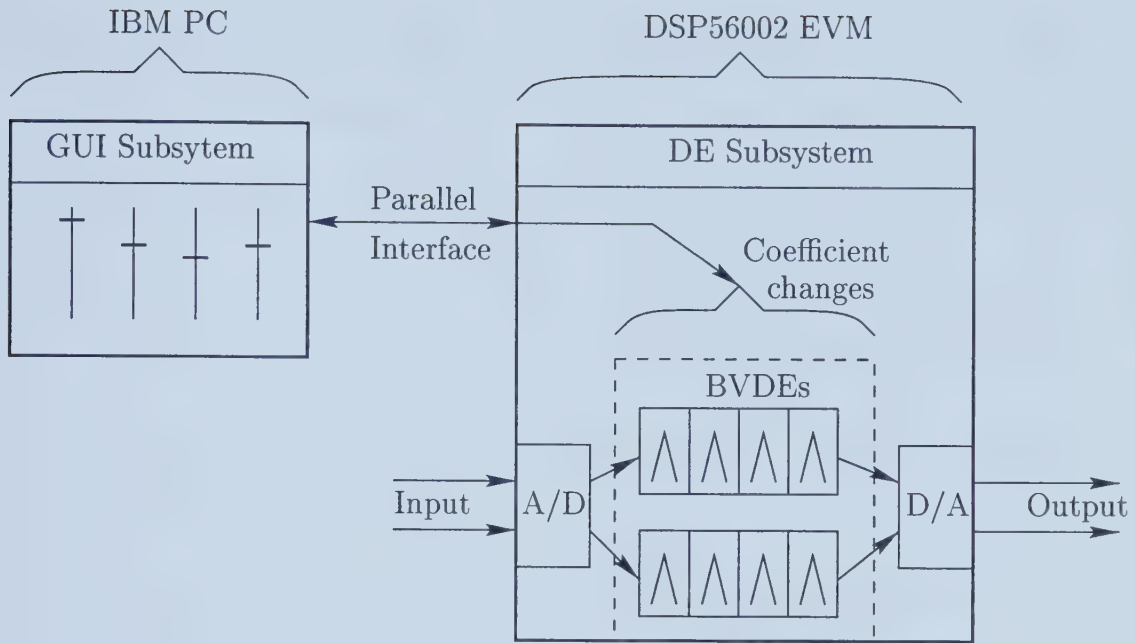


Figure 6.1: Digital graphic equalizer system overview

6.2 Overview of DSP56002EVM Microprocessor System

In this section, a general overview of the DSP56002EVM microprocessor system is given as pertains to the present digital equalizer implementation. The Motorola DSP5600x family of microprocessors was chosen for the digital graphic equalizer implementation due to its wide acceptance by industry and due to its use in numerous digital audio products (e.g. Denon, Yamaha, etc.).

The Motorola DSP56002EVM microprocessor system is based on the DSP56002 24-bit fixed-point digital signal processor [44–46]. The DSP56002 digital signal processor is capable of 20 million instructions per second (MIPS)

with a 50 ns instruction cycle (assuming a 40 MHz clock). The DSP56002 features a Harvard architecture which consists of four internal 24-bit data buses and three 16-bit address buses. Memory is divided into three components which can be accessed simultaneously: (1) Program memory, (2) X data memory, and (3) Y data memory. The DSP56002 comes standard with a 512×24 -bit on-chip program RAM and 256×24 -bit internal RAMs for both X and Y data memories.

The fundamental arithmetic operation of the DSP56002 digital signal processor is the multiply-accumulate (MAC) operation. The constituent data arithmetic logic unit of the DSP56002 consists of [46]: (a) a parallel, single-cycle MAC unit, (b) two 48-bit accumulator registers, (c) two 8-bit accumulator extension registers, (d) an accumulator shifter, (e) four 24-bit input registers, and (f) two data bus shifter/limiter circuits.

The DSP56002 digital signal processor provides a number of on-chip interfaces for external devices. The synchronous serial interface (SSI) provides direct communication with synchronous serial devices such as codecs. The on-chip emulation (OnCE) interface provides access to the processor's internal registers, peripherals, and memory. The DSP56002 also provides an I/O port that can be configured as a general parallel input/output port or as a host interface (HI) for communication with other microprocessors. All of these interfaces are exploited in the implementation of the graphic digital

equalizer system.

In addition to the DSP56002 digital signal processor, the DSP56002EVM system provides a number of additional features as shown in the block diagram given in Figure 6.2: (a) Crystal Semiconductor's CS4215 high-quality stereo sigma-delta A/D and D/A converter for audio input and output (accessed via the SSI interface), (b) $32k \times 24$ -bit external RAM, (c) MC68HC705K1 microcontroller for RS-232 to OnCE command conversion that allows programs to be downloaded, executed, and debugged on the DSP56002 by using an IBM-PC computer and a serial cable, and (d) external port for connection to the standard parallel port on an IBM-PC computer. The external parallel port is used for transmitting changes to the value of the variable digital multiplier from the IBM-PC computer running the user interface to the DSP56002.

6.3 Design and Implementation of the DE Subsystem

In this section, the techniques developed in Chapter 4 for the design of general-order Bode-type VA digital equalizers and their corresponding effective shaping transfer functions are exploited and applied to the design of a lowpass, two bandpass, and a highpass Bode-type VA digital equalizer for

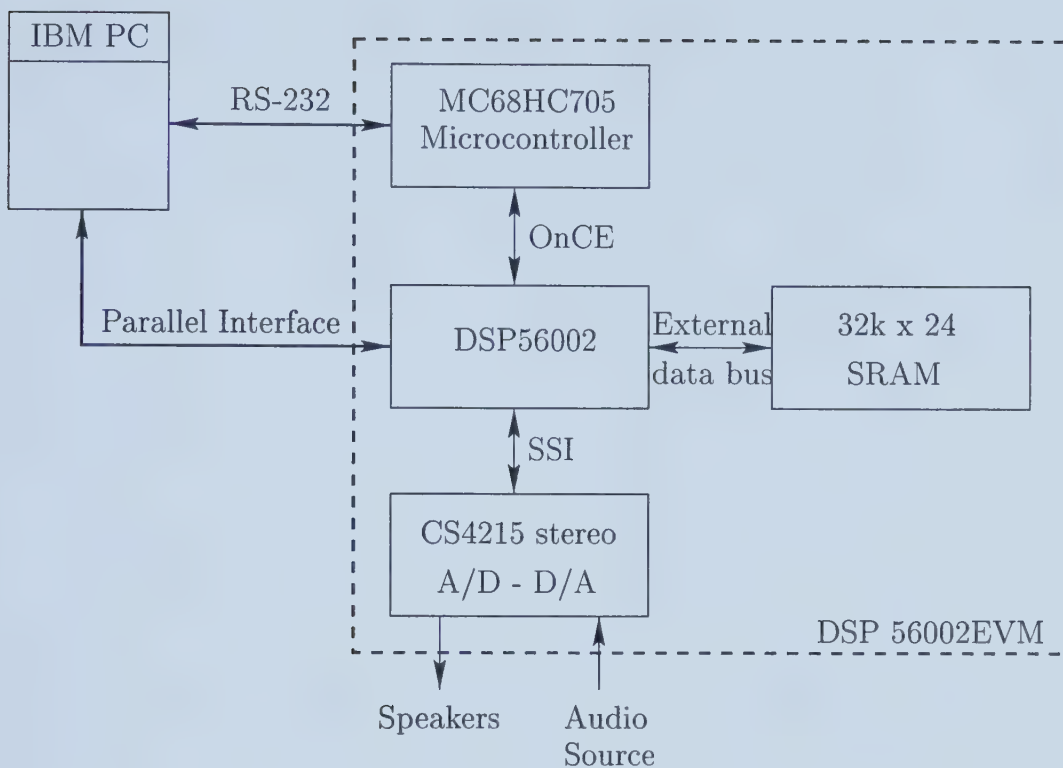


Figure 6.2: Block diagram of DSP56002EVM

use in the DE subsystem.

As observed in Section 4.6, the choice of values

$$V_I = -\infty, \quad V_o = -1, \quad \text{and} \quad V_F = 0. \quad (6.1)$$

leads to the simplified realizability conditions

$$t_{12}(z) = t_{22}(z) - 1 \quad (6.2)$$

$$t_{21}(z) = t_{22}(z) + 1. \quad (6.3)$$

A possible realization of the corresponding second-order Bode-type VA digital equalizer can be obtained as shown in Fig. 6.3. Note that $t_{22}(z)$ has been implemented using a Direct Form II realization, which lends itself to exploitation of the DSP56002's MAC architecture. Moreover, this single general structure can be used to implement lowpass, bandpass, and highpass Bode-type VA digital equalizers.

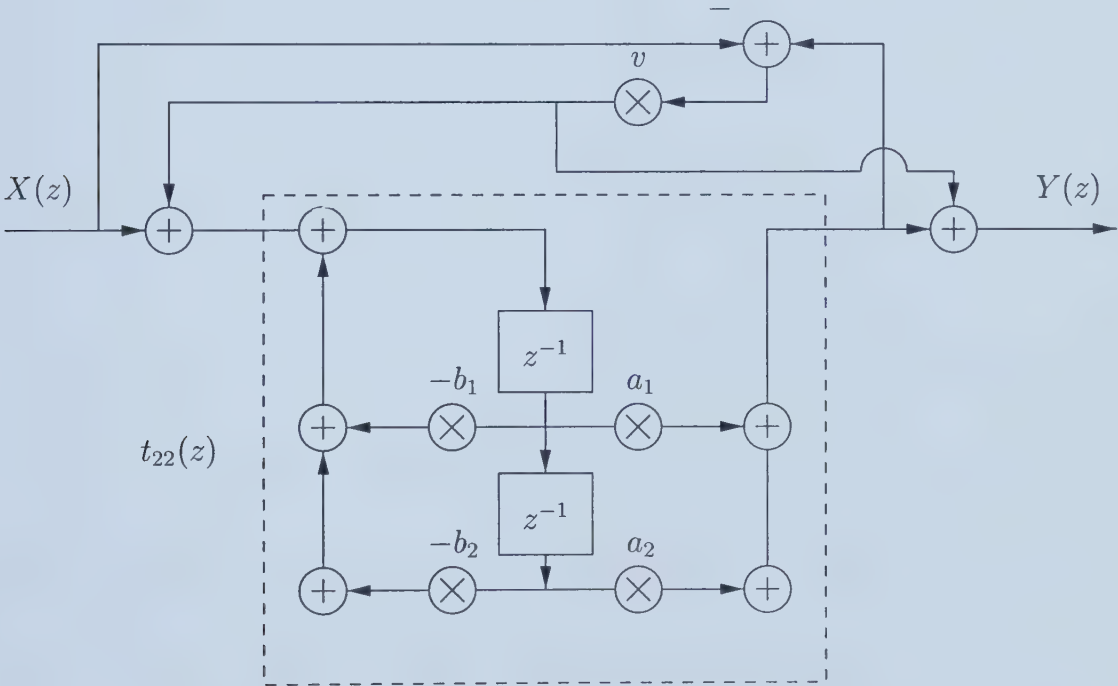


Figure 6.3: Schematic diagram for 2nd-order Bode-type VA digital equalizer

The magnitude-frequency responses of the desired shaping transfer functions $T_{se}(z)$ to be used in the DE subsystem are shown in Figure 6.4. Using the results of Section 4.4.2, the corresponding maximally flat shaping transfer functions $T_{se}(z)$ for Band 1, Band 2, Band 3, and Band 4 can be found

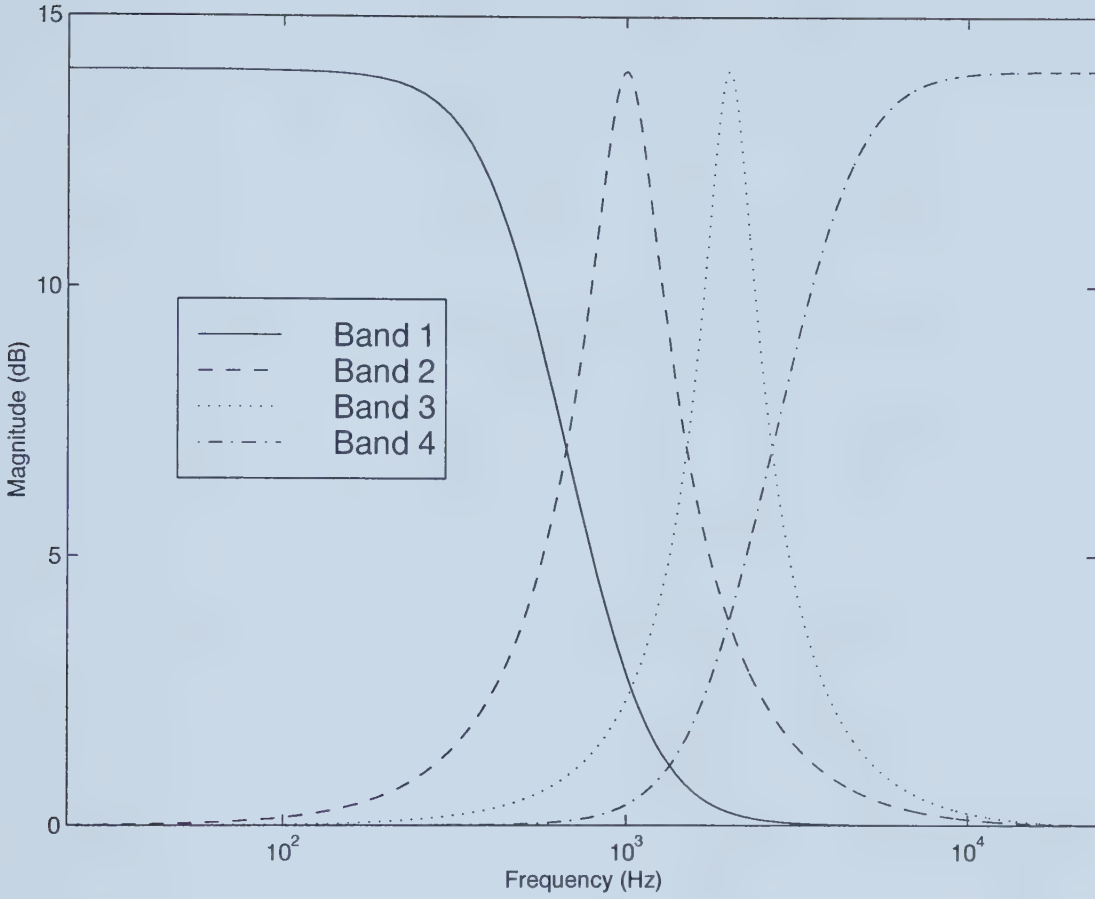


Figure 6.4: Desired DE subsystem response

in Tables 6.1, 6.2, 6.3, and 6.4, respectively. Note that $T_{se}(z)$ for all four

Table 6.1: Band 1 $T_{se}(z)$ coefficient values

i	α_i	β_i
0	1.052335	1
1	-1.910973	-1.917531
2	0.875020	0.920799

bands are minimum-phase BIBO-stable transfer functions that satisfy the BIBO stability condition developed in Section 4.5.2 (c.f. Eqn 4.91). Consequently, the resulting Bode-type VA digital equalizers are guaranteed to be

Table 6.2: Band 2 $T_{se}(z)$ coefficient values

i	α_i	β_i
0	1.095504	1
1	-1.935668	-1.935668
2	0.856884	0.952389

Table 6.3: Band 3 $T_{se}(z)$ coefficient values

i	α_i	β_i
0	1.132573	1
1	-1.867884	-1.867884
2	0.801336	0.933909

BIBO stable over the effective range of their variable digital multipliers v .

The effective range of the variable multiplier of each band can be determined by substituting Eqn. 6.1 into Eqns. 4.10 and 4.16 to obtain

$$V_{Fe} = -\alpha_0 \quad (6.4)$$

$$V_{Ie} = \frac{1}{V_{Fe}}. \quad (6.5)$$

By invoking Eqn. 4.92 in Eqns. 4.11 and 4.12, one obtains

$$a_i = \frac{\alpha_0 \beta_i - \alpha_i}{\alpha_0^2 - 1} \quad (6.6)$$

$$b_i = \frac{\alpha_0 \alpha_i - \beta_i}{\alpha_0^2 - 1}. \quad (6.7)$$

Then, the coefficients of $t_{22}(z)$, V_{Ie} and V_{Fe} can be obtained from the specified coefficients of $T_{se}(z)$ as given in Tables 6.5, 6.6, 6.7, 6.8 for Bands 1, 2, 3 and

Table 6.4: Band 4 $T_{se}(z)$ coefficient values

i	α_i	β_i
0	4.101127	1
1	-6.851324	-1.289778
2	2.943183	0.482765

4, respectively.

Table 6.5: Band 1 Bode-type VA digital equalizer coefficient values

i	a_i	b_i
1	-0.995363	-0.870075
2	0.874862	0.000149
$V_{Ie} = -1.052336$		$V_{Fe} = -0.950267$

Table 6.6: Band 2 Bode-type VA digital equalizer coefficient values

i	a_i	b_i
1	-0.923724	-0.923724
2	0.931703	-0.068296
$V_{Ie} = -1.095504$		$V_{Fe} = -0.912821$

Finally, by simple numerical optimization, the intermediate values of the variable multiplier v between V_{Ie} and V_{Fe} corresponding to 1 dB steps in the Bode-type VA digital equalizer magnitude-frequency response can be obtained as given in Table 6.9.

The DSP56002 assembly code implementing the above Bode-type VA digital equalizers can be found in Appendix B.

Table 6.7: Band 3 Bode-type VA digital equalizer coefficient values

i	a_i	b_i
1	-0.975883	-0.875883
2	0.906843	-0.093156
$V_{Ie} = -1.132573$		$V_{Fe} = -0.882945$

Table 6.8: Band 4 Bode-type VA digital equalizer coefficient values

i	a_i	b_i
1	0.098726	-1.694668
2	-0.060894	0.732500
$V_{Ie} = -0.243835$		$V_{Fe} = -4.101127$

6.4 Development of Parallel Interface

In this section, a brief overview is given of the parallel interface protocol designed and implemented for the transmission of changes to the variable digital multipliers from the GUI (on an IBM-PC) to the DSP56002EVM system.

As discussed in the previous chapter, the changes to the value v_i of the variable digital multiplier should be deferred until after the processing of the current sample n_i is complete so as to ensure stability of the Bode-type VA digital equalizer. In this way, the DE subsystem checks for a change in the GUI after the complete processing of the current audio sample. Note that this approach differs from the traditional polling or interrupt driven schemes used in conventional digital graphic equalizers [3].

When a slider in the GUI is changed by the user, it is necessary to transmit the slider number (1 byte) and slider value (1 byte) from the GUI to

the DSP56002EVM in the time interval between samples. To this end, a parallel interface was chosen instead of a serial interface to satisfy the time requirement. Moreover, a handshaking protocol was developed for the parallel interface so that data could be transmitted reliably and efficiently.

The implemented parallel interface requires that the parallel port on the IBM-PC computer be configured for bidirectional transmission and that Port B of the DSP56002 be configured for general purpose I/O. The interface consists of 8 data lines and three control lines: (a) *INI* which is used by the IBM-PC to indicate that it has data to transmit to the DSP56002EVM, (b) *STR* which is used by the IBM-PC to indicate that data has been placed on the data lines, and (c) *ACK* which is used by the DSP56002EVM system for acknowledgement purposes during various stages of handshaking. The handshaking protocol for the IBM-PC and the DSP56002EVM is given in Figures 6.4 and 6.4, respectively. The code for implementing this protocol on the IBM-PC and DSP56002EVM can be found in Appendices C and B.

6.5 The GUI Subsystem

The GUI subsystem was implemented on the IBM-PC using the TCL/TK toolkit [47–50] and Microsoft Visual C++ version 5.0. The use of TCL/TK facilitated the rapid development of the user interface for the Microsoft

- Step ①:** Set $INI = 1$ and $STR = 1$ to indicate that data is available
- Step ②:** Wait for $ACK = 1$ from the DSP56002EVM
- Step ③:** Write 1 data byte to data lines
- Step ④:** Set $STR = 0$ to indicate that data is available on the data lines.
- Step ⑤:** Wait for $ACK = 0$
- Step ⑥:** If more data to transmit then set $STR = 1$ and go to **Step ②**. Else set $INI = 0$.

Figure 6.5: Transmission protocol (IBM-PC side)

- Step ①:** After processing of current audio sample, check if $INI = 1$. If not, then process next audio sample. Else go to **Step ②**.
- Step ②:** Set $ACK = 1$ to indicate readiness to receive data.
- Step ③:** Wait for $STR = 0$
- Step ④:** Read 1 data byte from data lines.
- Step ⑤:** Set $ACK = 0$
- Step ⑥:** If $STR = 1$ then go to **Step ②**. Else data transfer complete.

Figure 6.6: Transmission protocol (DSP56002EVM side)

Win32 operating system. An example of the GUI subsystem is given in Figure 6.5. The digital graphic equalizer can be controlled by simply dragging the slider bars with the mouse. The source code for the GUI subsystem can be found in Appendix C.

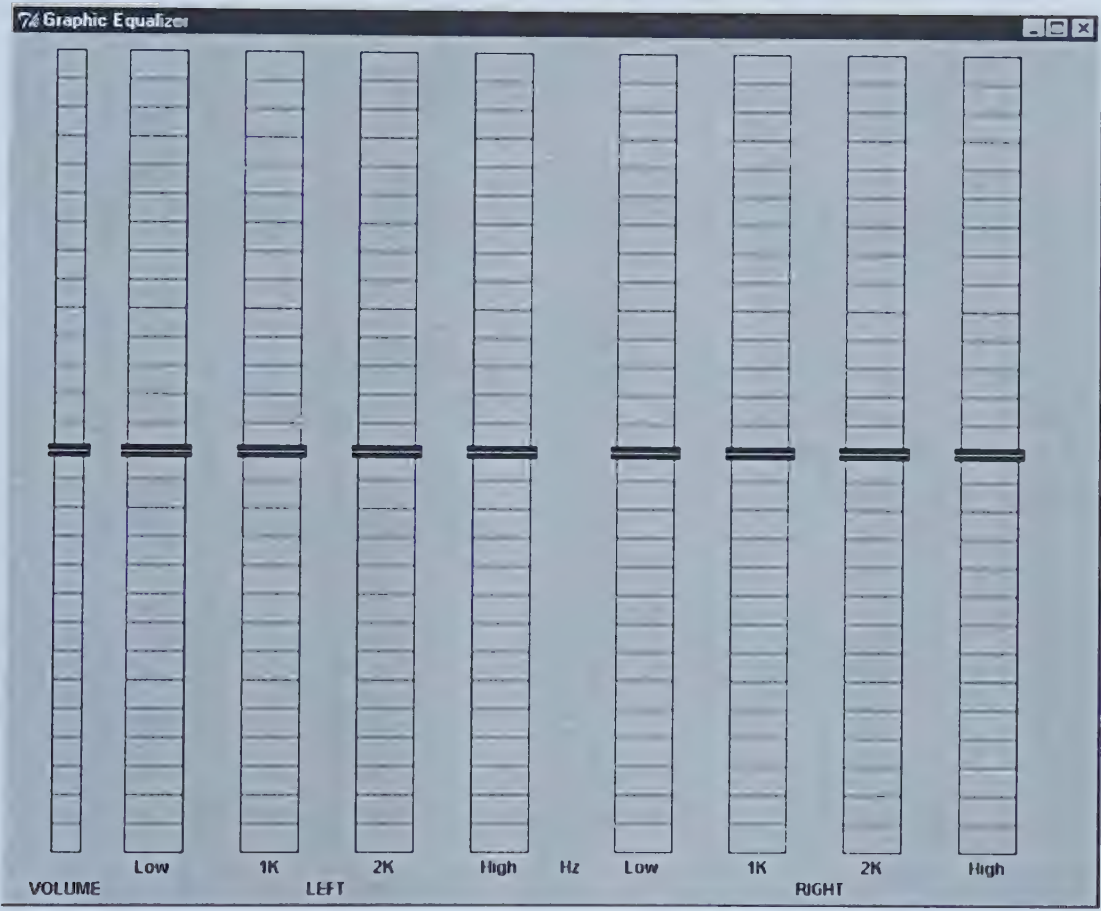


Figure 6.7: Digital graphic equalizer GUI

6.6 Conclusions

This chapter has presented the design and implementation of a real-time stereo 4-band digital graphic equalizer achieved by exploiting, (a) the realizability conditions for Bode-type VA digital equalizers developed in Chapter 3, and (b) the general-order design technique and the corresponding shaping transfer function approximations developed in Chapter 4. The resulting digital graphic equalizer provides CD-quality equalization of a 2-channel (stereo) audio input signal by using eight second-order Bode-type VA digital equalizer sections (4 Bode-type VA digital equalizer sections per channel). Subjective listening tests have confirmed the quality of the processed audio signals as well as the absence of zipper noise.

Table 6.9: Bode-type VA digital equalizer variable digital multiplier v values

Magnitude (dB)	Band 1	Band 2	Band 3	Band 4
14	-1.052333	-1.095504	-1.132572	-4.101127
13	-1.049667	-1.090543	-1.125571	-3.734908
12	-1.046808	-1.085232	-1.118089	-3.395481
11	-1.043753	-1.079572	-1.110132	-3.082320
10	-1.040505	-1.073569	-1.101711	-2.794254
9	-1.037068	-1.067234	-1.092845	-2.530010
8	-1.033450	-1.060585	-1.083560	-2.288251
7	-1.029663	-1.053644	-1.073892	-2.067598
6	-1.025720	-1.046440	-1.063885	-1.866659
5	-1.021640	-1.039010	-1.053590	-1.684048
4	-1.017443	-1.031392	-1.043065	-1.518406
3	-1.013154	-1.023633	-1.032374	-1.368415
2	-1.008798	-1.015780	-1.021586	-1.232809
1	-1.004404	-1.007885	-1.010770	-1.110383
0	-1.000000	-1.000000	-1.000000	-1.000000
-1	-0.995615	-0.992176	-0.989343	-0.900589
-2	-0.991278	-0.984464	-0.978869	-0.811155
-3	-0.987016	-0.976912	-0.968640	-0.730772
-4	-0.982855	-0.969562	-0.958712	-0.658585
-5	-0.978818	-0.962454	-0.949135	-0.593807
-6	-0.974924	-0.955620	-0.939950	-0.535716
-7	-0.971191	-0.949086	-0.931191	-0.483652
-8	-0.967631	-0.942875	-0.922883	-0.437014
-9	-0.964256	-0.937000	-0.915042	-0.395255
-10	-0.961071	-0.931472	-0.907678	-0.357877
-11	-0.958080	-0.926292	-0.900793	-0.324430
-12	-0.955284	-0.921461	-0.894382	-0.294509
-13	-0.952682	-0.916974	-0.888437	-0.267744
-14	-0.950269	-0.912821	-0.882945	-0.243835

Chapter 7

Conclusions

7.1 Review of Material Presented

This thesis has been concerned with the design and implementation of Bode-type variable-amplitude (VA) digital equalizers.

In Chapter 2, a synthesis technique for the design of first- and second-order Bode-type wave-digital VA equalizers was presented. The proposed first-order equalizer consists of one unit-delay and two digital multipliers and produces a fan-shaped magnitude-frequency response, while the proposed second-order equalizer consists of two unit-delays and three digital multipliers and produces a bump-shaped magnitude-frequency response. The salient feature of the resulting WD equalizers is that only one single variable digital multiplier is required to control the fan amplitude in the first-order equalizer

and the bump amplitude in the second-order equalizer without changing their other important magnitude-frequency response characteristics (e.g. the cut-off frequency in the fan equalizer and the center frequency and quality factor in the bump equalizer). Moreover, it was shown that these equalizers remain BIBO stable (under infinite-precision arithmetic) for all possible values of the variable digital multiplier. Application examples were given to illustrate the main results.

In Chapter 3, a novel approach was presented for the direct discrete-time z -domain design and enumeration of Bode-type VA digital equalizers. The salient feature of the proposed approach is threefold: (1) it does not make any recourse to the concept of a continuous-time s -domain prototype analog network or its transfer function, (2) it ensures that the frequency response of the resulting VA digital equalizers can be varied from that of an shaping transfer function, to its inverse for arbitrary shaping transfer functions, and (3) it only requires one single variable digital multiplier (of course, in addition to the required usual fixed digital multipliers). This approach was subsequently applied to the design and enumeration of two classes of second-order bump VA digital equalizers, one class including digital equalizers operating under infinite-precision arithmetic and the other including digital equalizers operating under finite-precision arithmetic operations.

In Chapter 4, a new approach was presented for the design of arbitrary-

order Bode-type VA digital equalizers which eliminates the constraint between the range of variable digital multiplier values and the shaping transfer function. This approach is based on replacing the conventional shaping transfer function with an effective shaping transfer function. The main salient feature of this approach is that it leads to a substantial simplification in the realizability conditions associated with the VA digital equalizer, and, in turn, leads to a reduction in the cost of the corresponding hardware implementation of the digital equalizer. In addition, a novel approximation technique was presented for the design of general-order shaping transfer functions with maximally flat or equiripple lowpass, highpass, or bandpass magnitude-frequency response characteristics. This was achieved by first deriving a corresponding normalized prototype lowpass shaping transfer function, and then by applying a lowpass-to-lowpass, lowpass-to-highpass, or lowpass-to-bandpass frequency transformation to obtain the desired (denormalized) shaping transfer function. These shaping transfer functions can be employed in the design of VA digital equalizers having magnitude-frequency responses with sharp transition bands and reduced interband interference in the corresponding digital graphic equalizers. Finally, the theoretical basis of Kharitonov's stability theorem was used for the development of a novel BIBO stability condition for general-order Bode-type VA digital equalizers.

In Chapter 5, the effect of the “dynamic” variations of the variable digital

multiplier on the stability and the transient signal behaviour of Bode-type VA digital equalizers was investigated. It was shown that the state-space representation of a Bode-type VA digital equalizer consisting of a dynamically-varying variable digital multiplier can be decomposed into a series of shift-invariant state-space representations. This fact was exploited for the investigation of the stability of the VA digital equalizer for two different cases, including the case corresponding to infinite precision arithmetic and that corresponding to finite-precision arithmetic hardware implementations of the digital equalizer. In addition, the transient behavior of VA digital equalizers in the presence of a dynamically-varying variable digital multipliers was investigated. By using the state-space representation of the digital equalizer together with Cayley-Hamilton theorem, an analytical approach was developed for the estimation of the time required for the transients in the digital equalizer output signal to reduce to a specified level. The results of the chapter were illustrated through an application example.

Finally, in Chapter 6, the realizability conditions for Bode-type VA digital equalizers together with the shaping transfer function approximations developed in previous chapters were exploited and applied to the design and implementation of a real-time stereo 4-band digital graphic equalizer. This digital graphic equalizer consists of two subsystems: (a) a graphical user interface (GUI) subsystem implemented on an IBM PC (or compatible)

running the Microsoft Win32 operating subsystem, and (b) a digital equalizer (DE) subsystem running on a Motorola DSP56002EVM microprocessor board. The GUI subsystem facilitates real-time changes to the variable digital multiplier values by the user via a set of 9 sliders (8 band controls and 1 volume control). The DE subsystem performs CD-quality equalization of a 2-channel (stereo) audio input signal using eight second-order Bode-type VA digital equalizer sections (4 Bode-type VA digital equalizer sections per channel).

7.2 Contribution of the Thesis

To the best of the author's knowledge, the following contributions of the present thesis are original.

7.2.1 Chapter 2

- The first-order wave-digital (WD) equalizer consisting of one unit-delay and two digital multipliers capable of realizing both lowpass and high-pass fan-shaped magnitude-frequency response characteristics.
- The fully WD second-order equalizer consisting of two unit-delays and three digital multipliers that realizes a bump-shaped magnitude-frequency response.

- The proof of the BIBO stability of the above WD equalizers under infinite-precision arithmetic for all possible values of the variable digital multiplier.

7.2.2 Chapter 3

- The three realizability conditions for Bode-type VA digital equalizers.
- The novel approach to the direct discrete-time z -domain design and enumeration of VA digital equalizers using the above realizability conditions.
- The class of 14 distinct VA digital equalizers operating under infinite-precision arithmetic operations.
- The class of 40 distinct VA digital equalizers operating under finite-precision operations.
- The BIBO stability condition for second-order Bode-type VA digital equalizers.

7.2.3 Chapter 4

- The approach for the design of arbitrary-order Bode-type VA digital equalizers which eliminates the interdependence between the range

of variable digital multiplier values and the shaping transfer function (accomplished by replacing the conventional shaping transfer function with an effective shaping transfer function).

- The general-order shaping transfer function approximations suitable for Bode-type VA digital equalizers.
- The BIBO stability condition for use in the realization general-order Bode-type VA digital equalizers.

7.2.4 Chapter 5

- The proof of the fact that under infinite-precision arithmetic operation, Bode-type VA digital equalizers remain BIBO stable if changes to the variable digital multiplier are deferred until the processing of the current input sample is completed.
- The analytical approach for the estimation of the time required for the transients in the digital equalizer output signal to reduce to a specified level.

7.2.5 Chapter 6

- The implementation of a CD-quality real-time stereo 4-band digital graphic equalizer using Bode-type VA digital equalizers.

7.3 Proposed Areas of Future Investigation

In Chapter 6, a digital graphic equalizer was developed and implemented, demonstrating the viability of Bode-type VA digital equalizers for digital audio applications. The same type of digital graphic equalizer based on Bode-type VA digital equalizers could find applications in hearing aids. To date, Bode-type VA digital equalizers have attracted some industrial interest for possible use in hearing aids. Further investigation into hearing aid requirements and issues could be useful in adapting this technology for use in hearing aids.

Another area for future investigation is that of audio equalization using multi-rate filter banks. Multi-rate filter banks have recently found widespread use in audio coding and compression based on perceptual criteria. However, their possible application to audio equalization has not been fully investigated. Moreover, further investigation should be undertaken into the “fusion” of audio equalization and audio compression into a single operation via multi-rate filter banks.

This thesis has focused primarily on the application of Bode-type VA digital equalizers to audio equalization. However, the application of these digital equalizers to other fields such as communications warrants further investigation. In particular, the application of Bode-type VA digital equalizers

to the equalization of communication channels over twisted pair cable could prove to be quite promising. For example, Bode-type VA digital equalizers could be potentially used in Discrete Multi-tone (DMT) systems [51, 52] to compensate for the change in channel characteristics of twisted pair cable due to temperature variations. Another possible application of Bode-type VA digital equalizers is in the equalization of Ethernet twisted pair cables to compensate for the loss due to the length of the cable.

In Chapter 4, a BIBO stability condition was developed for Bode-type VA digital equalizers under the assumption that only the value of the variable digital multiplier changed and that the remaining fixed multipliers remained constant at all times. Further investigation into the BIBO stability of VA digital equalizers under the assumption that the fixed digital multipliers undergo occasional changes in value would be useful in situations where the design specifications of the VA digital equalizer (e.g. centre frequency) change in real-time. Moreover, further investigation is warranted into the techniques used in the development of the BIBO stability condition for VA digital equalizers and their application to more general discrete-time digital filters with variable digital multipliers.

Finally, in Chapter 5, the dynamic stability of Bode-type VA digital equalizers with variable coefficients under finite-precision arithmetic was investigated under the simplifying assumption of infinite-precision signal wordlength.

However, in practical implementations, both signal and coefficient wordlengths will be finite. The effect of variable coefficients on the stability of such finite-precision digital systems has been relatively unexplored. Further investigation of finite-precision stability would find applications not only in Bode-type VA digital equalizers, but other applications such as adaptive signal processing, etc.

Bibliography

- [1] D.A. Bohn, “Constant-Q Graphic Equalizers”, *J. Audio Eng. Soc.*, vol. 34, pp. 611–626, Sept. 1986.
- [2] P. Regalia and S. Mitra, “Tunable Digital Frequency Response Equalization Filters”, *IEEE Transactions on Acoustics, Speech, and Signal Processing*, vol. ASSP-35, no. 1, pp. 118–120, Jan. 1987.
- [3] Motorola, *Digital Stereo 10-Band Graphic Equalizer Using the DSP56001*, vol. Application Note APR2/D, Motorola Inc., 1988.
- [4] B. Hardman, “Designing Digits into Audio Equalization”, *Electronics World*, pp. 998–1023, December 1991.
- [5] J. Henriquez, “A Phase Linear Audio Equalizer - Design and Implementation”, *Journal of the Audio Engineering Society*, vol. 38, pp. 653–664, September 1990.

- [6] P. H. Kraght, “A Linear Phase Digital Equalizer with Cubic-Spline Frequency Response”, *Journal of the Audio Engineering Society*, vol. 40, pp. 403–414, May 1992.
- [7] D. Massie, “Engineering Study of Four-Multiply Normalized Ladder Filter”, *J. Audio Eng. Soc.*, vol. 41, no. 7/8, pp. 564–582, July/August 1993.
- [8] S. A. White, “Design of Digital Biquadratic Filter Section for Parametric Filters”, *J. Audio Eng. Soc.*, vol. 34, no. 6, pp. 479–483, June 1986.
- [9] D. J. Shpak, “Analytic Design of Digital Biquadratic Filter Sections for Parametric Filters”, *J. Audio Eng. Soc.*, vol. 40, no. 11, pp. 876–885, Nov. 1992.
- [10] H.W. Bode, “Variable Equalizers”, *Bell Syst. Tech. J.*, vol. 17, pp. 229–244, April 1938.
- [11] F. Brglez, “Inductorless Variable Equalizers”, *IEEE Trans. on Circuits and Systems*, vol. CAS-22, pp. 415–419, May 1975.
- [12] F. Brglez, “Minimally Active RC Variable Equalizers”, *IEEE Trans. on Circuits and Systems*, vol. CAS-22, pp. 688–691, August 1975.

- [13] H.S. Malvar, “Active-RC Variable Equalizers with Minimum Number of Operational Amplifiers”, *IEEE Trans. on Circuits and Systems*, vol. CAS-30, pp. 496–500, July 1983.
- [14] M. Zyoute, “New Active RC Bode-Type Variable Equalizer”, *Proc. Inst. Elect. Eng.*, vol. 128, no. G, pp. 134–137, June 1981.
- [15] W. Saraga, “Some New Active Variable Equalizer Circuits”, in *Proceedings of the 1978 International Symposium on Circuits and Systems*, New York, U.S.A, 1978, pp. 141–145.
- [16] A. Fuller and B. Nowrouzian, “Design of First- and Second-Order Bode-Type Wave-Digital Variable-Amplitude Equalizers”, *Canadian Journal of Electrical and Computer Engineering*, vol. 23, no. 4, pp. 155–162, October 1998.
- [17] A. Fettweis, “Wave Digital Filters: Theory and Practice”, *Proceedings of the IEEE*, vol. 73, no. 2, pp. 270, Feb. 1988.
- [18] B. Nowrouzian and L.S. Lee, “Design of Bode-Type Wave Digital Variable Equalizers”, in *Proceedings of the 1988 Midwest Symposium on Circuits and Systems*, Sept. 1997, pp. 72–75.
- [19] A. Antoniou, *DIGITAL FILTERS Analysis, Design, and Applications*, McGraw-Hill Inc., New Jersey, 1975.

- [20] C.H. Houpis and G.B. Lamont, *DIGITAL FILTERS Analysis, Design, and Applications*, McGraw-Hill Inc., New York, 1992.
- [21] A.V. Oppenheim and R.W. Schaffer, *Discrete-time Signal Processing*, Prentice-Hall Inc., New Jersey, 1989.
- [22] E.C. Ifeachor and B.W. Jervis, *Digital Signal Processing: A Practical Approach*, Addison-Wesley Inc., Reading, Massachusetts, 1993.
- [23] A. Fuller and B. Nowrouzian, "Novel Realizability Conditions for the Exact Design of Second-Order Bode-Type Variable-Amplitude Digital Equalizers", in *Proceedings of the 1997 International Symposium on Circuits and Systems*, Hong Kong, June 1997, pp. 2220–2223.
- [24] A. Fuller and B. Nowrouzian, "A Novel Approach to the Design and Enumeration of Bode-Type Variable-Amplitude Digital Equalizers", in *Proceedings of the 1996 Midwest Symposium on Circuits and Systems*, Aug. 1996, pp. 719–722.
- [25] A. Fuller and B. Nowrouzian, "A New Set of Design and Realizability Conditions for Bode-Type Variable-Amplitude Digital Equalizers", in *Proceedings of CCECE 1996*, May 1996, pp. 478–481.
- [26] A. Fuller and B. Nowrouzian, "Finite-Precision Characterization of a Class of Bode-Type Variable-Amplitude Digital Equalizers", in *Proceed-*

ings of the 1997 Midwest Symposium on Circuits and Systems, Sacramento, California, Aug. 1997, pp. 429–432.

[27] L.O. Chua and P.M. Lin, *Computer Aided Analysis of Electronic Circuits: Algorithms and Computational Techniques*, Prentice-Hall Inc., New Jersey, 1975.

[28] L.M. Smith and B. Nowrouzian, “A Bit-Serial Multirate LDI Jau-mann Digital Filter for Digital Codec Applications”, in *Proceedings of CCVLSI’93*, Banff, AB, Nov. 1993, pp. 6A14–19.

[29] A. Fuller and B. Nowrouzian, “Design of General-Order Bode-Type Variable-Amplitude Digital Equalizers”, in *Proceedings of the 1998 International Symposium on Circuits and Systems*, Monterey, California, May 1998.

[30] A. Fuller and B. Nowrouzian, “Design of Gernal-Order Shaping Transfer Functions for Bode-Type Variable-Amplitude Digital Equalizers”, in *Proceedings of the 1998 Midwest Symposium on Circuits and Systems*, University of Notre Dame, Aug. 1998.

[31] A. Fuller and B. Nowrouzian, “An Exact BIBO Stability Condition for Bode-Type Variable-Amplitude Digital Equalizers”, in *Proceedings*

of the 1999 IEEE International Symposium on Circuits and Systems, Orlando, Florida, May 1999.

- [32] M.R. Spiegel, *Mathematical Handbook of Formulas and Tables*, McGraw-Hill Inc., New York, New York, 1968.
- [33] M.R. Spiegel, *Advanced Mathematics for Engineers and Scientists*, McGraw-Hill Inc., New York, New York, 1971.
- [34] F. Ashrafzadeh, B. Nowrouzian, and A. Fuller, "A Novel Modified Branch-and-Bound Technique for Discrete Optimization over Canonical Signed-Digit Number Space", in *Proceedings of the 1998 International Symposium on Circuits and Systems*, Monterey, California, May 1998.
- [35] B. Nowrouzian, A. Fuller, and F. Ashrafzadeh, "Development of and Interactive Graphical Software Environment for the Design and Min-Max Optimization of Multi-Rate FIR and IIR Digital Filters", in *Proceedings of WAC'98*, Anchorage, Alaska, May 1998.
- [36] B. Nowrouzian, A. Fuller and F. Ashrafzadeh, "Constrained Min-Max Optimization of Finite-Precision Multi-Rate Digital Filters Over the Canonical Signed-Digit Coefficient Space", in *Proceedings of the 1997 Midwest Symposium on Circuits and Systems*, Sacramento, California, August 1997, pp. 683–686.

- [37] R. Schaumann, M.S. Ghausi, and K.R. Laker, *Design of Analog Filters: Passive Active RC and Switched Capacitor*, Prentice-Hall Inc., New Jersey, 1990.
- [38] B.R. Barmish, *New Tools for Robustness of Linear Systems*, Macmillian Publishing Company, New York, 1994.
- [39] P.P. Vaidyanathan, *Multirate Systems and Filter Banks*, Prentice-Hall Inc., New Jersey, 1993.
- [40] D.G. Manolakis J.G. Proakis, *Introduction to Digital Signal Processing*, Macmillan Inc., New York, New York, 1988.
- [41] B. Kuo, *Digital Control Systems*, Saunders College Publishing, New York, 1992.
- [42] J.N. Mourjopoulos et al., "Theory and Real-Time Implementation of Time-Varying Digital Audio Filters", *J. Audio Eng. Soc.*, vol. 38, no. 7/8, pp. 523–535, July/Aug.. 1990.
- [43] R.A. Roberts and C.T. Mullis, *Digital Signal Processing*, Addison-Wesley Publishing Company, Reading, MA, 1987.
- [44] *DSP56002EVM Product Brief*, vol. DSP56002EVMP/D, Motorola Inc., 1994.

- [45] *DSP56002 User's Manual*, vol. DSP56002UM/AD, Motorola Inc., 1993.
- [46] *DSP56000 Family Manual*, vol. DSP56KFAMUM/AD, Motorola Inc., 1993.
- [47] J. Ousterhout, *TCL TK Toolkit*, Addison-Wesley Publishing Company, Reading, MA, 1994.
- [48] B. B. Welch, *Practical Programming in Tcl & Tk*, Prentice-Hall Press, New Jersey, 1997.
- [49] M. Harrison and M. McLennan, *Effective Tcl/Tk Programming*, Addison-Wesley Publishing Company, Reading, MA, 1997.
- [50] E. Foster-Johnson, *Graphical Applications with Tcl and Tk*, M & T Books, New York, 1997.
- [51] B.P. Lathi, *Modern Digital and Analog Communication Systems*, Oxford University Press, New York, New York, 1998.
- [52] J.S. Chow, J.C. Tu, and J.M. Cioffi, "A Discrete Multitone Transceiver System for HDSL Applications", *IEEE Journal on Selected Areas in Communications*, vol. 9, no. 6, pp. 895–908, August 1991.

Appendix A

MATLAB Design Files

A.1 Design of Maximally Flat Lowpass Transfer Function

```
function [n,d] = createfan( N, h, p )
%
% Function:  createfan
%
% Purpose:  This function creates a normalized lowpass maximally
flat
% shaping transfer function.  See Chapter 4 for details.
%
% Parameters:  N - order of resulting transfer function
% h - magnitude of passband
% p - magnitude at passband edge (w = PI)
%
% Returns:  n - numerator polynomial
% d - denominator polynomial
%
n = [1];
d = [1];

an = ( h ^2 - p^2 )/( tan(1/2)^(2*N)*(p^2 - 1 ) );

Kn = 1;
Kd = 1;

for k = 1:N
```



```

p = (1+exp(1j*(2*k+N-1)*pi/(2*N))*an^(-1/(2*N))) / ...
    (1-exp(1j*(2*k+N-1)*pi/(2*N))*an^(-1/(2*N)));

z = (1+exp(1j*(2*k+N-1)*pi/(2*N))*h^(1/N)*an^(-1/(2*N))) / ...
    ( 1- exp(1j*(2*k+N-1)*pi/(2*N))*h^(1/N)*an^(-1/(2*N)));
n = conv( n, [1 -z] );
d = conv( d, [1 -p] );
Kn = Kn*p;
Kd = Kd*z;
end

Kn = Kn*(h^2 + (-1)^N*an);
Kd = Kd*(1 + (-1)^N*an);
n = n * sqrt( Kn/Kd );

%The following is used to get rid of the imaginary part that
%sometimes appears due to numerical inaccuracies.
n = real(n);
d = real(d);

```

A.2 Design of Cheybshev Lowpass Transfer Function

```

function [n,d] = chebfan( N, h, p )
%
% Function:  chebfan
%
% Purpose:  This function creates a normalized lowpass shaping
% transfer function with equiripple passband.  See
% Chapter 4 for details.
%
% Parameters:  N - order of resulting transfer function
% h - magnitude of passband
% p - magnitude at passband edge (w = PI)
%
% Returns:  n - numerator polynomial
% d - denominator polynomial
%

```



```

an = ( h^2 - p^2 )/(cos(N*acos(1))^2 *( p^2 - 1 ) );
alpha = 1/tan(1/2);

C = chebpoly(N);
C = conv(C,C);

n = 1;
d = 1;
Kn = 1;
Kd = 1;

for k = 1:N
    F41 = 1j/alpha*cos((acos(-(2+an)/an)+2*pi*(k-1))/(2*N));
    F4h2 = 1j/alpha*cos((acos(-(2*h^2+an)/an)+2*pi*(k-1))/(2*N));
    p = (1+F41)/(1-F41);
    z = (1+F4h2)/(1-F4h2);
    n = conv( n, [1 -z] );
    d = conv( d, [1 -p] );
    Kn = Kn/z;
    Kd = Kd/p;
end

sum = 0;

for k = 0:N
    sum = sum + C(2*N + 1 - 2*k)*(-1)^k*alpha^(2*k);
end

Kn = Kn*(h^2 + an*sum);
Kd = Kd*(1+an*sum);

n = n*sqrt(Kn/Kd);

n = real(n);
d = real(d);

```


A.3 Calculation of Cheybshev Polynomial

```
function [C] = chebpoly( n )
%
% Function:  chebpoly
%
% Purpose:  This function creates the chebyshev polynomial
% of a given order.  See Chapter 4 for details.
%
% Parameters:  n - order
%
% Returns:  C - resulting chebyshev polynomial (in vector form)
%

if n < 0
    error('Invalid negative value for n');
end

if n == 0
    C = 1;
elseif n == 1
    C = [1 0];
else
    C = polyadd( conv( [2 0], chebpoly(n-1) ), -chebpoly(n-2) );
end
```

A.4 Design of Inverse-Cheybshev Lowpass Transfer Function

```
function [n,d] = invfan( N, h, p )
%
% Function:  chebpoly
%
% Purpose:  This function creates the chebyshev polynomial of a
% given order.  See Chapter 4 for details.
%
% Parameters:  n - order
%
% Returns:  C - resulting chebyshev polynomial (in vector form)
```



```

%

an = (cos(N*acos(2))^2*(h^2 - p^2))/(p^2 - 1);
alpha = 2/tan((pi-1)/2);

n = 1;
d = 1;
Kn = 1;
Kd = 1;

C = chebpoly(N);
C = conv(C,C);

for k = 1:N
    F61 = 1j/alpha*cos((acos(-2*an-1)-2*pi*k)/(2*N));
    F6h2 = 1j/alpha*cos((acos((-2*an-h^2)/(h^2))-2*pi*k)/(2*N));
    p = (F61-1)/(F61+1);
    z = (F6h2-1)/(F6h2+1);
    n = conv( n, [1 -z] );
    d = conv( d, [1 -p] );
    Kn = Kn*p;
    Kd = Kd*z;
end

sum = 0;

for k = 0:N
    sum = sum + C(2*N + 1 - 2*k)*(-1)^k*alpha^(2*k);
end

Kn = Kn*(h^2*sum + an);
Kd = Kd*(sum+an);
n = n*sqrt( Kn/Kd );

%The following is used to get rid of the imaginary part that
%sometimes appears due to numerical inaccuracies.
n = real(n);
d = real(d);

```


A.5 Normalized Lowpass to Lowpass Transformation Function

```
function [nlp,dlp] = dlp2lp( n, d, wp );
%
% Function:  dlp2lp
%
% Purpose:  This function performs a lowpass to lowpass transform.
% This can be used to create denormalized lowpass shaping
% transfer functions from normalized lowpass prototypes.
% Based on transformations given in A. Antonious' DIGITAL
% FILTERS Analysis, Design, and Applications.
%
% Parameters:  n - numerator of normalized lowpass prototype
% d - denominator of normalized lowpass prototype
% wp - passband edge (in radians) of resulting denormalized
% lowpass transfer function.
%
% Returns:  nlp - numerator polynomial of resulting denormalized
% shaping transfer function
% dlp - denominator polynomial of resulting denormalized
% shaping transfer function
%

N = size( d,2 ) - 1;

A = sin( (1-wp)/2 )/sin( (1+wp)/2 );

nt = [1 -A];
dt = [-A 1];

nz = zeros(1,N+1);
dz = nz;

for i = 0:N
    DT = polypow(dt,i);
    NT = polypow(nt,N-i);
    prod = conv(NT,DT);
    prod = polypad(prod,N+1);
    nz = nz + n(i+1)*prod;
```



```

        dz = dz + d(i+1)*prod;
end

```

```

c = dz(1);
dz = dz/c;
nz = nz/c;

```

```

nlp = nz;
dlp = dz;

```

A.6 Normalized Lowpass to Highpass Transformation Function

```

function [nhp,dhp] = dlp2hp( n, d, wp );
% % Function:  dlp2hp
%
% Purpose:  This function performs a lowpass to highpass tranform.
% This can be used to create denormalized highpass shaping
% transfer functions from normalized lowpass prototypes.
% Based on transformations given in A. Antonious' DIGITAL
% FILTERS Analysis, Design, and Applications.
%
% Parameters:  n - numerator of normalized lowpass prototype
% d - denominator of normalized lowpass prototype
% wp - passband edge (in radians) of resulting denormalized
% highpass transfer function.
%
% Returns:  nhp - numerator polynomial of resulting denormalized
% shaping transfer function
% dhp - denominator polynomial of resulting denormalized
% shaping transfer function
%
N = size( d,2 ) - 1;

A = cos( (1-wp)/2 )/cos( (1+wp)/2 );
A = 1/A;

```



```

nt = -[1 -A];
dt = [-A 1];
nz = zeros(1,N+1);
dz = nz;

for i = 0:N
    DT = polypow(dt,i);
    NT = polypow(nt,N-i);
    prod = conv(NT,DT);
    prod = polypad(prod,N+1);
    nz = nz + n(i+1)*prod;
    dz = dz + d(i+1)*prod;
end

c = dz(1);
dz = dz/c;
nz = nz/c;

nhp = nz;
dhp = dz;

```

A.7 Normalized Lowpass to Bandpass Transformation Function

```

function [nbp,dbp] = dlp2bp( N, num, den, wp1, wp2 )
%
% Function:  dlp2bp
%
% Purpose:  This function performs a lowpass to bandpass tranform.
% This can be used to create denormalized bandpass shaping
% transfer functions from normalized lowpass prototypes.
% Note that the resulting transfer function is order 2N.
% Based on transformations given in A. Antonious' DIGITAL
% FILTERS Analysis, Design, and Applications.
%
% Parameters:  n - numerator of normalized lowpass prototype
% d - denominator of normalized lowpass prototype
% wp1 - lower passband edge (in radians) of resulting

```



```

% denormalized bandpass transfer function.
% wp2 - upper passband edge (in radians) of resulting
% denormalized bandpass transfer function.
%
% Returns:  nbp - numerator polynomial of resulting
% denormalized shaping transfer function
% dbp - denominator polynomial of resulting denormalized
% shaping transfer function
%

if rem(N,2) = 0
    error('Order N must be even');
end

A = cos( (wp2+wp1)/2 )/cos( (wp2-wp1)/2 );
K = tan(1/2)*cot(( wp2 - wp1 )/2);

nt = -[1 -2*A*K/(K+1) (K-1)/(K+1)];
dt = [(K-1)/(K+1) -2*A*K/(K+1) 1];
nz = zeros(1,N+1);
dz = nz;
Nfan = N/2;

for i = 0:Nfan
    DT = polypow(dt,i);
    NT = polypow(nt,Nfan-i);
    prod = conv(NT,DT);
    prod = polypad(prod,N+1);
    nz = nz + num(i+1)*prod;
    dz = dz + den(i+1)*prod;
end

c = dz(1);
dz = dz/c;
nz = nz/c;

n = nz;
d = dz;

```


A.8 Polynomial Addition Function

```
function [result] = polyadd(p1,p2)
%function [result] = polyadd(p1,p2)

l1 = size(p1,2);
l2 = size(p2,2);

if l1 > l2
    p2 = polypadl(p2,l1-l2);
elseif l1 < l2
    p1 = polypadl(p1,l2-l1);
end

result = p1+p2;
```

A.9 Polynomial Power Function

```
function [p] = polypow( x, n )
%
% Function:  polypow
%
% Purpose:  This function raises a polynomial to a given power.
%
% Parameters:  x - input polynomial (in vector form)
% n - power
%
% Returns:  p - x**n (in vector form)
%

p = 1;

for i = 1:n
    p = conv( p, x );
end
```


A.10 Polynomial Pad Function

```
function [p] = polypad( x, n )
%
% Function:  polypad
%
% Purpose:  This function pads a polynomial with zeros to the
% right effectively increasing the order of the polynomial.
%
% Parameters:  x - input polynomial (in vector form)
% n - length of new polynomial
%
% Returns:  p - polynomial (in vector form) with new length n
%

p = zeros( 1, n );
for i = 1:size(x,2)
    p(i) = x(i);
end
```

A.11 Polynomial Pad Left Function

```
function [p] = polypadl( x, n )
%
% Purpose:  This function pads a polynomial with zeros to the
% left to create a new polynomial of length n.
%
% Parameters:  x - input polynomial (in vector form)
% n - length of new polynomial
%
% Returns:  p - polynomial (in vector form) with new length n
%

sz = size(x,2);
p = zeros( 1, n+sz );

for i = 1:sz
    p(i+n) = x(i);
end
```


Appendix B

DSP56002EVM Code for 4-Band Equalizer Implementation

```
*****
;EQUAL.ASM : 4-Band Graphic Equalizer
;              (based on Motorla Framework)
;*****
;---Port-B bit position names
ACK      equ      13              ;acknowledge back to host
STR      equ      12              ;data strobe from host
INI      equ      11

START    EQU      $40

;set start vector
org      p:$0
jmp      START

org      p:$000c
jsr      ssi_rx_isr      ;SSI receive data
jsr      ssi_rx_isr      ;SSI receive data with exception
jsr      ssi_tx_isr      ;SSI transmit data
jsr      ssi_tx_isr      ;SSI transmit with exception

org      p:START

movep    #$261009,x:PLL  ;these labels are defined in the
```



```

movep    #0000,x:BCR        ;ada_init.asm program
ori      #3,mr              ;mask interrupts
movec    #0,sp              ;clear hardware stack pointer
move     #0,omr             ;operating mode 0
move     #$D0,r3            ; initialise stack pointer
move     #-1,m3             ; linear addressing

movep    #$0000,X:PBC       ;set up port-B for parallel out
movep    #$2000,X:PBDDR     ; PB12(STR)=input, PB13(ACK)=output
movep    #$0000,X:PBD       ; start with ack low
;-----
;    Set runtime variables
;-----
MOVE     #$200000,X0        ;Constants used for data scaling.
MOVE     X0,X:>$1D
MOVE     #>$80,X0
MOVE     X0,X:>$1E

include 'ada_init.asm'

TONE_OUTPUT    EQU    HEADPHONE_EN+LINEOUT_EN
                  +(4*LEFT_ATTEN)+(4*RIGHT_ATTEN)

TONE_INPUT     EQU    MIC_IN_SELECT+(15*MONITOR_ATTEN)

loop_1

jset     #2,x:SSISR,*        ;wait for frame sync to pass
jclr     #2,x:SSISR,*        ;wait for frame sync

move     x:RX_BUFF_BASE,x0   ;receive left

jsr      process_Lchannel    ;process left
move     x0,x:TX_BUFF_BASE   ;transmit left

move     x:RX_BUFF_BASE+1,x0 ;receive right
jsr      process_Rchannel    ;process right

```



```

move    x0,x:TX_BUFF_BASE+1      ;transmit right

move    #TONE_OUTPUT,y0          ;set up control words
move    y0,x:TX_BUFF_BASE+2
move    #TONE_INPUT,y0
move    y0,x:TX_BUFF_BASE+3

;-----
;| After processing a pair of samples,
;| check to see if the sliders have changed
;-----

loop_2
jclr    #INI,x:PBD,done1 ;if INI is lowm then no data
doack   bset    #ACK,x:PBD      ;tell PC we are ready to
                                   ;receive

l1      jset     #STR,x:PBD,l1    ;Wait until PC outputs data
jset    #STR,x:PBD,l1      ; Check again to be sure

ready1  move     x:PBD,x0         ; Read the data

bclr    #ACK,x:PBD          ;tell PC we received data

l2      jclr     #INI,x:PBD,done1 ; no more data to be received
jset    #STR,x:PBD,nextByte
jmp     l2

nextByte
bset    #ACK,x:PBD          ;tell PC we are ready to receive

l3      jset     #STR,x:PBD,l3    ;Wait until PC outputs data
jset    #STR,x:PBD,l3      ; Check again to be sure

ready2  move     x:PBD,x1         ; Read the data

bclr    #ACK,x:PBD          ;tell PC we received data

```



```

        ; no more data to be received
l4      jclr      #INI,x:PBD,doneData
jmp     l4

```

doneData

```

;-----
; at this point, we have slider number in x0 and value in x1
;-----

```

```

move     #>$00ff,y1
move     x0,a
and      y1,a
move     a,x0

```

```

move     x1,a
and      y1,a
move     a,x1

```

```

clr      a
move     #>$0014,a
sub      x0,a
jeq      adjustvolume

```

```

;-----
; Changing band setting
;-----

```

```

move     #pointers,n2
move     x0,r2

```

```

move     x1,r1

```

```

move     y:(r2+n2),n1
move     x0,r2
move     y:(r1+n1),y0

```

```

move     #current,n2
nop
move     y0,x:(r2+n2)

```

```

jmp      done1

```

adjustvolume


```

move    #GVol,n2
move    x1,r2
nop
move    x:(r2+n2),x1
move    x1,y1
move    y1,y:$1e

done1    jmp        loop_1

;*****
;* Subroutines
;*****

process_Lchannel
;*****
;  LEFT CHANNEL SERVICE ROUTINE  *
;*****

move    #>$10000,y0          ;scale input by 2^-3
mpy     x0,y0,b
move    b,x0

move    #fixedcoeffs,r1
move    #lstates,r4
move    #lvariablev,r2

;-----
;  4-Band EQ
;-----
DO      #4,LFBAND            ;For all 4 bands

clr     a                    x:(r1)+,x1      y:(r4)+,y1

mac     x1,y1,a x:(r1)+,x1      y:(r4)-,y1
mac     x1,y1,a                    y:(r4),y0

move    a,b

```



```

sub      x0,b

rnd      b          x:(r2)+,x1

move     b,y1

mpy      x1,y1,b
asl      b
asl      b
asl      b

add      b,a
add      x0,b      x:(r1)+,x1      y:(r4)+,y1

asr      b

mac      -x1,y1,b      x:(r1)+,x1      y:(r4),y1
macr     -x1,y1,b      y0,y:(r4)-

asl      b

rnd      a          b,y:(r4)+

move     a,x0      y:(r4)+,y0

```

LFBAND

```

;-----
;   Volume Scaling
;-----
MOVE     Y:$1E,Y0          ;X:$1D=$200000.

MPY      X0,Y0,B          ;Y0=volume gain.

ASL      B
ASL      B          ;Scale result
ASL      B
ASL      B

```



```

ASL      B
ASL      B

MOVE     b,x0                      ;move b to x0
;to force
;limiting

```

```

;-----
;   Left EQ Complete
;-----

```

```

rts

```

```

process_Rchannel
;*****
;   RIGHT CHANNEL SERVICE ROUTINE *
;*****

```

```

move     #>$10000,y0              ;scale input by 2^-3
mpy      x0,y0,b
move     b,x0

```

```

move     #fixedcoeffs,r1
move     #rstates,r4
move     #rvariablev,r2

```

```

;-----
;   For all 4 bands
;-----

```

```

DO       #4,RFBAND

```

```

clr      a          x:(r1)+,x1      y:(r4)+,y1

```

```

mac      x1,y1,a x:(r1)+,x1      y:(r4)-,y1
mac      x1,y1,a                  y:(r4),y0

```

```

move     a,b
sub      x0,b

```



```

rnd      b          x:(r2)+,x1

move     b,y1

mpy      x1,y1,b
asl      b
asl      b
asl      b

add      b,a
add      x0,b      x:(r1)+,x1      y:(r4)+,y1

asr      b

mac      -x1,y1,b      x:(r1)+,x1      y:(r4),y1
macr     -x1,y1,b      y0,y:(r4)-

asl      b

rnd      a          b,y:(r4)+

move     a,x0      y:(r4)+,y0

```

RFBAND

```

;-----
;   Volume Scaling
;-----

```

```

MOVE     Y:$1E,Y0          ;Y0=volume gain.

MPY      X0,Y0,B          ;Scale total left
;data by volume.
ASL      B
ASL      B          ;Scale result
ASL      B
ASL      B
ASL      B
ASL      B

```



```
MOVE      B,X0                                ;move b to x0
```

```
;-----  
;      EQ Complete  
;-----
```

```
rts
```

```
include 'txrx_isr.asm'      ;Motorola ISR for DAC/ADC
```

```
ORG      X:$20
```

```
;-----  
;      Fixed Coefficients Entered Here  
;-----
```

```
fixedcoeffs
```

```
DC      -9.9536251231873485e-01      ;band1 a1  
DC      8.7486235917265265e-01      ;band1 a2  
DC      -8.7007491980318896e-01/2.0  ;band1 b1/2.0  
DC      1.4995168823989490e-04/2.0   ;band1 b2/2.0
```

```
DC      -9.2372434472688736e-01      ;band2 a1  
DC      9.3170350611254904e-01      ;band2 a2  
DC      -9.2372434472688736e-01/2.0  ;band2 b1/2.0  
DC      -6.8296493887452681e-02/2.0  ;band2 b2/2.0
```

```
DC      -8.7588351136690579e-01      ;band3 a1  
DC      9.0684358334815629e-01      ;band3 a2  
DC      -8.7588351136690579e-01/2.0  ;band3 b1/2.0  
DC      -9.3156416651843349e-02/2.0  ;band3 b2/2.0
```

```
DC      9.8726397940360283e-02      ;band4 a1  
DC      -6.0894263922046839e-02      ;band4 a2  
DC      -1.6946682264383299e+00/2.0  ;band4 b1/2.0  
DC      7.3250036045664368e-01/2.0  ;band4 b2/2.0
```

```
ORG      X:$40
```

```
;-----
```


; Volume Gain (GVol) Coefficients
;-----
GVol

DC	0.9999
DC	0.9999
DC	0.9999
DC	0.9000
DC	0.8000
DC	0.7000
DC	0.6000
DC	0.5000
DC	0.4500
DC	0.4000
DC	0.3500
DC	0.3000
DC	0.2500
DC	0.2000
DC	0.1500
DC	0.1200
DC	0.1000
DC	0.0800
DC	0.0600
DC	0.0400
DC	0.0300
DC	0.0200
DC	0.0150
DC	0.0100
DC	0.0030
DC	0.0010
DC	0.0005
DC	0.0002
DC	0.0000


```

ORG      X:$B0
;-----
;      Initial Gain Coefficients
;-----
current

lvariablev      DC      -1.000/8.0
DC      -1.000/8.0
DC      -1.000/8.0
DC      -1.000/8.0
rvariablev      DC      -1.000/8.0
DC      -1.000/8.0
DC      -1.000/8.0
DC      -1.000/8.0

ORG      Y:$1E
;-----
;      Initial Volume Coefficient
;-----
DC      0.15

ORG      Y:$20
;-----
;      Filter States
;-----
lstates
bsc      8,0
rstates
bsc      8,0

ORG      Y:$40
;-----
;      Pointer Array for band settings
;-----
pointers      DC      band1
DC      band2
DC      band3
DC      band4

```


DC	band1
DC	band2
DC	band3
DC	band4

band1

DC	-1.0523335904170381e+00/8.0
DC	-1.0496679000529345e+00/8.0
DC	-1.0468081697904186e+00/8.0
DC	-1.0437534459860451e+00/8.0
DC	-1.0405053883240112e+00/8.0
DC	-1.0370685910894504e+00/8.0
DC	-1.0334508252851677e+00/8.0
DC	-1.0296632258879794e+00/8.0
DC	-1.0257203284635807e+00/8.0
DC	-1.0216400231260667e+00/8.0
DC	-1.0174433358179313e+00/8.0
DC	-1.0131540843963023e+00/8.0
DC	-1.0087983922835837e+00/8.0
DC	-1.0044040862080050e+00/8.0
DC	-1.0000000000000000e+00/8.0
DC	-9.9561522472032937e-01/8.0
DC	-9.9127834426493577e-01/8.0
DC	-9.8701669904026468e-01/8.0
DC	-9.8285571765634649e-01/8.0
DC	-9.7881834830643044e-01/8.0
DC	-9.7492461858281876e-01/8.0
DC	-9.7119133213444819e-01/8.0
DC	-9.6763191390752690e-01/8.0
DC	-9.6425637473938974e-01/8.0
DC	-9.6107142857832284e-01/8.0
DC	-9.5808066919030788e-01/8.0
DC	-9.5528486389269385e-01/8.0
DC	-9.5268227212585066e-01/8.0
DC	-9.5026901080265014e-01/8.0

band2

DC	-1.0955046213363762e+00/8.0
DC	-1.0905431129120489e+00/8.0
DC	-1.0852320669280859e+00/8.0

DC	-1.0795723128700443e+00/8.0
DC	-1.0735695223856259e+00/8.0
DC	-1.0672348727569241e+00/8.0
DC	-1.0605854296828221e+00/8.0
DC	-1.0536443617148614e+00/8.0
DC	-1.0464409129674266e+00/8.0
DC	-1.0390101683456556e+00/8.0
DC	-1.0313925523035778e+00/8.0
DC	-1.0236330604767112e+00/8.0
DC	-1.0157802815525576e+00/8.0
DC	-1.0078852242920513e+00/8.0
DC	-1.0000000000000000e+00/8.0
DC	-9.9217646602807386e-01/8.0
DC	-9.8446486721671889e-01/8.0
DC	-9.7691256624155420e-01/8.0
DC	-9.6956294455155434e-01/8.0
DC	-9.6245448838314174e-01/8.0
DC	-9.5562012876987712e-01/8.0
DC	-9.4908684214135364e-01/8.0
DC	-9.4287548368362861e-01/8.0
DC	-9.3700086600127652e-01/8.0
DC	-9.3147204642868042e-01/8.0
DC	-9.2629274396774663e-01/8.0
DC	-9.2146189785070742e-01/8.0
DC	-9.1697429304718270e-01/8.0
DC	-9.1282134326382602e-01/8.0

band3

DC	-1.1325726588845859e+00/8.0
DC	-1.1255712473218253e+00/8.0
DC	-1.1180893933485438e+00/8.0
DC	-1.1101324853467724e+00/8.0
DC	-1.1017114812520623e+00/8.0
DC	-1.0928451510708563e+00/8.0
DC	-1.0835604750826691e+00/8.0
DC	-1.0738928183327441e+00/8.0
DC	-1.0638857741931640e+00/8.0
DC	-1.0535906717745893e+00/8.0
DC	-1.0430657416448286e+00/8.0
DC	-1.0323749257164232e+00/8.0
DC	-1.0215864193507673e+00/8.0

DC	-1.0107709612140989e+00/8.0
DC	-1.0000000000000000e+00/8.0
DC	-9.8934381612906519e-01/8.0
DC	-9.7886970799348938e-01/8.0
DC	-9.6864034091688500e-01/8.0
DC	-9.5871234196905231e-01/8.0
DC	-9.4913520666965934e-01/8.0
DC	-9.3995053252628169e-01/8.0
DC	-9.3119162632313224e-01/8.0
DC	-9.2288342274916046e-01/8.0
DC	-9.1504272038917933e-01/8.0
DC	-9.0767865908371015e-01/8.0
DC	-9.0079338565399214e-01/8.0
DC	-8.9438286951736456e-01/8.0
DC	-8.8843776205139524e-01/8.0
DC	-8.8294555952361586e-01/8.0

band4

DC	-4.1011278315101380e+00/8.0
DC	-3.7349081313970713e+00/8.0
DC	-3.3954810731636731e+00/8.0
DC	-3.0823206591510663e+00/8.0
DC	-2.7942541114920183e+00/8.0
DC	-2.5300106820385655e+00/8.0
DC	-2.2882517243373788e+00/8.0
DC	-2.0675988746686773e+00/8.0
DC	-1.8666594059129915e+00/8.0
DC	-1.6840482124714948e+00/8.0
DC	-1.5184062205756619e+00/8.0
DC	-1.3684152409844907e+00/8.0
DC	-1.2328094546926758e+00/8.0
DC	-1.1103838524984193e+00/8.0
DC	-1.0000000000000000e+00/8.0
DC	-9.0058946530062545e-01/8.0
DC	-8.1115536240698904e-01/8.0
DC	-7.3077233433951039e-01/8.0
DC	-6.5858528926526494e-01/8.0
DC	-5.9380722748573123e-01/8.0
DC	-5.3571636948460644e-01/8.0
DC	-4.8365280724978393e-01/8.0
DC	-4.3701485696009923e-01/8.0

DC	-3.9525524816924734e-01/8.0
DC	-3.5787725815174359e-01/8.0
DC	-3.2443087873778204e-01/8.0
DC	-2.9450907793406417e-01/8.0
DC	-2.6774420275390876e-01/8.0
DC	-2.4383536458354554e-01/8.0

end

Appendix C

IBM-PC Code for 4-Band Equalizer Implementation

C.1 C Code

```
#include <math.h>
#include <stdlib.h>
#include <stdio.h>
#include <conio.h>

#define INIHIGH 0x04
#define INILOW 0x00
#define STRHIGH 0x00
#define STRLOW 0x01

#define DATA 0x378
#define STATUS 0x379
#define CONTROL 0x37A

int slider, pos;

void send2Bytes( char c1, char c2 );

ET_PROC(send_change )
{
    int slider, pos;
    sscanf( argv[1], "%d", &slider );
    sscanf( argv[2], "%d", &pos );
```



```

send2Bytes( (char)(slider-1), (char)(30-pos) );
return ET_OK;
}

/*
** This file implements a simple ASCII text editor
*/
void Et_Main(int argc, char **argv){
    ET_INSTALL_COMMANDS;
    ET_INCLUDE( sliders.tcl );
}

#if UNIX
int main(int argc, char **argv){
    Et_Init(&argc,argv);
    Et_Main(argc,argv);
    Et_MainLoop();
    return 0;
}
#endif

void send2Bytes( char c1, char c2 )
{
    int ack1,ack2,ack3;

    /* select input mode, STR  high  */
    _outp(CONTROL, INIHIGH | STRHIGH );
    /* INI~ high for sync req.          */
    do {
        /* wait here until ack=high */
        ack1 = (_inp(STATUS) & 0x40); /* read ACK 3 times... */
        ack2 = (_inp(STATUS) & 0x40); /*...to avoid noise... */
        ack3 = (_inp(STATUS) & 0x40);
        ack1 = ack1 | ack2 | ack3;
    } while (!ack1);

    _outp(DATA, c1); /*Put data on D0-D7 */

    /* toggle STR  low to indicate that data is ready */
    _outp(CONTROL, INIHIGH | STRLOW);

```



```

do {
    /* wait here until ack=low*/
    ack1 = (_inp(STATUS) & 0x40); /* read ACK 3 times... */
    ack2 = (_inp(STATUS) & 0x40); /*...to avoid noise... */
    ack3 = (_inp(STATUS) & 0x40);
    ack1 = ack1 | ack2 | ack3;
    } while (ack1 != 0);

/* Signal that transmission is finished */
_outp(CONTROL, INIHIGH | STRHIGH );

do {
    /* wait here until ack=high*/
    ack1 = (_inp(STATUS) & 0x40); /* read ACK 3 times...*/
    ack2 = (_inp(STATUS) & 0x40); /*...to avoid noise...*/
    ack3 = (_inp(STATUS) & 0x40);
    ack1 = ack1 | ack2 | ack3;
    } while (!ack1);

_outp(DATA, c2); /*Put data on D0-D7 */

    /* toggle STR low to indicate that data is ready */
_outp(CONTROL, INIHIGH | STRLOW);

do {
    /* wait here until ack=low */
    ack1 = (_inp(STATUS) & 0x40); /* read ACK 3 times... */
    ack2 = (_inp(STATUS) & 0x40); /*...to avoid noise... */
    ack3 = (_inp(STATUS) & 0x40);
    ack1 = ack1 | ack2 | ack3;
    } while (ack1 != 0);

    /* Signal that transmission is finished */
_outp(CONTROL, INILOW | STRLOW );

}

```

C.2 TCL/TK Code

```

global sliders

wm title . "Graphic Equalizer"

```



```

frame .base
pack .base
canvas .base.canvas -width 750 -height 600
pack .base.canvas

proc DrawSlider {w startX startY endX stepSize \
                stepNum startPos number} {
global sliders
set endY [expr ($startY + $stepSize*($stepNum-1))]
$w create rect $startX $startY $endX $endY -fill grey -tag slider
for { set i 1 } { $i < [expr ($stepNum-1)] } { incr i } {
set tempY [expr ($startY+$i*$stepSize)]
$w create line $startX $tempY $endX $tempY -fill red -tag slider
}
set tempY [expr ($startY + ($startPos-1)*$stepSize)]
$w create rect [expr ($startX - 4)] [expr ($tempY - 4)] \
[expr ($endX + 4)] [expr ($tempY+4)] -fill black -tag s$number
$w create line [expr ($startX-4)] $tempY [expr ($endX+4)] $tempY \
                -fill cyan -tag s$number
set sliders($number,steps) $stepNum
set sliders($number,stepSize) $stepSize
set sliders($number,startY) $startY
set sliders($number,endY) $endY
set sliders($number,pos) [expr ($startPos-1)]

set control {MarkSlider %y }
append control $number
$w bind s$number <Button-1> $control
set control {DragSlider %W %y }
append control $number
$w bind s$number <B1-Motion> $control
}

proc MarkSlider {y number} {
global sliders
set sliders($number,mark) $y
}

proc DragSlider {w y number} {

```



```

global sliders
if { ( $y <= $sliders($number,endY) ) && \
    ( $y >= $sliders($number,startY) ) } {

set interval [expr ($y-$sliders($number,startY)) \
                /$sliders($number,stepSize)]
set subint [expr ($y - $sliders($number,stepSize)*$interval - \
    $sliders($number,startY))/( $sliders($number,stepSize)/2 )]

if { $subint == 1 } {
set newPos [expr ($interval + 1)]
} else {
set newPos $interval
}
if { $newPos >= $sliders($number,steps) } {
set newpos [expr ($sliders($number,steps) - 1)]
}
set dy [expr ($newPos - $sliders($number,pos))* \
        $sliders($number,stepSize)]
$w move s$number 0 $dy
if { $newPos != $sliders($number,pos) } {
set sliders($number,pos) $newPos
send_change $number $newPos
}
}
}

DrawSlider .base.canvas 30 10 50 20 29 15 21

DrawSlider .base.canvas 80 10 120 20 29 15 1

DrawSlider .base.canvas 160 10 200 20 29 15 2

DrawSlider .base.canvas 240 10 280 20 29 15 3

DrawSlider .base.canvas 320 10 360 20 29 15 4

DrawSlider .base.canvas 420 10 460 20 29 15 5

```


DrawSlider .base.canvas 500 10 540 20 29 15 6

DrawSlider .base.canvas 580 10 620 20 29 15 7

DrawSlider .base.canvas 660 10 700 20 29 15 8

.base.canvas create text 40 595 -text VOLUME -justify center

.base.canvas create text 220 595 -text LEFT -justify center

.base.canvas create text 565 595 -text RIGHT -justify center

.base.canvas create text 390 580 -text Hz -justify center

.base.canvas create text 100 580 -text Low -justify center

.base.canvas create text 180 580 -text 1K -justify center

.base.canvas create text 260 580 -text 2K -justify center

.base.canvas create text 340 580 -text High -justify center

.base.canvas create text 440 580 -text Low -justify center

.base.canvas create text 520 580 -text 1K -justify center

.base.canvas create text 600 580 -text 2K -justify center

.base.canvas create text 680 580 -text High -justify center

University of Alberta Library



0 1620 1250 6166

B45365